ALMA MATER STUDIORUM
UNIVERSITÀ DEGLI STUDI DI BOLOGNA

Dottorato di Ricerca in Ingegneria Elettronica, Telecomunicazioni e Tecnologie dell'Informazione

Dipartimento di Ingegneria dell'Energia Elettrica e dell'Informazione "Guglielmo Marconi" - DEI

Ciclo XXIX

Settore concorsuale: 09/F2 - TELECOMUNICAZIONI

Settore scientifico disciplinare: ING-INF/03 - TELECOMUNICAZIONI

DEVICE-TO-DEVICE WIRELESS COMMUNICATIONS

Presentata da:
ASHRAF S.A. ALHALABI

Coordinatore Dottorato:
Chiar.mo Prof. Ing.
ALESSANDRO
VANELLI-CORALLI

Relatore:
Chiar.mo Prof. Ing.
DAVIDE DARDARI

ESAME FINALE 2017

INDEX TERMS

Stochastic Geometry

Device-to-Device

Link lifetime

Interference

Blockage

Contents

Typeset using LaTeX.

List of Acronyms

5G fifth generation

AP access point

AWGN additive white Gaussian noise

BW bandwidth

BS base station

CARE community database on Accidents on the roads in Europe

CASY center of complex automated systems

CDF cumulative distribution function

D2D Device-to-Device

EU European Union

GPS global positioning system

GDOP geometric dilution of person

HGVs heavy goods vehicles

HMIs human machine interface

IEEE Institute of Electrical and Electronics Engineers

i.i.d. independent and identically distributed

IR-UWB impulse radio UWB

LOS line-of-sight

MAE mean absolute error

MCU micro-controller unit

MS mobile stations

MIMO multiple-input multiple-output

mmW millimeter-wave

NLOS non-line-of-sight

NHPPP non-homogeneous PPP

OFDM orthogonal frequency division multiplexing

p.d.f. probability density function

PL path-loss

PPP Poisson point process

PHY physical layer

PEB position error bound

RA risk assessment

RFID radio frequency identification

RTLs real time locating systems

RV random variable

SPI serial peripheral interface

TDMA time division multiple access

TDOA time difference-of-arrival

TOA time-of-arrival

TWR two way ranging

UHF ultra-high frequency

UWB ultra-wideband

VRUs Vulnerable road users

WiFi Wi-Fi

WSN Wireless Sensor Network

Executive Summary

Device-to-Device (D2D) is one of the important proposed solutions to increase the capacity, offload the traffic, and improve the energy efficiency in next generation cellular networks. D2D communication is known as a direct communication between two users without using cellular infrastructure networks. Despite of large expected benefits in terms of capacity in D2D, the coexistence of D2D and cellular networks in the same spectrum creates new challenges in interference management and network design. To limit the interference power control schemes on cellular networks and D2D networks are typically adopted. Even though power control is introduced to limit the interference level, it does not prevent cellular and D2D users from experiencing coverage limitation when sharing the same radio resources. Therefore, the design of such networks requires the availability of suitable methods able to properly model the effect of interference in the presence of random terminals deployment. To this purpose in this PhD dissertation studied a new analytical model based on stochastic geometry to characterize the coverage probability on both cellular and D2D networks taking into account the impact of power control, shadowing and user's random locations.
The above mentioned work focus on static wireless networks while in dynamic mobility model user mobility poses several challenges especially at millimeter-wave (mmW). When transmitting at high frequencies, and using beamforming techniques, the presence of obstacles and user mobility might severely impact the wireless link blockage properties thus translating into frequent handovers and channel estimate updates causing significant signaling overhead. Unfortunately an analysis based on the coverage probability does not provide information about link blockages duration/rate as its evaluation usually does not include spatial/time correlation of the link state. In this context, the link lifetime represents an important performance index able to properly capture the dynamic behavior of the wireless link. For this reason, in this thesis I have also addressed the effect of blockages and user mobility in wireless networks on link lifetime.

When users in D2D communications are machines, then I refer to machine-

to-machine (M2M) communications. Examples of M2M networks are those devoted to improve the safety of read users like cars and cyclists. In the last part of the Thesis, the experimental activity carried out within the European H2020 project XCYCLE is reported. Such an activity regards the investigation of a communication and localization architecture to determine potentially dangerous situations and provide a real-time feedback to road users. Summarizing, the main contributions of this dissertation are:

- Chapter 1: *Analytical Characterization of Device-to-Device and Cellular Networks Coexistence:* In chapter 1 a new analytical framework based on stochastic geometry for the characterization of the reciprocal impact of D2D communications and an underlay cellular network in terms of coverage probability is presented. I consider a random number of D2D groups where in each group devices are distributed according to different spatial distributions to model users' behavior. The effect of power control, users' spatial distribution, shadowing and random base station (BS) deployment are accounted for in the analysis and closed form expressions for coverage probability for both cellular network and D2D networks are derived. The validity of the framework developed is assessed via simulation in the numerical results where the effect of key system parameters as well as devices spatial distribution on cellular and D2D coverage is investigated and the amount of the traffic that could be offloaded through D2D communications is studied. Part of the materials (text, tables and illustrations) of this chapter have been published in [J1], [C1], [C2], © IEEE.

- Chapter 2: *Characterization of Link Lifetime in the Presence of Random Blocking Object-Part I:* In chapter 2 the statistical characterization of the link lifetime is addressed by introducing a new mathematical framework to model randomly deployed obstacles distributed according to Poisson point process (PPP) and user's mobility. I show that the link lifetime can be computed through a Markov chain model. In the numerical results the interplay of between obstacles' density, transmission range and user's speed is investigated for two different mobility models. Part of the materials (text, tables and illustrations) of this chapter have been submitted for publication in [J2], © IEEE.

- Chapter 3: *Characterization of Link Lifetime in the Presence of Random Blocking Object-Part II:* In chapter 3 I extend the model that I proposed in chapter 2 where the size of obstacles are taken into account. I derive an analytical framework to characterize the statistics of the link lifetime of a moving user in the presence of random obstacles

with different sizes for two different mobility models. Using statistical geometry arguments, closed-forms of the cumulative distribution function and the average link lifetime are obtained as a function of the distance, user's speed and direction, obstacles' density and size. The analytical framework is validated through simulations and allows to get insights on the impact of system parameters on the link lifetime. Part of the materials (text, tables and illustrations) of this chapter have been submitted for publication in [J3], and [C3] © IEEE.

- Chapter4:*Device-to-Device (D2D) communication and localization for road users:* In chapter 4, an ultrawide-band localization system and high-level architectures to improve the cyclists' safety are presented. They consist of tags placed on bikes, whose positions have to be estimated, and anchors, acting as reference nodes, located at intersections and/or on vehicles. The peculiarities of the localization system in terms of accuracy and cost enable its adoption in enhanced risk assessment systems situated on the infrastructure/vehicle, depending on the architecture chosen, as well as real-time warning to road users. Part of the materials (text, tables and illustrations) of this chapter have been submitted for publication in [J4] © IEEE.

Author's Contributions

The PhD activity has been conducted at the Department of Electrical, Electronic, and Information Engineering "Guglielmo Marconi" at University of Bologna (UNIBO) Italy for about three years.

During the work at University of Bologna, three different activities have been conducted. First, the analytical model for coverage characterization to scenarios involving D2D links sharing the same frequency resources of an underlay cellular network is developed. Secondly, a new analytical framework to characterize the statistics of the link lifetime of a moving user in the presence of random obstacles with different sizes for different mobility models are derived. for both activities stochastic geometry are used and the performance assessment are obtained through a mix of analytical and simulation tools. Chapter 1 shows the results of analytical characterization of coverage probability whereas the results that show the characterization of link lifetime of dynamic mobility models are presented in Chapters 2 and 3 .

A third activity is experimental. Here a localization and communication system based on the ultra-wideband (UWB) technology and high-level architectures to improve the cyclists' safety are proposed. This work has been carried on in collaboration with the Tutor Prof.Davide Dardari, Nicoló Decarli and Anna Guerra. This project is funded by the Horizon 2020 project Xcycle of the European Union which aims to develop technologies improving detection of cyclists, systems informing both drivers and cyclists of an hazard at junctions, effective methods of presenting information in vehicles and on-site and cooperation systems aimed at reducing collisions with cyclists.

Within this project I participated to meetings, contributed to the writing of Deliverables, cooperated with other researchers at European level, and

carried out experimental activity.

Finally, The research activity led to the publication of 1 accepted journal paper, 1 minor revision and 2 under submission. In addition, 3 conference papers are accepted.

Introduction

Thesis motivations

In the last few years, user data traffic and the corresponding cellular network load are increasing exponentially [1]. Most of this growth is being generated in indoor environments where service coverage is more critical and new heterogenous networks (HetNets), comprising a mix of small and large overlapped cells, are being considered [2].
One of the most promising solution to offload data traffic of cellular networks is given by D2D communications underlaid cellular networks. D2D communications have been recently proposed to increase spectral efficiency, improve service coverage, and reduce handset power consumption [3]. They take advantage of the physical proximity of devices by enabling direct links between them [3, 4] and allow for extremely high bit rates, low delays, and low power consumption. It is expected that, besides ad hoc designed standards such as Zigbee, Wi-Fi and cellular, D2D networks will result particularly attractive thanks to the worldwide availability of wireless infrastructures. However, the perspective to have trillions of seamless connected objects poses several technical challenges in the choice and design of D2D networks. Differently from the traditional cellular architecture, to fully realize their potential advantages, D2D networks require new peer discovery methods, physical and MAC layer procedures as well as radio resource management algorithms, which make their design and adoption still an open issue.

Despite the large expected benefits in terms of capacity, the coexistence of D2D and cellular networks in the same spectrum creates new challenges

in interference management [3]. In fact, interference and propagation effects are the main factors impacting the cellular network capacity. These factors are highly dependent on network topology and devices spatial distribution. Starting from these considerations the following research lines have been identified and investigated:

a) Need for a general analytical model for the characterization of the mutual interference between heterogeneous networks.

b) Inclusion of shadowing propagation effects into the coexistence characterization.

c) Evaluation of the impact of power control strategies.

d) Characterization of the coverage probability in D2D and cellular networks to understand how much traffic can be off-loaded.

e) Characterization of the link lifetime in the presence of obstacles.

Interference Characterization in Heterogeneous Networks

The availability of analytical models for the characterization of the mutual interference is fundamental to gain a full insight on the key parameters affecting the cellular network performance. In this perspective, stochastic geometry is a better suited mathematical tool in scenarios where devices are randomly deployed. One of the simplest process and most interesting to model devices' random position is the so called Poisson Point Process (PPP). The PPP is widely used to model random "points" in time and space. PPP may be homogeneous and non-homogeneous. In homogeneous Poisson point process (HPPP) a random number of points distributed randomly and uniformly in any given set and it is described by a single parameter called the intensity (number of points per unit area). Further, it considers that the number of points falling in two disjoint sets are independent random variables whereas, the points in non-homogeneous PPP (NHPPP) are not uniformly distributed and they are distributed according to the intensity function of the process.

In this thesis, I use PPP as a reference model for the distribution of BSs,

Blockages, and D2D devices in which I consider the deployment of BSs and Blockages according to HPPP with density ρ_{BS} and ρ_B, respectively. Instead, in D2D networks I consider a random number of D2D groups in which D2D are characterized by HPPP spatial distribution with density ρ_{D2D}, where within each group devices are distributed according to a general spatial distribution (HPPP and NHPPP) to model user's behavior.

Shadowing Propagation Effects

For a downlink cellular scenario, each base station serves a mobile stations (MS) using the same radio resource. The power coming from the serving BS will often encounters a lot of obstacles, such as building, tree, animals, etc. The radio will be reflected, difracted and scattered by these obstacles. Further, the received power varies as the distance between transmitter and receiver changes. One finds several effects appearing: path loss, shadowing and fading.

According to author's knowledge there are several papers in stochastic geometry related to D2D communications focusing on the uplink scenario and a few papers focusing on the downlink scenario. Most of them account only for fast fading and neglect the effect of shadowing [19]-[22]. In addition, it is well-known that the effect of the shadowing is significant and should not be neglected in the cellular network [33]. Further, the results shown in [34] illustrate that the log-normal distribution seems to better describe the interference probability density function (p.d.f.). It is worthwhile to remark that only shadowing (slow fading) concurs in determining the coverage in wireless networks as fast fading is typically averaged out by the coding and/or diversity scheme employed in the demodulation process and accounted for in the SINR threshold η. In our models I consider the effect of the log-normal shadowing which is a model commonly used in the cellular network to describe large-scale fluctuations of the signal and interference strength [5]. In other words, the shadow loss represents the actual local-mean power received, statistically fluctuating about the area-mean power. I use a log-normal distribution to characterize the changing of local mean power.

Power Control

Power control is an effective approach to mitigate interference in cellular networks; it is widely used in current cellular system. In this thesis, I propose power control method for interference coordination and analyze their performance in both cellular and D2D networks. In particular, I consider (decentralized) power control against the joint effect of path loss and shadowing. In the absence of power control the received signal of a MS near a BS would be much stronger than a signal received from a MS far away. In this case, near far problem would occur. Therefore, in cellular systems power control is always applied.

On the other hand, for D2D links I consider both the above strategy and one in which the transmitted power is kept constant (no power control) to evaluate the impact of power control on the coxesistence between D2D links and a cellular network.

Coverage Probability

Coverage probability of small cells is a very important index of the system performance since small cells deployment will dominate the topology in the next generation cellular networks. Coverage probability is defined as the probability that the signal-to-interference plus noise ratio (SINR) of a user in a cell is higher than some trarget SINRs. The majority of prior works on coverage probability focuses on the anlysis of outage probability or sucess probability. For instance, in [6] the authors provide an overview of how a PPP is successfully applied to make the analysis of outage probability tractable under some random access protocols. In [5] the authors proposed an analytical model based on a PPP to characterize a more realistic distribution of BSs in the network. Simple path loss and Rayleigh fading models are used to obtain some tractable results of the coverage probability and achievable rate. However, they only obtain the "worse-case" results that would detach far away from the reality. In [7] the average rate of downlink heterogeneous cellular networks with a general fading assumption is found. The analysis of

the coverage probability does not consider the shadowing.

Link Lifetime

Unfortunately coverage probability does not provide information about link blockages duration/rate as its evaluation usually does not include spatial/-time correlation of the link state. In this context, the link lifetime represents an important performance index able to properly capture the dynamic behavior of the wireless link. Link blockage can arise due to the presence of big obstacles, such as walls or cars in vehicular ad hoc networks, but also small obstacles like furniture and people in a crowded scenario might determine serious link blockages especially at mmW. Together with user's mobility, blockages due to obstacles may force frequent handovers between access points (APs) and consequent signaling overhead or connection drops, especially if narrow beamforming is performed as expected in future mmW wireless systems. This could have a strong impact especially on device-to-device or vehicular communications.

The aim of the second part of this thesis is to fill the gap in characterizing the link lifetime by proposing a new analytical framework (for dynamic mobility model) able to account for both users mobility and effects of blockages. In other words, I address for the first time, based on our best knowledge, the problem of characterizing the statistics of the link lifetime in the presence of random blocking objects. Specifically, I consider one of the most realistic scenario where I assume a mobile device moving along the straight line with constant speed. Further, a random number of obstacles located in random positions with different sizes is present. I derive closed-form expressions for the statistical distribution of link lifetime accounting for the shadowing effect caused by obstacles depending on their dimension and distance from the AP. In the numerical results I investigate the joint effect of the main system parameters such as the density and size of obstacles and the communication distance, from which network design guidelines can be easily obtained. Analytical results are compared with simulations with the purpose to assess their validity.

D2D communication and localization for road user safety improvement

Today several technologies are available for the direct communications between road users and localizationn capabilities to predict dangerous situations for cyclists. The choice of the proper technology requires a deep analysis of the most dangerous scenarios and situations and must account for several aspects in order to make it effective, reliable, user-friendly, and low-cost.

The performance of the implemented UWB-based tracking system has been experimentally characterized as discussed in chapter 4. The availability of accurate real-time tracking of road users opens the door to the introduction of advanced risk assessment (RA) units, both on vehicles and in the infrastructure (on-site), capable of predicting critical situations and providing a suitable feedback to the road user through ad-hoc human machine interfaces (HMIs). Moreover, it also enables the possibility of offering additional services to cyclists, such as enhancing the functionality of green waves by accounting for the amount of people approaching the traffic light.[1]

[1]These applications are currently being investigated in the Europe-funded project XCycle (http://www.xcycle-h2020.eu/).

Chapter 1

Analytical Characterization of Device-to-Device and Cellular Networks Coexistence

1.1 Introduction

1.1.1 Related Works

The trend towards heterogeneous networks in 4G and 5G systems characterized by different cell sizes, from macro to small, and partially overlapped coverages, has made inadequate classical analytical design tools based on the assumption of uniform hexagonal cells [8]. A prominent approach is stochastic geometry which is more accurate in modeling irregular deployment of BS and MS, and D2D links as well. Typically, nodes are assumed to be randomly deployed according to a HPPP.

Most of theoretical frameworks address only cellular networks without the presence of D2D links and a rich literature is available [5, 9–14]. In [5] the authors developed general models for coverage characterization in the presence of multi-cell SINR using stochastic geometry. They assume that the cellular network model consists of BS distributed according to a HPPP, and the MS according to some independent stationary point process. Each

MS is connected to the closest BS, and channel fading plus shadowing are considered. The mean rate and the coverage gain from static frequency reuse are evaluated. The extension to generalized fading channels and MIMO systems can be found in [11, 14]. In [9] a tractable, flexible and accurate model for k-tier downlink heterogenous cellular networks is developed to evaluate the probability of coverage per tier. The model considers that BS in the i-th tier and the mobiles are distributed according to a HPPP, and each tier has different transmit power levels and different SINRs requirements. Moreover, each MS is connected to the BS having the highest received SINR. Exponential fast fading but no shadowing is assumed. In [10] a closed form expression for the coverage probability of both macrocells and femtocells is obtained for downlink femtocell-tier with power control. The authors assume that the location of BS and femto base stations are modeled as HPPP, and each MS is connected to the closest BS. They include path loss and small scale fading, whereas the transmitted power of femto BS depends on different power control techniques. In [12] the downlink coverage probability under constraints on the transmitted power and BS density is studied.

To better fit the non-uniform deployment of BS in some urban scenarios, other spatial distributions have been introduced. Recently, several progresses have been obtained by applying stochastic geometry theory in modeling BS and MS irregular spatial distribution [6, 15–17]. In [15] the authors proposed accurate models for both macrocell and microcell based on Strauss point process and Matern cluster process (MCP), respectively. Specifically, In [16] the authors introduced a two tier heterogeneous cellular network model with intra-tier dependence, where macro BS and pico BS are deployed as HPPP and MCP, respectively. Their results show that the model appears closer to the real deployment than HPPP in same practical scenarios. In [17] the authors investigated the impact of different spatial processes. Specifically, they selected data from urban area and rural area separately, and verified that the capacity-centric BS deployment in urban areas can be modeled by a typical aggregative process such as the MCP, while the coverage centric BS deployment in rural areas can be modeled by representative repulsive processes such as the Strauss hard-core process.

The above mentioned papers do not consider D2D communications, and most of them account only for fast fading and neglect the shadowing. A few works address D2D communications from an analytical perspective and consider the deployment of D2D follows a HPPP [18] and NHPPP [19]. In [18] and [19] the border effects on the coverage probability of finite cellular network in presence D2D links are investigated. From simulation results it can be seen that the border effects become negligible when the radius of cellular network is at least 2-3 times the average cell radius since there are no significant changes on coverage probability. In [20] a simple power control scheme for the D2D communication underlaid cellular network in a single-cell is proposed, where the D2D transmit power is regulated to protect the existing cellular links. In [21] an analytical expression for coverage probability of D2D underlaid uplink cellular networks under power constraint is derived, by investigating both centralized and decentralized power control algorithms. In [22] resource allocation for D2D communication is addressed to maximize the overall network throughput, whereas in [23] a dynamic power control mechanism is proposed to reduce interference and improve the performance of cellular systems.

In [24] the authors present a resource allocation method for D2D communications underlay cellular networks to maximize the overall network throughput, while guaranteeing the quality-of-service requirements for both D2D and cellular users. In [25] a new power control scheme to improve the reliability of D2D communications is proposed. Again the location of D2D pairs is modeled as a HPPP. The optimum transmitted power is calculated for different D2D communication distances and different noise-variance levels. In [26] interference management for D2D communications underlay cellular networks at the cell edge is studied. Power control and resource allocation policies are introduced to reduce the mutual interference inside the interference-suppression-area which contains downlink and uplink parts. In [27] the authors propose a mechanism for spectrum allocation and mode selection for overlay D2D communications.

In all these papers the authors concentrate on the HPPP model which is quite unrealistic as D2D users tend to work in groups. Indeed they consider

only fast fading and neglect shadowing effects that are predominant when characterizing the coverage in cellular networks. At author's knowledge, no downlink analytical works modeling the reciprocal impact of D2D and cellular network are available.

1.1.2 Author's Contribution

In this chapter I investigate a cellular downlink scenario in the presence of underlay D2D links. A new analytical framework based on stochastic geometry to evaluate the coverage probability for both cellular network and D2D communication by properly characterizing the impact of interference from D2D links and other BSs is proposed. I consider a random number of D2D groups where D2D groups are characterized by a HPPP spatial distribution, whereas within each group devices are distributed according to a general spatial distribution (homogeneous and not) to model users' behavior. Some particular distributions are considered as examples in the numerical results but the analytical framework accounts for any spatial distribution, included those coming from experimental data. Both power control, compensating path loss and shadowing, and fixed power strategies for the D2D link are investigated. For infinite size cellular network I derive the closed form expressions for coverage probability for cellular and D2D networks. In the numerical results I study the amount of the traffic that could be offloaded through D2D communications and I use the proposed analytical framework model to investigate the reciprocal effect of D2D and cellular networks under different conditions in terms of devices' spatial distribution. Finally, I validate my analytical framework through simulations.

1.2 System Model

As shown in Figure 1.1, I consider a downlink cellular scenario where BS are distributed according to a HPPP with spatial density ρ_{BS} and each BS serves a MS using the same radio resource. In addition, a random number of groups of D2D users is present, where in each one only a D2D link is active

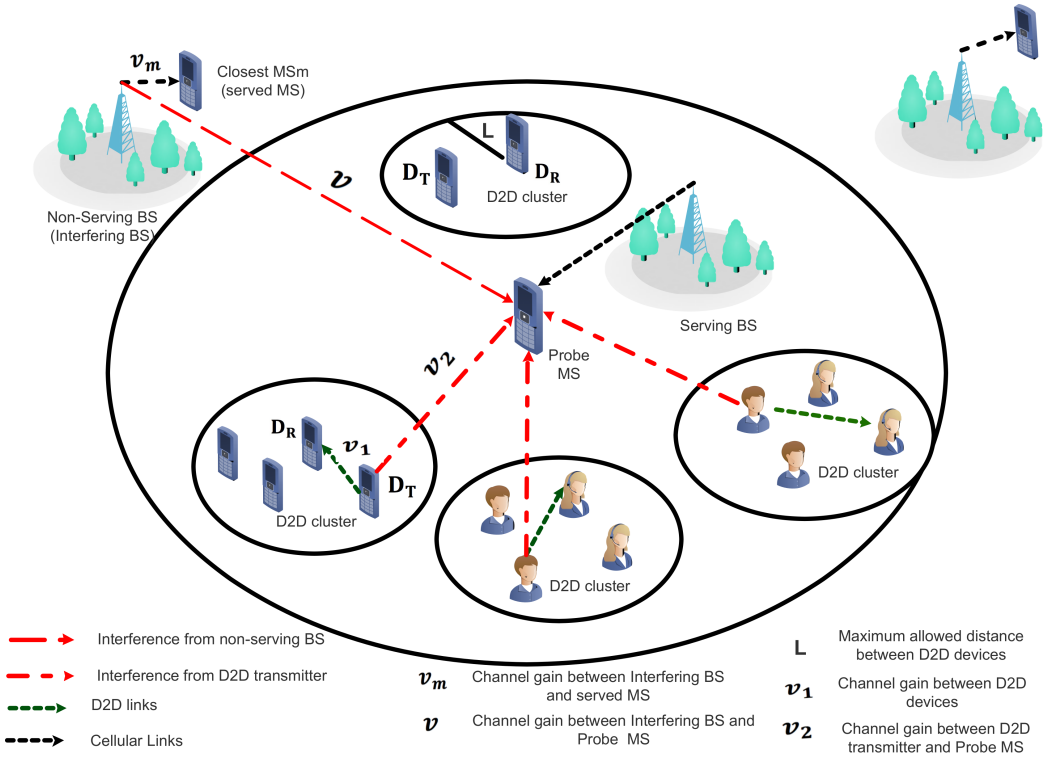

Figure 1.1: System model considered

at the same time sharing the same radio resource as that used by the cellular network as long as such use does not cause the SINR of the cellular link to fall below the required minimum SINR threshold η [28]. Denote with D_T and D_R the couple of active users communicating in the generic D2D group where, without loss of generality, D_T is the transmitter and D_R is the receiver. The D2D groups (links) are distributed according to a HPPP with density ρ_D.

To take properly into account the tendency of D2D users to work in groups, devices involved in each D2D group are supposed to be distributed according to different spatial models (uniform [29] and non-uniform [30] distributions). Here, I consider the following spatial distribution models for the distance between D_T and D_R that will be used in the numerical results even though the analytical framework applies to any spatial distribution, even obtained from experimental data.

- *Uniform spatial distribution*: I assume D_T is uniformly distributed

within a circle of radius L centered on D_R being L the maximum allowed communication distance between D2D devices. Actually, the distance between D2D device is not more than 100 meters [29, 31]. This is a conservative assumption motivated by the fact that at low SNR it is difficult for a D2D link to acquire beacon signals and discover other D2D devices [32].

The corresponding probability density function (p.d.f.) of the reciprocal distance r_1 is

$$f_{R_1}(r_1) = \frac{2\, r_1}{L^2}\,, \tag{1.1}$$

for $r_1 \in [0, L]$, zero otherwise.

- *Way-point spatial distribution*: I assume D_T is non-uniformly distributed around D_R according to the following distance distribution [33]

$$f_{R_1}(r_1) = \frac{1}{L^2}\left(\frac{-4\, r_1^3}{L^2} + 4\, r_1\right)\,, \tag{1.2}$$

for $r_1 \in [0, L]$, zero otherwise.

- *Exponential spatial distribution*: I assume D_T is non-uniformly distributed around D_R according to the following exponential distance distribution

$$f_{R_1}(r_1) = \alpha \exp\left(-\alpha\, r_1\right)\,, \tag{1.3}$$

where $r_1 \in [0, \infty)$ and α is the distribution rate [34].

From the above mentioned distribution models, which are examples taken from literature, it can be noted that the uniform one can be used when no priori knowledge on user spatial distribution is available whereas the other two models (Way-point and Exponential models) correspond to devices concentrated around the receiver thus resulting in a NHPPP spatial distribution

of D2D nodes in each group. The exponential nature of the contact distribution implies that the process is memoryless in nature.

Further, a model based on the exponential distribution can be of great importance to provide an insight into the mobile nodes arrival pattern [35,36] whereas, the other distribution (way-point model [37]) considers nodes more concentrated in the middle than at the border of the D2D group. In this chapter, these distributions will be considered as examples in the numerical results, even though the analytical framework here proposed is more general and can account for any spatial distribution, even obtained from experimental data. It will be demonstrated that the only parameter affecting the coverage is the second moment of the spatial distribution regardless its shape.

1.2.1 Coverage Probability on Cellular Downlink

I am interested in investigating the joint effect of the interference coming from the surrounding BS and the D2D links on the downlink coverage probability. The coverage is related to the SINR at the probe MS which is given by

$$\mathsf{SINR} = \frac{P_{\mathrm{u}}}{\sum_{i=0}^{n} P_i + \sum_{j=0}^{m} P_{\mathrm{j}}^{(d)} + \sigma_0^2}\,, \tag{1.4}$$

where P_u is the power received from the serving BS, P_i is the power of the interference coming from the ith non-serving BS, $P_{\mathrm{j}}^{(d)}$ is the power of the interference from the jth D2D link, n and m are the (random) number of interfering BS and D2D, respectively, and σ_0^2 is the thermal noise power. Even though quality-based power control strategies typically guarantee better performance [30], their analytical characterization is prohibitive. Moreover, most of them require a significant signaling between devices which could be not feasible when considering heterogeneous networks. Therefore, I consider, as conservative approach a power control strategy [21], [38] and [39] which purpose is to keep the signal-to-noise ratio (SNR) constant against the joint effect of path loss and shadowing so that P_{u} results constant regardless the distance and channel conditions.

Moreover, for D2D links I consider both the above strategy and one in

which the transmitted power is kept constant (no power control) to evaluate the impact of power control on the coxesistence between D2D links and a cellular network. It is worthwhile to remark that under particular channel conditions the transmitted power level necessary to compensate scarce path loss events would end up to be unrealistically high. In practice this situation is avoided by setting a saturation level in the power amplifier. Depending on results in [40] it can be noted that there is a slight difference when considering saturation with respect to unbounded power in terms of coverage and for mathematical convenience, I do not consider power saturation being aware that the probability of the saturation events is very low. As a consequence, in (1.4) only the interfering terms P_i, and $P_{\mathrm{j}}^{(d)}$ are random variables (RVs) in addition to n and m.[1] The probability of coverage of the cellular network is given by

$$\begin{aligned} P_c =& \text{Prob}\left(\mathsf{SINR} > \eta\right) = \text{Prob}\left(\sum_{i=0}^{n} P_i + \sum_{j=0}^{m} P_{\mathrm{j}}^{(d)} < \gamma\right) \\ =& \text{Prob}\left(10\log_{10}\left(\sum_{i=0}^{n} 10^{P_i(\mathrm{dBm})/10} + \sum_{j=0}^{m} 10^{P_{\mathrm{j}}^{(d)}(\mathrm{dBm})/10}\right) < 10\log_{10}\gamma\right) \\ \approx& \text{Prob}\left(\max_{i,j}\left(P_i\left(\mathrm{dBm}\right), P_j^{(d)}\left(\mathrm{dBm}\right)\right) < 10\log_{10}\gamma\right), \end{aligned} \tag{1.5}$$

with

$$\gamma = P_{\mathrm{u}}/\eta - \sigma_0^2 = P_{\mathrm{u}}\left(\frac{1}{\eta} - \frac{1}{\eta_0}\right), \tag{1.6}$$

where η is the target SINR and η_0 is the target SNR at the cell boundary in the absence of interference. In (1.5) I exploited the approximation $\ln(\sum_{i=0}^{n}\exp(a_i) + \sum_{j=0}^{m}\exp(b_j)) \approx \max_{i,j}(a_i, b_j)$ [41]. The accuracy of the approximation in (1.5) will be assessed in the numerical results through simulation.

For analysis convenience, I start considering a finite circular area of radius R_0 centered at the probe MS, then we will take the limit for R_0 to infinity

[1] Their randomness is caused by the joint effect of the random position of BS and MS, shadowing, and power control at the interfering nodes, when present.

in order to account for an infinite plane.
In the circular area R_0 the number n and m of interferes for the probe MS are Poisson distributed RVs with mean $\rho_{\mathrm{BS}}\pi R_0^2$, and $\rho_{\mathrm{D}}\pi R_0^2$, respectively. Moreover, the random number of D2D links is Poisson distributed with mean $\rho_{\mathrm{D}}\pi R_0^2$ and the generic transmitter D_T is uniformly distributed in the circle. Since $\{P_i\}$s, and $\left\{P_j^{(d)}\right\}$s have the same statistical characterization then the coverage probability with the limited circular area is given by

$$\begin{aligned} P_{c_0} = \mathbb{E}[P_{c_0}|_{n,m}] &= \sum_{m=0}^{\infty}\sum_{n=0}^{\infty} P_{c_0}|_{n,m} \frac{(\rho_{\mathrm{BS}}\pi R_0^2)^n}{n!}\frac{(\rho_{\mathrm{D}}\pi R_0^2)^m}{m!}\exp\left(-(\rho_{\mathrm{BS}}+\rho_{\mathrm{D}})\pi R_0^2\right) \\ &= \exp\left(-\rho_{\mathrm{D}}\pi R_0^2(1-F_{\mathrm{D}}(\gamma)) - \rho_{\mathrm{BS}}\pi R_0^2(1-F_{\mathrm{I}}(\gamma))\right)\,, \end{aligned} \tag{1.7}$$

with

$$P_{c_0}|_{n,m} = F_{\mathrm{I}}^n(\gamma)\, F_{\mathrm{D}}^m(\gamma) \tag{1.8}$$

$$F_{\mathrm{I}}(\gamma) = \mathrm{Prob}\left(P_i < \gamma\right) \qquad \forall\, i = 0, 1, \ldots n \tag{1.9}$$

$$F_{\mathrm{D}}(\gamma) = \mathrm{Prob}\left(P_{\mathrm{j}}^{(d)} < \gamma\right) \qquad \forall\, j = 0, 1, \ldots m\,. \tag{1.10}$$

Denote with

$$\lambda_{\mathrm{BS}_0}(\gamma) = \rho_{\mathrm{BS}}\pi R_0^2(1-F_{\mathrm{I}}(\gamma))\,, \tag{1.11}$$

and

$$\lambda_{\mathrm{D}_0}(\gamma) = \rho_{\mathrm{D}}\pi R_0^2(1-F_{\mathrm{D}}(\gamma))\,, \tag{1.12}$$

where (1.11) and (1.12) represent, respectively, the average number of BS in R_0 providing an interference contribution to the probe MS such that $P_i(\mathrm{dBm}) \geq \gamma$ and the average number of D2D links in R_0 providing an interference contribution to the probe MS such that $P_j^{(d)}(\mathrm{dBm}) \geq \gamma$. In order to compute (1.5), here I am interested in finding closed-form expressions for $\lambda_{\mathrm{BS}_0}(\gamma)$ and $\lambda_{\mathrm{D}_0}(\gamma)$ when $R_0 \to \infty$, in particular

$$\lambda_{\mathrm{BS}}(\gamma) = \lim_{R_0\to\infty} \lambda_{\mathrm{BS}_0}(\gamma)\,. \tag{1.13}$$

and

$$\lambda_{\mathrm{D}}(\gamma) = \lim_{R_0 \to \infty} \lambda_{\mathrm{D}_0}(\gamma)\,, \tag{1.14}$$

By considering (1.14), (1.13) and (1.7) the coverage probability in (1.5) can be obtained as

$$P_c = \lim_{R_0 \to \infty} P_{c_0} = \exp\left(\lambda_{\mathrm{BS}}(\gamma)\right) \exp\left(\lambda_{\mathrm{D}}(\gamma)\right)\,. \tag{1.15}$$

1.2.2 Coverage Probability on D2D Links

The same approach can be used to characterize the effect of the cellular network and other D2D groups on a probe D2D communication in terms of coverage probability. This can be done by considering the D2D receiver D_R as the probe receiver and by referring all quantities to it. Therefore the SINR at the probe D2D device is given by

$$\mathsf{SINR}^{(\mathrm{d})} = \frac{P_{\mathrm{u}}^{(\mathrm{d})}}{\sum_{i=0}^{n} P_i + \sum_{j=0}^{m} P_{\mathrm{j}}^{(d)} + \sigma_0^2}\,, \tag{1.16}$$

where now P_i and $P_{\mathrm{j}}^{(d)}$ are, respectively, the power of the interference coming from the ith non-serving BS and the power of the interference coming from the jth D2D link impinging the D2D probe receiver D_R.
Following the same method as in the previous section, the D2D coverage probability considering a finite circular area of radius R_0 centered at the probe receiver is

$$\begin{aligned} P_{c_0}^{(\mathrm{d})} &= \mathrm{Prob}\left(\mathsf{SINR}^{(\mathrm{d})} > \eta^{(d)}\right) \\ &= \exp\left(-\rho_{\mathrm{D}}\pi R_0^2 \left(1 - F_{\mathrm{D}}\left(\gamma^{(\mathrm{d})}\right)\right) - \rho_{\mathrm{BS}}\pi R_0^2 \left(1 - F_{\mathrm{I}}\left(\gamma^{(\mathrm{d})}\right)\right)\right)\,, \end{aligned} \tag{1.17}$$

with $F_{\mathrm{I}}(\gamma)$ and $F_{\mathrm{D}}(\gamma)$ given by (1.9) and (1.10), respectively, and

$$\gamma^{(\mathrm{d})} = P_{\mathrm{u}}^{(\mathrm{d})} \left(\frac{1}{\eta^{(d)}} - \frac{1}{\eta_0^{(d)}}\right)\,, \tag{1.18}$$

being $P_{\mathrm{u}}^{(\mathrm{d})}$ the useful power received by D_R (kept constant by the power control strategy.)
In the same way the D2D coverage probability under the condition $R_0 \to \infty$ is given by

$$P_c^{(\mathrm{d})} = \exp\left(\lambda_{BS}(\gamma^{(\mathrm{d})})\right) \exp\left(\lambda_D(\gamma^{(\mathrm{d})})\right) . \tag{1.19}$$

The characterization of (1.15) and (1.19) requires the derivation of the functions $\lambda_{BS}(\gamma)$ and $\lambda_D(\gamma)$. This will be done in the next section after having introduced a proper channel model describing the effect of path loss and shadowing.

1.3 Analytical Characterization of the Channel Model

In this section I derive the statistics of the power gain of all wireless links involved in the scenario considered with the purpose to obtain a full characterization of the interference impinging the probe MS and D2D receivers.
Let us introduce the widely-used channel gain model (in dB) of the generic wireless link

$$z = k_0 - 10\beta \log_{10}(r) + \xi \,, \tag{1.20}$$

where k_0 is the channel gain at the reference distance of 1 meter, β is the path loss exponent, r is the distance between the involved devices, and ξ is a zero mean Gaussian RV with standard deviation σ modeling the log-normal shadowing [42].
Denote with

$$\nu = k_0 - 10\beta \log_{10}(r) \,, \tag{1.21}$$

the average channel gain with respect to the log-normal shadowing depending only on the path loss. As well-known from the literature, the effect of shadowing is significant and should not be neglected when characterizing the probability of coverage in cellular network [43]. Further, the results shown in [44] illustrate that the log-normal distribution seems to be better describe

of the interference p.d.f. Therefore, in our model I consider the effect of the log-normal shadowing which is a model commonly used in the cellular network to describe large-scale fluctuations of the signal and interference strength [6]. It is worthwhile to remark that only shadowing (slow fading) concurs in determining the coverage in wireless networks as fast fading is typically averaged out by the coding and/or diversity scheme employed in the demodulation process and accounted for in the SINR threshold η. In this thesis, fast fading has not been included, even though several papers consider it and neglect the shadowing for mathematical convenience.

1.3.1 Channel Gain Statistics with Uniform Nodes Distribution

Consider a node randomly located within a disk of radius R_0 centered in the origin with uniform distribution. Then the p.d.f. of its distance r from the origin is given by

$$f_R(r) = \frac{2\,r}{R_0^2}\,, \tag{1.22}$$

for $r \in [0, R_0]$, zero otherwise.
By means of the transform method of RVs, from (1.21) and (3.3) the p.d.f. and cumulative distribution function (CDF) of the average channel gain ν are, respectively,

$$f_V(\nu) = \frac{\log(10)10^{\left(\frac{-(\nu-k_0)}{5\beta}\right)}}{5\,\beta\,R_0^2} \qquad F_V(\nu) = 1 - R_0^{-2}10^{\frac{-(\nu-k_0)}{5\,\beta}}\,, \tag{1.23}$$

for $\nu \in [k_0 - 10\beta\log_{10}(R_0), \infty)$, and zero otherwise
The p.d.f. of the channel gain $z = \nu + \xi$, which includes also the shadowing, can be derived as

$$f_Z(z) = f_V(z) \otimes f_\xi(z)\,, \tag{1.24}$$

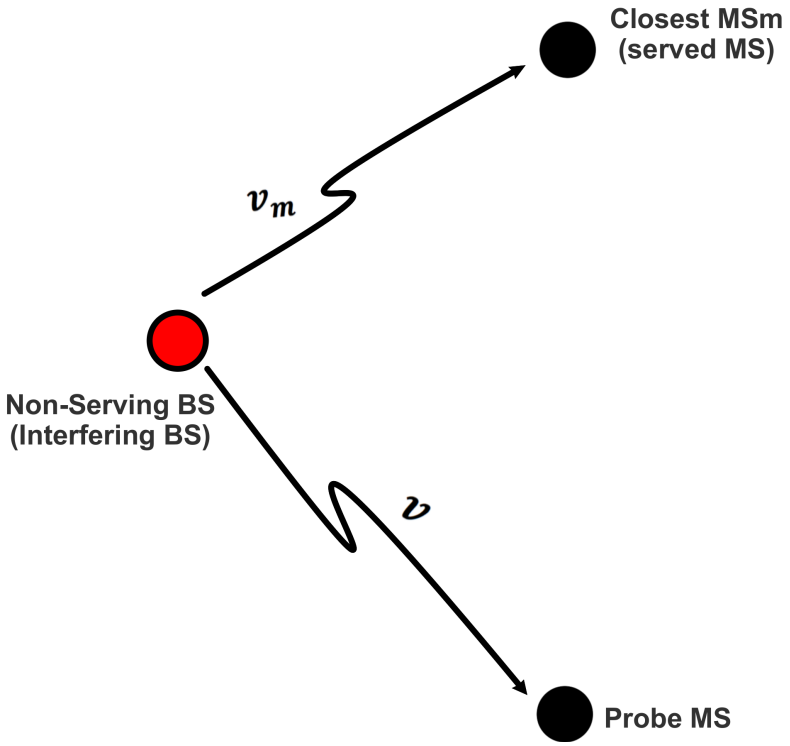

Figure 1.2: Generic interfering BS and served MS.

where $f_\xi(z)$ is the Gaussian p.d.f. with zero mean and variance σ^2, resulting in

$$f_Z(z) = c(z; R_0)\,\sigma\sqrt{\pi}\exp\left(\sigma^2\left(\frac{\log(10)}{5\beta} - \frac{z}{\sigma^2}\right)^2\right) \times \left(1 - \frac{1}{2}\text{erfc}\left(\left(\frac{\log(10)}{5\beta} - \frac{z}{\sigma^2}\right)\frac{\sigma}{\sqrt{2}}\right)\right), \tag{1.25}$$

with $\text{erfc}(\cdot)$ being the complementary error function and

$$c(z; R_0) = \frac{\log(10)}{5\beta R_0^2}\exp\left(\frac{k_0\log(10)}{5\beta} - \frac{z^2}{2\sigma^2}\right) \tag{1.26}$$

defined in $(-\infty, \infty)$.

1.3.2 Channel Gain Statistics from Serving BS

Consider a generic MS and denote with r_i, $i = 1, 2, \ldots, \infty$, the corresponding distances from the surrounding BS. Recalling that BS are spatially distributed according to a HPPP with density ρ_{BS}, the number n of the surrounding BS in a circle of radius R_0 and centered on the MS is Poisson distributed with mean $\rho_{\mathrm{BS}}\,\pi\,R_0^2$ conditioned to the presence of at least one MS. I denote with ν_m the average channel gain with respect to the closest BS which is supposed to be also the serving one (see Figure 1.2). The corresponding p.d.f. is

$$\begin{aligned} f_{V_m}(\nu_m) =& \sum_{N=1}^{\infty} \mathrm{P}\left\{n = N | n \geq 1\right\} N\, F_V(\nu_m)^{N-1} f_V(\nu_m) \\ =& \sum_{N=1}^{\infty} \frac{(\rho_{\mathrm{BS}}\pi R_0^2)^N \exp\left(-\rho_{\mathrm{BS}}\pi R_0^2\right)}{N!\,\left(1-\exp(-\rho_{\mathrm{BS}}\pi R_0^2)\right)} N F_V(\nu_m)^{N-1} f_V(\nu_m) \\ =& \frac{\rho_{\mathrm{BS}}\pi \log(10)}{5\beta} 10^{-\frac{(\nu_m - k_0)}{5\beta}} \sum_{N=0}^{\infty} \frac{\left[-\rho_{\mathrm{BS}}\pi 10^{-\frac{(\nu_m-k_0)}{5\beta}}\right]^N}{N!\,\left(1-\exp(-\rho_{\mathrm{BS}}\pi R_0^2)\right)} \\ =& \frac{\rho_{\mathrm{BS}}\pi \log(10)}{5\beta\,\left(1-\exp(-\rho_{\mathrm{BS}}\pi R_0^2)\right)} 10^{-\frac{(\nu_m - k_0)}{5\beta}} \exp\left(-\rho_{\mathrm{BS}}\pi 10^{-\frac{(\nu_m-k_0)}{5\beta}}\right), \end{aligned} \tag{1.27}$$

for $\nu_m \in [k_0 - 10\beta \log_{10}(R_0), \infty)$, and zero otherwise.

Note that the approach in (1.27) is not exact because the serving BS is in general the closest one conditioned it belongs to the same Voronoi cell as the MS. However in [45] it is shown that the problem can be overcome by considering the unconditional closest BS with an overestimated ρ_{BS} by a factor 1.25.

1.3.3 Statistics of the Interference from Non-serving BS

With reference to Figure 1.2, I evaluate the p.d.f. of the channel gain averaged with respect to the log-normal shadowing regarding the generic interfering

BS and the probe MS. A part from a constant term, the *effective* average channel gain is $x = \nu - \nu_m$, including the effect of power control affecting v_m, where the p.d.f.s of ν and ν_m are given respectively by (1.23) and (1.27). Here I am considering that the transmitted power of the interfering BS is inversely proportional to the average gain ($-\nu_m$ in dB) of the channel between the BS and its serving MS as a result of the power control policy aimed at keeping the received power fixed to the target value P_{u}. From Appendix A we have

$$f_X(x) = \frac{\rho_{\mathrm{BS}}\pi R_0^2 \log(10)}{5\beta\ (1-\exp(-\rho_{\mathrm{BS}}\pi R_0^2))} 10^{\frac{x}{5\beta}} \frac{1+(A(x)-1)e^{A(x)}}{A(x)^2} \tag{1.28}$$

having defined $A(x) = -\rho_{\mathrm{BS}}\pi R_0^2 10^{\frac{x}{5\beta}}$ for $x \in (-\infty, \infty)$.
To account also for the presence of the log-normal shadowing in both links (interfering BS-served MS and interfering BS-probe MS) we have to sum a Gaussian RV ξ_2 with zero mean and double variance $2\sigma^2$ (the sum of the two Gaussian RVs). Denote with $y = x + \xi_2$ the effective channel gain between the generic interfering BS and the probe MS and with $f_{\xi_2}(\xi)$ the p.d.f. of ξ_2. Now let us define the quantity

$$\Pi_{\mathrm{BS}}(y) = \lim_{R_0 \to \infty} \rho_{\mathrm{BS}}\pi R_0^2 \left(1 - F_y(y)\right) , \tag{1.29}$$

where the CDF of RV y is derived in Appendix A. Then (1.29) is given by

$$\Pi_{BS}(y) = 10^{-\frac{y}{5\beta}} 10^{\frac{\log(10)\sigma^2}{(5\beta)^2}} . \tag{1.30}$$

It can be noted that we can write the explicit expression of $\lambda_{\mathrm{BS}}(\gamma)$ in (1.13) as

$$\lambda_{\mathrm{BS}}(\gamma) = \Pi_{\mathrm{BS}}(10\log_{10}(\gamma/P_{\mathrm{u}})) . \tag{1.31}$$

1.3.4 D2D Channel Gain Statistics

With reference to Figure 1.3, denote with

$$\nu_1 = k_0 - 10\beta\log_{10}(r_1) \tag{1.32}$$

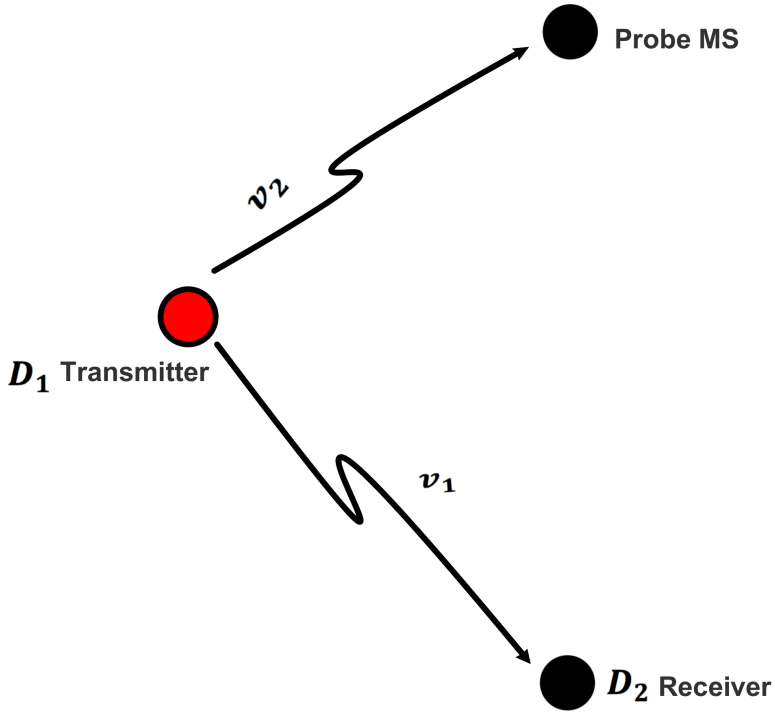

Figure 1.3: Generic interfering D2D devices.

the (average) channel gain between D_T and D_R of the generic D2D link. Define the quantity

$$\int_0^\infty \pi {r_1}^2 f_{R_1}(r_1) dr_1 = \delta^2 \,, \tag{1.33}$$

where $f_{R_1}(r_1)$ is a general distribution function for D2D link that could be obtained from experimental data.

By means of the transform method of RVs, from (1.32) and general distribution function $f_{R_1}(r_1)$, the p.d.f. of the average channel gain v_1 is given by

$$\begin{aligned} f_{V_1}(v_1) &= |\frac{dr_1}{d\nu_1}| f_{R_1}(r_1(v_1)) \\ &= \frac{\log(10)}{10\beta} 10^{-\frac{v_1 - k_0}{10\beta}} f_{R_1}(r_1(v_1)) \end{aligned} \tag{1.34}$$

defined in $(-\infty, \infty)$.

In the following, by using (1.34) we derive the average channel gain ν_1 for

the three models of devices' spatial distribution introduced in Sec. 3.2.

Uniform Spatial Distribution

From (1.1) and (1.34) the p.d.f. and CDF of the average channel gain ν_1 are, respectively,

$$f_{V_1}(\nu_1) = \frac{\log(10)10^{\left(\frac{-(\nu_1-k_0)}{5\beta}\right)}}{5\,\beta\,L^2} \qquad F_{V_1}(\nu_1) = 1 - L^{-2}10^{\frac{-(\nu_1-k_0)}{5\,\beta}}\,, \tag{1.35}$$

for $\nu_1 \in [k_0 - 10\beta\log_{10}(L), \infty)$, and zero otherwise
The p.d.f. of the channel gain $z_1 = \nu_1 + \xi$, which includes also the shadowing, can be derived as

$$f_{Z_1}(z_1) = f_{V_1}(z_1) \otimes f_{\xi}(z_1)\,, \tag{1.36}$$

where $f_{\xi}(z_1)$ is the Gaussian p.d.f. with zero mean and variance σ^2, resulting in

$$\begin{aligned} f_{Z_1}(z_1) =& c(z_1; L)\,\sigma\sqrt{\pi}\exp\left(\sigma^2\left(\frac{\log(10)}{5\beta} - \frac{z_1}{\sigma^2}\right)^2\right) \\ &\times\left(1 - \frac{1}{2}\mathrm{erfc}\left(\left(\frac{\log(10)}{5\beta} - \frac{z_1}{\sigma^2}\right)\frac{\sigma}{\sqrt{2}}\right)\right)\,, \end{aligned} \tag{1.37}$$

with $\mathrm{erfc}(\cdot)$ being the complementary error function and

$$c(z_1; L) = \frac{\log(10)}{5\beta L^2}\exp\left(\frac{k_0\log(10)}{5\beta} - \frac{z_1^2}{2\sigma^2}\right) \tag{1.38}$$

defined in $(-\infty, \infty)$.

Way-point Spatial Distribution

From (1.2) and (1.34) the p.d.f. and CDF of the average channel gain ν_1 are, respectively,

$$f_{V_1}(\nu_1) = \frac{-4\log(10)}{10\beta L^4} 10^{-4\left(\frac{\nu_1-k0}{10\beta}\right)} + \frac{4\log(10)}{10\beta L^2} 10^{-2\left(\frac{\nu_1-k0}{10\beta}\right)} \tag{1.39}$$

$$F_{V_1}(\nu_1) = 1 + \frac{1}{L^4} 10^{-2\left(\frac{\nu_1-k_0}{5\beta}\right)} - \frac{2}{L^2} 10^{\left(-\frac{\nu_1-k_0}{5\beta}\right)}, \tag{1.40}$$

for $\nu_1 \in [k_0 - 10\beta\log_{10}(L), \infty)$, and zero otherwise.
The p.d.f. of the channel gain $z_1 = \nu_1 + \xi$, which includes the shadowing, results

$$\begin{aligned} f_{Z_1}(z_1) =& \frac{-\log(10)}{5\beta L^4} 10^{\frac{2k_0}{5\beta}} \exp\left(-\frac{z_1^2}{2\sigma^2}\right) \\ & \times \operatorname{erfc}\left(\frac{k_0 - 10\beta\log_{10}(L)}{\sqrt{2}\sigma} - \frac{\sigma}{\sqrt{2}}\left(\frac{z_1}{\sigma^2} - \frac{2\log(10)}{5\beta}\right)\right) \\ & + \frac{\log(10)}{5\beta L^2} 10^{\frac{k_0}{5\beta}} \exp\left(-\frac{z_1^2}{2\sigma^2}\right) \\ & \times \operatorname{erfc}\left(\frac{k_0 - 10\beta\log_{10}(L)}{\sqrt{2}\sigma} - \frac{\sigma}{\sqrt{2}}\left(\frac{z_1}{\sigma^2} - \frac{\log(10)}{5\beta}\right)\right). \end{aligned} \tag{1.41}$$

Exponential Spatial Distribution

In this case the distance distribution is given by (1.3). From (1.3) and (1.34) the p.d.f. and CDF of the average channel gain ν_1 are

$$f_{V_1}(\nu_1) = \frac{\alpha\log(10)}{10\beta} 10^{-\frac{\nu_1-k_0}{10\beta}} \exp\left(-\alpha 10^{-\frac{\nu_1-k_0}{10\beta}}\right) \tag{1.42}$$

$$F_{V_1}(\nu_1) = \exp\left(-\alpha 10^{-\frac{\nu_1-k_0}{10\beta}}\right) \tag{1.43}$$

respectively, and defined in $(-\infty, \infty)$.
The p.d.f. of the channel gain $z_1 = \nu_1 + \xi$ is

$$f_{Z_1}(z_1) = c(z_1;\alpha) \sum_{k=0}^{\infty} \frac{\sqrt{2\pi}\sigma(-\rho\pi)^k}{k!} \exp\left(\left(\frac{\ln(10)}{5\beta} + \frac{\ln(10)k_0}{5\beta} - \frac{z_1}{\sigma^2}\right)^2 \frac{\sigma^2}{2}\right). \tag{1.44}$$

1.3.5 Statistics of the Interference from the D2D Link

The interference caused by the generic D2D link to the probe MS is due to D_T. For the integrated D2D communications scenario, I consider the following options:

- No power control scheme (NPC): with NPC, the transmit power of the D2D transmitter is set to some fixed value P (in dBm), then the effective average channel gain between the interfering D2D and probe MS is $x_d = v_2 - P$, where v_2 is the average channel gain between D_T and the probe MS having p.d.f. $f_{V_2}(\nu_2)$ given by (1.23) where $f_{V_2}(v_2) = f_V(v_2)$. The p.d.f. of $f_{X_d}(x_d)$ is similar to the p.d.f. $f_{V_2}(v_2)$ with a shift value P, so

$$f_{X_d}(x_d) = f_{V_2}(x_d - P)\,. \tag{1.45}$$

  The channel gain, including also the effect of shadowing in both involved links, is $y_d = x_d + \xi$, where ξ is a Gaussian RV with zero mean and variance σ^2.
  Define the quantity

$$\Pi_{\mathrm{D}}\left(y_d\right) = \lim_{R_0 \to \infty} \rho_D \pi R_0^2 (1 - F_D(y_d))\,, \tag{1.46}$$

  where the CDF of y_d derived in Appendix B. Then (1.46) is given by

$$\Pi_{\mathrm{D}}\left(y_d\right) = \frac{\rho_D \pi}{2} 10^{-\frac{y_d}{5\beta}} 10^{\frac{\log(10)\sigma^2}{(5\beta)^2} + \frac{\mathrm{Ko}+P}{5\beta}}\,. \tag{1.47}$$

- Power control scheme (PC) : In this case, I consider the average channel gain between the interfering D2D transmitter and the probe MS, including also this power control strategy in the D2D link, is $x_d = \nu_2 - \nu_1$, where ν_1 is the average channel gain between the D2D nodes with p.d.f. given by (1.34), depending on the spatial distribution model, and ν_2 is the average channel gain between D_T and the probe MS having p.d.f. $f_{V_2}(\nu_2)$ given by (1.23). The channel gain, including also the effect of shadowing in both involved links, is $y_d = x_d + \xi_2$, where ξ_2 is a Gaussian

RV with zero mean and variance $2\sigma^2$ in which the CDF of y_d is derived in Appendix C.

For the general spatial distribution case, the p.d.f. and CDF of y_d are derived in Appendix C and are given by

$$f_{Y_d}(y_d) = \frac{\delta^2}{\pi}\left(\frac{\log(10)}{5\beta R_0^2}\right) 10^{\frac{\log(10)\sigma^2}{(5\beta)^2}} 10^{\frac{-y_d}{10\beta}} . \tag{1.48}$$

and

$$F_{Y_d}(y_d) = 1 - \frac{2\delta^2}{\pi} 10^{\frac{\log(10)\sigma^2}{(5\beta)^2}} 10^{\frac{-y_d}{10\beta}} \tag{1.49}$$

defined in $(-\infty, \infty)$.
For the uniform, way-point, and exponential distributions $\delta^2 = \frac{\pi L^2}{2}$, $\frac{\pi L^2}{3}$ and $\frac{2\pi}{\alpha^2}$, respectively.
By substituting values of δ^2 in (1.49) and substituting the results in (1.46) then the quantity $\Pi_D(y)$ for uniform, way-point, and exponential distributions distributions can be obtained.

Finally, we can write the explicit expression for $\lambda_D(\gamma)$ in (1.14) as

$$\lambda_{\mathrm{D}}(\gamma) = \Pi_{\mathrm{D}}\left(10\log_{10}\left(\gamma/P_{\mathrm{u}}^{(d)}\right)\right) . \tag{1.50}$$

It can be noted that I analyze the case of constant power in the D2D links thus comparing the effect of interference caused by the power control strategy. In general it is true that some links suffering from deep fading might cause strong interference, but on average this might be compensated by the lower transmitted power caused by good links. In addition, It can be observed that the terms P_{u} and $P_{\mathrm{u}}^{(\mathrm{d})}$ defined in (1.31) and (1.50), respectively, account for the fact that the nominal transmitted power at each link is controlled in such a way at the D2D and MS receivers the average received power levels are set to the target values, respectively, P_{u}, and $P_{\mathrm{u}}^{(\mathrm{d})}$ at the maximum distance of interest, R_{m} (average cell radius) and L, respectively, for cellular and D2D links. This is done by setting the nominal transmitted power to

Table 1.1: Simulation Parameters

Parameter	value
Average cell radius R_m	500 m
channel gain at reference distance of 1 meter k_0	-38.5 dB
System Bandwidth	10 MHz
Carrier Frequency	2 GHz
path loss exponent β	4
Normalized received power at probe MS P_u	-116 dBm
Normalized received power at probe D2D receiver $P_u^{(d)}$	-78 dBm
BS density ρ_{BS}	30 BS/km^2
D2D groups density ρ_{D2D}	130 Links/km^2
shadowing spread for cellular network σ	7 dB
Target SNR at cell boundary η_0	10 dB
Target SNR at D2D boundary $\eta_0^{(d)}$	4 dB

$P_{\mathrm{t}}(\mathrm{dBm}) = P_{\mathrm{u}}(\mathrm{dBm}) - \nu$, where the average channel gain ν is evaluated through (1.23) with $r = R_{\mathrm{m}}$. Similarly for the D2D link. Finally, From (1.49) it can be noted that the analytical framework can be used to account for any spatial distribution, included those coming from experimental data.

1.4 Numerical Results

I validate my analytical framework model by Monte Carlo Simulation where 100,000 randomly generated scenarios were considered. With reference to the scenario shown in Figure 1.1, when not otherwise specified, I simulate 1000 m $\times$ 1000 m area where I consider a probe MS located at the center of the plane, and I assume number of BSs and D2D groups located around probe MS and distributed randomly according to PPP. Path-loss and log-normal shadowing are considered and the main simulation parameters are given in Table I. Analytical results have been obtained using the derived closed-form expressions (1.15) and (1.19), as well as the results in sec.1.3.

Figs. 1.4 and 1.5 show the effect of different spatial distributions on the cellular and D2D coverage probability, respectively. In particular, Fig.1.4 shows the coverage probability of the cellular network in the presence of

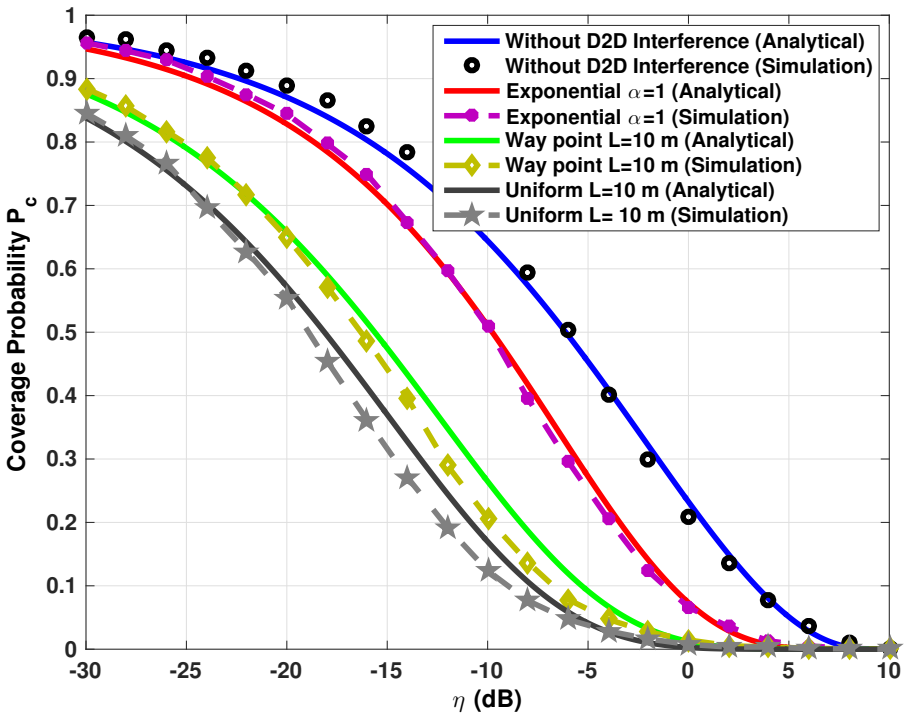

Figure 1.4: Impact of different D2D distributions on the cellular coverage probability.

self-interference and D2D interference, whereas Fig. 1.5 shows the coverage probability of D2D links in the presence of interference from the cellular network and other D2D links. It is evident how the spatial distribution of D2D devices could have a significant impact both on cellular and D2D coverage. This calls for accurate models well describing the actual behavior of D2D links. Given a particular model, also its parameters (e.g. L) might strongly affect the performance. For comparison, the different slope near $\eta = 10$ dB indicates that D2D links are less impaired from interference mainly because of the shorter distance between D2D nodes with respect to the distance between MS and BS. In addition, as can be noted the impact of D2D links can be important and must be properly taken into account when designing or during the operation of the cellular network. To this purpose, our analytical framework can be efficiently used to investigate the maximum

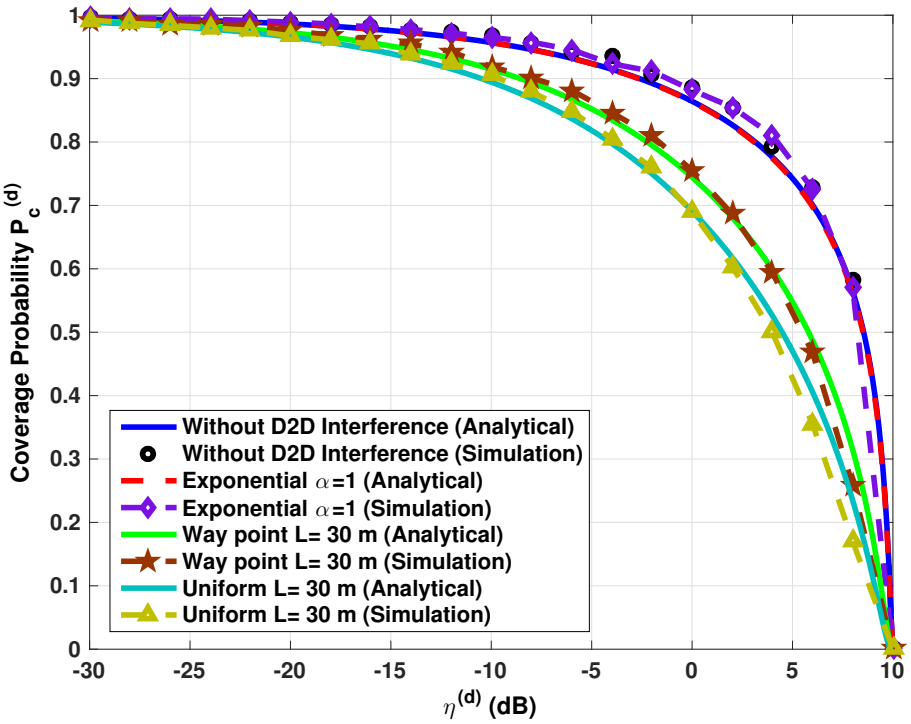

Figure 1.5: Impact of different D2D distributions on the D2D coverage probability.

allowable D2D link distance L, and hence the maximum transmitted power, given a target cellular network coverage. For example, in Fig. 1.6 we study the impact of the maximum D2D link distance L for different D2D densities ρ_{D} on the cellular coverage probability. From the results it can be seen that the coverage probability decreases with L and ρ_{D}. In fact, since the channel gain of the D2D link reduces when increasing L, on average more transmitted power is required for the D2D pair to guarantee the requirement on $P_{\mathrm{u}}^{(\mathrm{d})}$, thus causing higher interference to the probe MS. Similar considerations can be drawn from Fig. 1.7 where the impact of the interference on a probe D2D link is evaluated using (1.19). Results reported in Figs. 1.6 and 1.7 indicate that D2D links are less sensitive to interference than cellular links provided that their density is kept small. In particular, the maximum D2D distance L is typically much less than the distance from the interference. This is evident

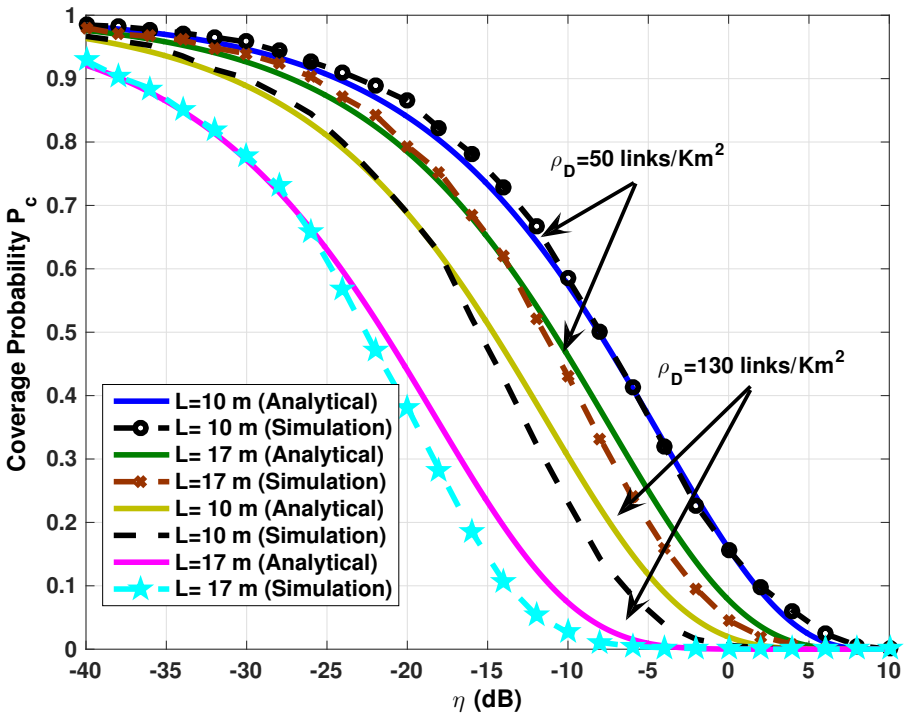

Figure 1.6: Impact of uniform D2D distribution on the cellular coverage probability.

in Fig. 7 in which higher robustness is obtained with lower L and D2D links density (less interference from D2D links). On the other hand, the density ρ_{D} of D2D groups has a strong impact on both links, especially if associated to large L.

In Figure 1.8 the effect of power control applied to D2D links on cellular coverage is investigated. As expected power control reduces the interference thus increasing the coverage probability even though the gain achieved of power control due to the short distance of D2D links.

Finally, the analytical framework is used to get engineering insights regarding the amount of traffic that can be offloaded from cellular network through D2D communications. Specifically, suppose a given density ρ of users has to be splitted between the cellular and D2D networks according to the distribution factor d. i.e, $\rho_{BS} = (1-d)\rho$ and $\rho_D = \rho d$ while mantaining

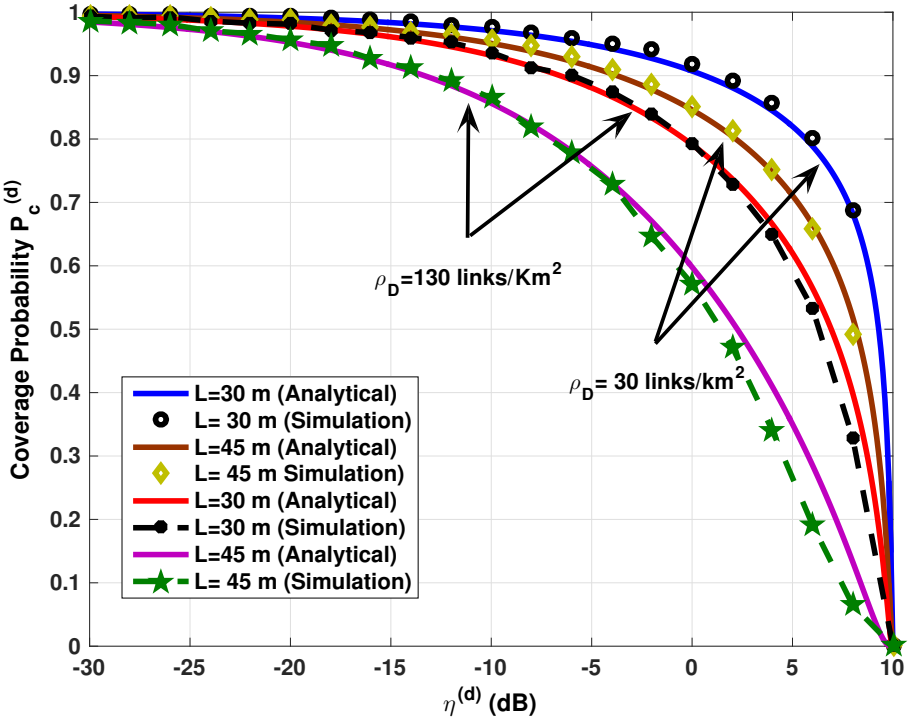

Figure 1.7: Impact of uniform D2D distribution on the D2D coverage probability.

the same coverage probabilities by supposing $P_c = P_c^{(d)}$ given by (1.15) and (1.19). Figure 1.9 shows the distribution of users between cellular network and D2D network for different values of ρ. For example, at a fixed target SINR, $\eta^{(d)} = 4$dB and $\rho = 500$ links/km^2 it can be observed that the best solution is to distribute 60% of users to the D2D network and 40 % of users to the cellular network. Moreover, it can be noted that with lower users' densities, the optimum distribution ratio decreases.

1.5 Conclusions

In this work I have presented a new analytical framework for analyzing the coverage probability in coexisting cellular and D2D networks. The closed-form expressions derived are based on the spatial HPPP model, for the distri-

bution of BSs, and for any non-uniform distribution of D2D links to capture the tendency of D2D users to work in groups. Both power control, compensating path loss and shadowing, and fixed power strategies for the D2D link have been investigated. The reciprocal impact of D2D and cellular communications on the downlink coverage has been investigated as a function of the D2D links maximum range and density. The analytical framework model has been used to get engineering insights regarding to the amount of the traffic that could be offloaded through D2D communications. Finally, the accuracy of our theoretical analysis has been corroborated by simulation results.

Appendix A: Derivation of the average channel gain $F_Y(y)$ between non serving BS and probe MS

With reference to Figure 1.2. Since the average channel gain is given by $x = v - v_m$, from (1.23) and (1.27) it is $f_X(x) = f_V(x) \otimes f_{V_m}(-x)$ which gives

$$\begin{aligned} f_X(x) =& \int_{\max(0,x)+k_0-10\beta\log_{10} R_0}^{\infty} f_V(\nu) f_{V_m}(-x+\nu) d\nu \\ =& \int_{k_0-10\beta\log_{10}(R_0)}^{\infty} \frac{(\log(10))^2 \rho_{\mathrm{BS}} \pi}{(5\beta)^2 R_0^2 (1-\exp\left(-\rho_{\mathrm{BS}}\pi R_0^2\right))} 10^{-\frac{\nu-k_0}{5\beta}} \\ & \times 10^{-\frac{-x+v-k_0}{5\beta}} \exp\left(-\rho_{\mathrm{BS}}\pi 10^{-\frac{-x+\nu-k_0}{5\beta}}\right) d\nu \\ =& \frac{\rho_{\mathrm{BS}}\pi(\log(10))^2}{(5\beta)^2 R_0^2 (1-\exp\left(-\rho_{\mathrm{BS}}\pi R_0^2\right))} 10^{\frac{x}{5\beta}} \int_{k_0-10\beta\log_{10}(R_0)}^{\infty} \\ & \times 10^{-2\frac{\nu-k_0}{5\beta}} \exp\left(-\rho_{\mathrm{BS}}\pi 10^{\frac{x}{5\beta}} 10^{-\frac{\nu-k_0}{5\beta}}\right) d\nu \,. \end{aligned} \tag{1.51}$$

By expanding the exponential function in Taylor series and solving the resulting integral it is

$$f_X(x) = \frac{\rho_{\mathrm{BS}}\pi R_0^2 \log(10)}{5\beta\ (1-\exp(-\rho_{\mathrm{BS}}\pi R_0^2))} 10^{\frac{x}{5\beta}} \sum_{n=0}^{\infty} \frac{\left[-\rho_{\mathrm{BS}}\pi R_0^2 10^{\frac{x}{5\beta}}\right]^n}{n!(n+2)}\,, \tag{1.52}$$

from which we get the final p.d.f. in (1.28).
To account for the presence of the log-normal shadowing in both links, the effective channel gain between the generic interfering BS and the probe MS is $y = y + \xi_2$. It turns out that the p.d.f. $f_Y(y)$ is given by convolving (1.28) and $f_{\xi_2}(\xi_2)$, i.e.,

$$f_Y(y) = \frac{\rho_{\mathrm{BS}}\pi R_0^2 \log(10)}{5\beta} \sum_{n=0}^{\infty} \frac{\left[-\rho_{\mathrm{BS}}\pi R_0^2\right]^n}{n!(n+2)} 10^{\frac{(n+1)y}{5\beta}} 10^{\frac{\sigma^2(n+1)^2}{(5\beta)^2}}\,. \tag{1.53}$$

and the CDF of $F_Y(y)$ can be expressed as

$$\begin{aligned} F_Y(y) =& \rho_{\mathrm{BS}} \pi R_0^2 \sum_{n=0}^{\infty} \frac{(-\rho_{\mathrm{BS}} \pi R_0^2)^n}{n!(n+2)} \frac{1}{(n+1)} \\ & \times 10^{\frac{\sigma^2 (n+1)^2}{(5\beta)^2}} 10^{\frac{(n+1)y}{5\beta}} \\ =& 1 - \frac{10^{-\frac{y}{5\beta}} 10^{\frac{\sigma^2 \log(10)}{(5\beta)^2}}}{\rho_{\mathrm{BS}} \pi R_0^2} \,. \end{aligned} \tag{1.54}$$

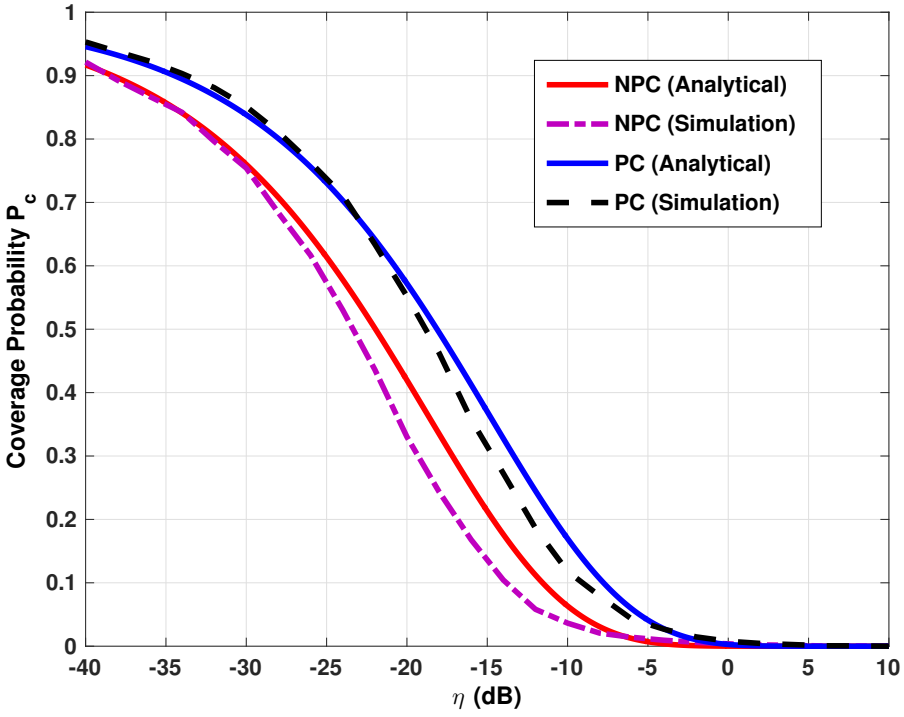

Figure 1.8: The impact power control on cellular coverage probability: $L = 10$ m, $P = 1$ mW.

Appendix B: Derivation of the average channel gain $F_{Y_d}(y_d)$ between D2D and probe MS :Fixed power strategy

From the definition of $x_d = v_2 - P$ the p.d.f. $f_{X_d}(x_d)$ is similar to the p.d.f. $f_{V_2}(\nu_2)$ with a shift value P, so

$$f_{X_d}(x_d) = \frac{\log(10)10^{-\frac{x_d+P-k_0}{5\beta}}}{5\beta R_0^2} \tag{1.55}$$

for $x_d \in [k_0 - P - 10\beta \log 10(R_0), \infty)$.
The p.d.f. and CDF of the average channel gain $y_d = x_d + \xi_2$, respectively,

are given by

$$f_{Y_d}(y_d) = \frac{\log(10)10^{\frac{\sigma^2\log(10)}{(5\beta)^2}+\frac{k_0+P}{5\beta}-\frac{y}{5\beta}}\left(\operatorname{erf}\left(\frac{\log(10)\left(\log(10)\sigma^2-5\beta k_0+5\beta P\right)+50\beta^2\log(R_0)}{5\sqrt{2}\beta\sigma\log(10)}\right)+1\right)}{10\beta R_0^2} \tag{1.56}$$

$$F_{Y_d}(y_d) = 1 - \frac{10^{\frac{\sigma^2\log(10)}{(5\beta)^2}+\frac{k_0+P}{5\beta}-\frac{y}{5\beta}}\left(\operatorname{erf}\left(\frac{\log(10)\left(\log(10)\sigma^2-5\beta k_0+5\beta P\right)+50\beta^2\log(R_0)}{5\sqrt{2}\beta\sigma\log(10)}\right)+1\right)}{2R_0^2}, \tag{1.57}$$

with $\operatorname{erf}(\cdot)$ being the error function.

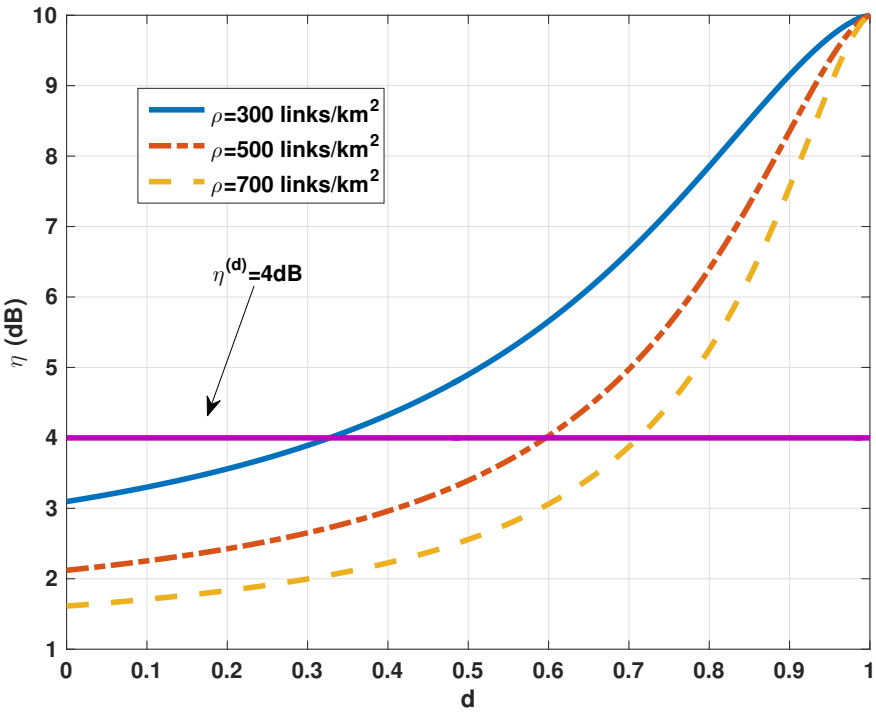

Figure 1.9: example on the split of users between cellular network and D2D network (Uniform spatial distribution): $P_c = P_c^{(d)}$ and $L = 50$ m.

Appendix C: Derivation the average channel gain $F_{Y_d}(y_d)$ between D2D and probe MS: General case

With reference to Figure 1.3. Since the average channel gain is given by $x_d = v_1 - v_2$ in which the p.d.f. of $f_{V_1}(v_1)$ and $f_{V_2}(v_2)$ expressed in (1.34) and (1.23), respectively, then the p.d.f. of $f_{X_d}(x_d)$ is

$$\begin{aligned} f_{X_d}(x_d) &= \int_{-\infty}^{\infty} f_{V_1}(-v) f_{V_2}(x-v) dv \\ &= \left(\frac{(\log(10))^2}{50\beta^2 R_0^2} \right) 10^{\frac{-x_d}{10\beta}} \int_{-\infty}^{-k_0+10\beta\log_{10}(R_0)} 10^{-3\frac{-\nu-k_0}{10\beta}} f_{R_1}(r_1(-v)) dv \,. \end{aligned} \tag{1.58}$$

The integral in (1.58) can be calculated by using transform method between RVs r_1 and ν_1 in (1.33) where

$$\int_{-\infty}^{-k_0+10\beta\log_{10}(R_0)} 10^{-3\frac{-\nu-k_0}{10\beta}} f_{R_1}(r_1(-v))dv = \left(\frac{10\beta}{\log(10)}\right)\int_0^{\infty} 2\pi {r_1}^2 f_{R_1}(r_1)dr_1$$
$$= \left(\frac{10\beta}{\log(10)}\right)\frac{\delta^2}{\pi} \tag{1.59}$$

By substituting (1.59) in (1.58), then

$$f_{X_d}(x_d) = \frac{\delta^2}{\pi}\left(\frac{\log(10)}{5\beta R_0^2}\right) 10^{\frac{-x_d}{10\beta}}\,. \tag{1.60}$$

The p.d.f. of the average channel gain $y_d = y_d + \xi_2$ can be obtained as

$$f_{Y_d}(y_d) = f_{X_d}(x_d) \otimes f_{\xi_2}(x_d)\,, \tag{1.61}$$

where RVs is a Gaussian random variable with zero mean and variance $2\sigma^2$. Then the p.d.f. $f_{Y_d}(y_d)$ is

$$f_{Y_d}(y_d) = \int_{-\infty}^{\infty} f_{X_d}(y-x) f_{\xi_2}(x)dx$$
$$= \frac{1}{\sqrt{2\pi}\sigma}\frac{\delta^2}{\pi}\left(\frac{\log(10)}{5\beta R_0^2}\right) 10^{\frac{-y_d}{10\beta}} \int_{-\infty}^{\infty} \exp\left(\frac{\log(10)x}{10\beta} - \frac{x^2}{4\sigma^2}\right) dx\,. \tag{1.62}$$

The integral in (1.62) can be evaluated by using

$$\int_{-\infty}^{\infty} \exp\left(-p^2x^2 + qx\right) dx = \exp\left(\frac{q^2}{4p^2}\right)\frac{\sqrt{\pi}}{p}\,. \tag{1.63}$$

Then the p.d.f. $f_{Y_d}(y_d)$ can be expressed as

$$f_{Y_d}(y_d) = \frac{\delta^2}{\pi}\left(\frac{\log(10)}{5\beta R_0^2}\right) 10^{\frac{\log(10)\sigma^2}{(5\beta)^2}} 10^{\frac{-y_d}{10\beta}}\,. \tag{1.64}$$

Finally, the CDF $F_{y_d}(y_d)$ is given by

$$\begin{aligned} F_{Y_d}(y_d) &= \int_{-\infty}^{y} f_{Y_d}(y_d) dy_d \\ &= 1 - \int_{y}^{\infty} f_{Y_d}(y_d) dy_d \,. \end{aligned} \tag{1.65}$$

By substituting (1.64) in (1.65) the CDF $F_{Y_d}(y_d)$ results

$$F_{Y_d}(y_d) = 1 - \frac{2\delta^2}{\pi} 10^{\left(\frac{\log(10)\sigma^2}{(5\beta)^2}\right) 10^{\frac{-y_d}{10\beta}}} \tag{1.66}$$

defined in $(-\infty, \infty)$.

Chapter 2

Characterization of Link Lifetime in the Presence of Random Blocking Objects - Part I

2.1 Related Work

Nowadays mmW spectrum represents a great opportunity to increase the capacity of next generation cellular systems, since it offers high bandwidth communication channels and small wavelength. The latter makes it possible to pack a large number of antenna elements in a small space and hence realize high directional beamforming to boost the received signal power and reduce the impact of out-of-cell interference. Moreover, large number of antennas enables the exploitation of multiple-input multiple-output (MIMO) communication techniques to further enhance spectral efficiency. In general dense mmW networks are expected to achieve higher data rates and comparable coverage relative to conventional microwave networks [46].

In addition to the above mentioned advantages, mmW technology poses also new challenges such as the strong sensitivity to non-line-of-sight (NLOS) channel conditions that, in most cases, lead to link blockages that prevent

reliable communications. Link blockage can arise due to the presence of big obstacles, such as walls or cars in vehicular ad hoc networks, but also small obstacles like furniture and people in a crowded scenario might determine serious link blockages at mmW. This could have a strong impact on system performance and, subsequently, on network design. As a consequence, such a phenomenon has received particular attention in the scientific community. Specifically, in addition to experimental campaigns, also theoretical frameworks have been developed to get insights on the key parameters affecting the coverage probability. Among them, approaches based on stochastic geometry, percolation and graph theories are of particular interest as they allow an elegant and efficient modeling of the random nature of obstacles present in the propagation environment, especially in indoor scenarios. For example, the coverage probability of an ad hoc network at mmW with directional antennas and random building blockages is analyzed in [47] using stochastic geometry, in which the transmission capacity is derived in the presence of noise and both line-of-sight (LOS) and NLOS interference. Percolation and graph theories have been adopted to model the size and shape of extended obstacles [48–52]. For instance, a general framework for modeling random blockages is derived in [52], where buildings are modeled as a process of rectangles with random sizes and orientations. The blockage model incorporates the height of the transmitter, receiver and buildings.

Together with user's mobility, blockages may force frequent handovers between APs and consequent signaling overhead or connection drops, especially if narrow beamforming is performed as expected in future mmW wireless systems. This could have a strong impact on device-to-device or vehicular communications. The results of [53] show that the user's mobility increases handovers between APs while, in indoor environment where the coverage area of APs is small, user mobility causes significant and rapid load fluctuation in each AP [54]. Moreover, link properties have direct impact on connection time, end-to-end delay, throughput, and packet losses. All these performance figures are closely dependent on node's mobility and time-varying radio channel characteristics [55, 56].

Unfortunately coverage probability does not provide information about

such effects as its evaluation usually does not include spatial/time correlation of the link state. *Link lifetime* is the proper figure of merit that should be introduced and characterized in order to account for user's mobility. In particular, link lifetime is defined as the time elapsed until a blockage or an out-of-range (i.e., distance larger than the transmission range) are encountered when the mobile user is traveling along a certain path.

While many progresses have been made in the analytical characterization of coverage probability, as previously summarized, less results considering the link lifetime are available so far. In [56] the probability distribution of link lifetime in vehicular ad-hoc networks is presented by considering free flow traffic state and uniformly random distribution of vehicle speed. In [57] the Authors provide a set of requirements necessary to define a mobility metric and investigate the effect of link lifetime on the performance of mobile ad hoc networks. In [58] the probability distribution for the link distance between two randomly mobile radios is presented by considering two different deployment scenarios for the mobile locations, whereas in [59] the Authors studied the impact of radio channels and node's mobility on link dynamics in wireless networks by finding that the probability density function of the link lifetime can be approximated by the exponential distribution with parameter dependent on the ratio between the average node's speed and the effective transmission range.

In all mentioned papers the authors studied the impact of nodes' mobility on the link lifetime distribution by considering only the effect of mobility and finite transmission range but none of them includes the impact of blockages in the analysis.

In this context the aim of this chapter is to fill the gap in characterizing the link lifetime by proposing a new analytically framework able to account for both user's mobility and effects of blockages. I consider the presence of random obstacles modeled according to a PPP and a finite transmission range.

Based on the proposed framework, I derive the statistical distribution of link lifetime from which network design guidelines can be easily obtained. In the numerical results I investigate the joint effect of the main network

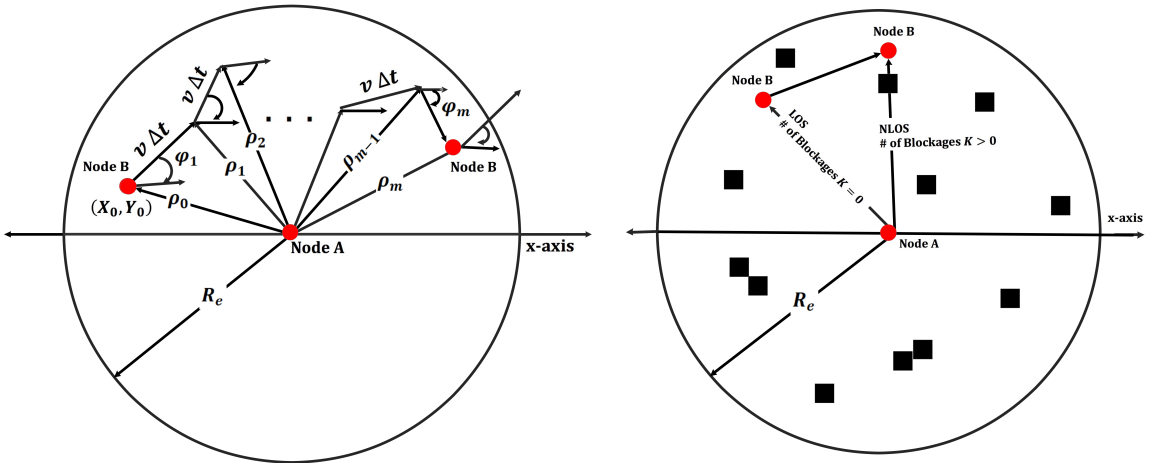

(a) User's mobility model.

(b) Random obstacles.

Figure 2.1: Scenario considered with the presence of a mobile user and obstacles.

parameters such as the density of obstacles and user's speed for two different mobility models.

2.2 System Model

I consider the scenario shown in Figure 2.1 where node A is located at the center of the circle with radius R_e, being R_e its transmission range, and a second node B (mobile user), communicating with A, which is in movement with respect to A. The communication link between B and A is affected by the presence of static obstacles that might create signal blockage during the movement of B. Obstacles are modeled as points distributed in the space according to a homogeneous PPP with density λ. Node B starts moving from position (X_0, Y_0) at time t_0 with constant speed v following a certain mobility model. The following mobility models of interest are considered:

Random Walk Model (RW) In this model, node B chooses at random a new direction every Δt seconds (step). During the total observation interval of T seconds, node B changes its direction $m = \lfloor \frac{T}{\Delta t} \rfloor$ times.[1] Specifically, at

[1]Operator $\lfloor x \rfloor$ denotes the smallest integer larger than x.

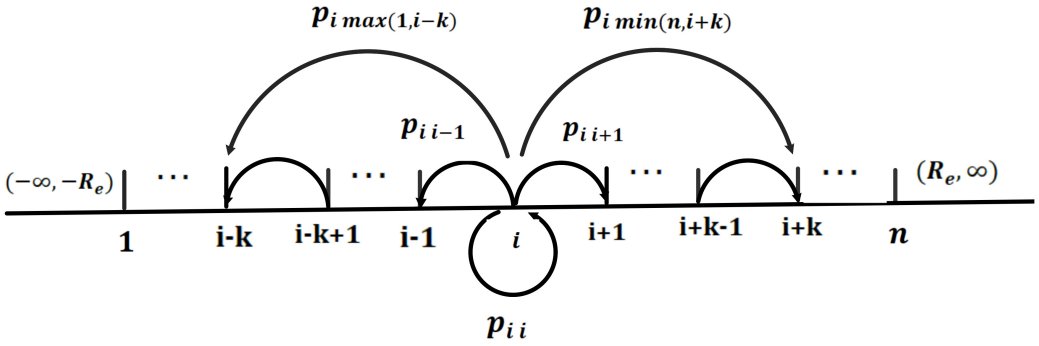

Figure 2.2: Valid states when starting from state S_i.

the mth step the direction of movement is $\psi_m = \psi_{m-1} + \theta_m - \pi/2$, where θ_m is a RV uniformly distributed in $[0 - \pi)$. As illustrated in Figure 2.1 (a), the distance ρ_m between A and B at the mth step is a RV that depends on the current and next positions of node B in relation to node A. In particular, from geometrical considerations, ρ_m is given by

$$\rho_m = \sqrt{\rho_{m-1}^2 + (v\Delta t)^2 - 2\rho_{m-1}\, v\, \Delta t \cos(\theta_m)} \tag{2.1}$$

from which it is

$$\theta_m = \cos^{-1}\left(\frac{\rho_{m-1}^2 + (v\Delta t)^2 - \rho_m^2}{2\rho_{m-1} v \Delta t}\right). \tag{2.2}$$

Straight Line Model (SL) In the second model, node B moves in a straight line along a random direction for the entire observation interval so that it never changes its direction. Note that this model can be seen as a particular case of the previous one by setting $\Delta t = T$ and $m = 1$.

Now define the link drop condition as the event in which at least one obstacle is present between A and B (blockage) or the distance between A and B becomes larger than R_e. The *link lifetime* T_{L} is the time elapsed from t_0 until the first link drop condition occurs. Our purpose is to characterize the statistics of T_{L} as a function of λ and the mobile user's mobility.

2.3 Characterization of the Link Lifetime

2.3.1 Finite-state Approximation

To make the analysis tractable, I discretize the RV ρ_m into n uniform intervals of width ϵ meters in the range $[0 - R_e]$. Moreover, inspired by [60], I model the RVs $\{\rho_1, \rho_2, \ldots, \rho_m\}$ as a finite-state Markov chain in which each interval $[(i-1)\epsilon, i\epsilon], i = 1, 2, \ldots, n$, is associated to a state $S_i = i\,\epsilon$ approximating the distance between A and B. The accuracy of this discretization is expected to increase with the number n of states as it will be verified in the numerical results. In order to account for the link drop condition, I introduce an additional state S_{n+1} which takes the role of absorbing state. If during the movement the absorbing state is reached it means a link drop condition has been encountered.

Denote with $\mathbf{P}$ the $n+1$ by $n+1$ transition probability matrix modeling the distance transition at each time step. With reference to Figure 2.2, the transition matrix $\mathbf{P}$ takes the following form

$$\mathbf{P} = \begin{bmatrix} p_{1,1} & \ldots & p_{1,k+1} & 0 & 0 & 0 & 1 - \sum_{j=1}^{n} p_{1,j} \\ \vdots & \ddots & \ddots & \ddots & 0 & 0 & \vdots \\ p_{k+1,1} & \ddots & \ddots & \ddots & \ddots & 0 & \vdots \\ 0 & \ddots & \ddots & \ddots & \ddots & p_{i,j} & 1 - \sum_{j=1}^{n} p_{i,j} \\ 0 & 0 & \ddots & \ddots & \ddots & \vdots & \vdots \\ 0 & 0 & 0 & p_{n,n-k} & \ldots & p_{n,n} & 1 - \sum_{j=1}^{n} p_{n,j} \\ 0 & 0 & 0 & 0 & \ldots & 0 & 1 \end{bmatrix}$$

where $p_{i,j}$ indicates the transition probability from the current state S_i to the next state S_j after one time step. In my model, I consider that state S_j subsequent to S_i can be only one out of the possible $2k + 1$ hops from S_i, where $j \in [\max(1, i-k), \min(n, i+k)]$, $i = 1, 2, \ldots, n$, because of the maximum distance $v\Delta t$ that can be traveled when moving at speed v at each step. The actual hop depends on the random direction θ taken by the mobile user at each time step.[2] The transition probabilities $p_{i,j}$ can be expressed as

[2]For the sake of notation simplicity I dropped the time step index m.

$$p_{i,j} = \begin{cases} \text{Prob}\left[0 \leq \theta \leq \theta_{ij}\right] \text{Prob}\left[K_{ij} = 0\right] & i = j = 1 \\ \text{Prob}\left[0 \leq \theta \leq \theta_{ij}\right] \text{Prob}\left[K_{ij} = 0\right] & j = L(i), i \neq 1 \\ \frac{1}{a(i)} \text{Prob}\left[\theta_{ii-1} \leq \theta \leq \theta_{ii}\right] \text{Prob}\left[K_{ii} = 0\right] & L(i) < j < U(i), i \neq 1 \\ \text{Prob}\left[\theta_{ii} \leq \theta \leq \theta_{ij}\right] \text{Prob}\left[K_{ij} = 0\right] & j = U(i), i \neq n \\ 1 - \sum_{z=1}^{n} p_{i,z} & j = n+1, i \neq n+1 \\ 1 & i = j = n+1 \\ 0 & o.w \end{cases} \tag{2.3}$$

where $L(i) = \max(1, i-k)$, $U(i) = \min(n, i+k)$, and $a(i) = U(i) - L(i)$. K_{ij} denotes the (random) number of obstacles falling inside the triangle formed between state S_i and state S_j. The area A_{ij} of such a triangle can be calculated by applying the Heron's formula [61]

$$A_{ij} = \sqrt{c_{ij}(c_{ij} - i\epsilon)(c_{ij} - j\epsilon)(c_{ij} - v\Delta t)} \tag{2.4}$$

where c_{ij} is the semiperimeter of the triangle which is given by

$$c_{ij} = \frac{i\epsilon + j\epsilon + v\Delta t}{2} \,. \tag{2.5}$$

The distribution of the number K_{ij} of blockages in the triangle follows the Poisson distribution and it is given by [42]

$$\text{Prob}\left[K_{ij} = k\right] = \frac{e^{-\lambda A_{ij}} (\lambda A_{ij})^k}{k!} \,. \tag{2.6}$$

It turns out that the probability no obstacles are present in A_{ij} is

$$\text{Prob}\left[K_{ij} = 0\right] = e^{-\lambda A_{ij}} \,. \tag{2.7}$$

According to the analysis reported in Appendix, (2.3) can be rewritten as

$$p_{i,j} = \begin{cases} \frac{\theta_{ij}}{\pi} e^{-\lambda A_{ij}} & j = i = 1 \\ \frac{\theta_{ij}}{\pi} e^{-\lambda A_{ij}} & j = L(i), i \neq 1 \\ \frac{\theta_{ii} - \theta ii - 1}{\pi a(i)} e^{-\lambda A_{ii}} & L(i) < j < U(i), i \neq 1 \\ \frac{\theta_{ij} - \theta_{ii}}{\pi} e^{-\lambda A_{ij}} & j = U(i), i \neq n \\ 1 - \sum_{z=1}^{n} p_{i,z} & j = n+1, i \neq n+1 \\ 1 & i = j = n+1 \\ 0 & o.w \end{cases} \tag{2.8}$$

The derivation of the threshold angles θ_{ij} and θ_{ii} can be found in Appendix. By substituting their expression we obtain the final equation of the $p_{i,j}$'s as follows

$$p_{i,j} = \begin{cases} \frac{1}{\pi} \cos^{-1}\left(\frac{v\Delta t}{2\epsilon}\right) e^{-\lambda A_{ij}} & j = i = 1 \\ \frac{1}{\pi} \cos^{-1}\left(\frac{(i\epsilon)^2 + \left(\frac{|j-i|v\Delta t}{k}\right)^2 - (j\epsilon)^2}{2i\epsilon\frac{|j-i|v\Delta t}{k}}\right) e^{-\lambda A_{ij}} & j = L(i), i \neq 1 \\ \frac{1}{\pi(a(i))}\left(\cos^{-1}\left(\frac{v\Delta t}{2i\epsilon}\right) - c_1(i)\right) e^{-\lambda A_{ij}} & L(i) < j < U(i), i \neq 1 \\ \frac{1}{\pi}\left(\cos^{-1}\left(c_2(i,j)\right) - \cos^{-1}(\frac{v\Delta t}{2i\epsilon})\right) e^{-\lambda A_{ij}} & j = U(i), i \neq n \\ 1 - \sum_{z=1}^{n} p_{i,z} & j = n+1, i \neq n+1 \\ 1 & i = j = n+1 \\ 0 & o.w \end{cases}$$

where

$$c_1(i) = \frac{1}{k} \cos^{-1}\left(\frac{(i\epsilon)^2 + \left(\frac{|L(i)-i|v\Delta t}{k}\right)^2 - (L(i)\epsilon)^2}{2i\epsilon\frac{v\Delta t}{k}|L(i)-i|}\right) \tag{2.9}$$

$$c_2(i,j) = \frac{(i\epsilon)^2 + (U(i)\frac{v\Delta t}{k})^2 - (j\epsilon)^2}{2iv\Delta t\epsilon}\,. \tag{2.10}$$

2.3.2 Link Lifetime Distribution

The CDF of the link lifetime T_{L} is defined as

$$\begin{aligned} P_{\mathrm{L}}(T) =& \mathrm{Prob}[T_{\mathrm{L}} \leq T] = \mathrm{Prob}[T_{\mathrm{L}} \leq m\Delta t] && (2.11)\\ =& 1 - \mathrm{Prob}\left[\rho_1 < R_e, K_1 = 0, \rho_2 < R_e, K_2 = 0, ..., \rho_m < R_e, K_m = 0\right] \\ =& \left[\pi^{(0)}\mathbf{P}^m\right]_{(n+1)} && (2.12) \end{aligned}$$

where $m = \left\lfloor \frac{T}{\Delta t} \right\rfloor$, K_i is the number of obstacles encountered when moving from step $i-1$ to step i, and $\pi^{(0)}$ is the probability vector of the initial state at time t_0. The latter is given by

$$\pi^{(0)} = \left(\pi_1^{(0)}, \pi_2^{(0)}, ..., \pi_n^{(0)}, 0\right) \tag{2.13}$$

with $\pi_i^{(0)}$ being the probability node B is in state S_i at time t_0.

Note that the evaluation of (3.9) for the straight line mobility model leads to

$$P_{\mathrm{L}}(T) = \mathrm{Prob}[T_{\mathrm{L}} \leq T = \Delta t] = \left[\pi^{(0)}\mathbf{P}\right]_{(n+1)} . \tag{2.14}$$

From the previous analysis, the average link lifetime T_{A} is given by

$$T_{\mathrm{A}} = \Delta t \sum_{m=1}^{\infty} m \left([\pi^{(0)}\mathbf{P}^m]_{(n+1)} - [\pi^{(0)}\mathbf{P}^{m-1}]_{(n+1)} \right) . \tag{2.15}$$

The last expression can be easily computed by resorting to the properties of absorbing Markov chains. In fact by defining $\mathbf{Q}$ as the $n \times n$ sub-matrix of $\mathbf{P}$ the fundamental matrix of the absorbing Markov chain is

$$\mathbf{N} = \sum_{m=0}^{\infty} \mathbf{Q}^m = (\mathbf{I}_n - \mathbf{Q})^{-1} \tag{2.16}$$

where $\mathbf{I}_n$ is the $n \times n$ identity matrix. The average link lifetime when starting from state S_i is the ith entry of the vector

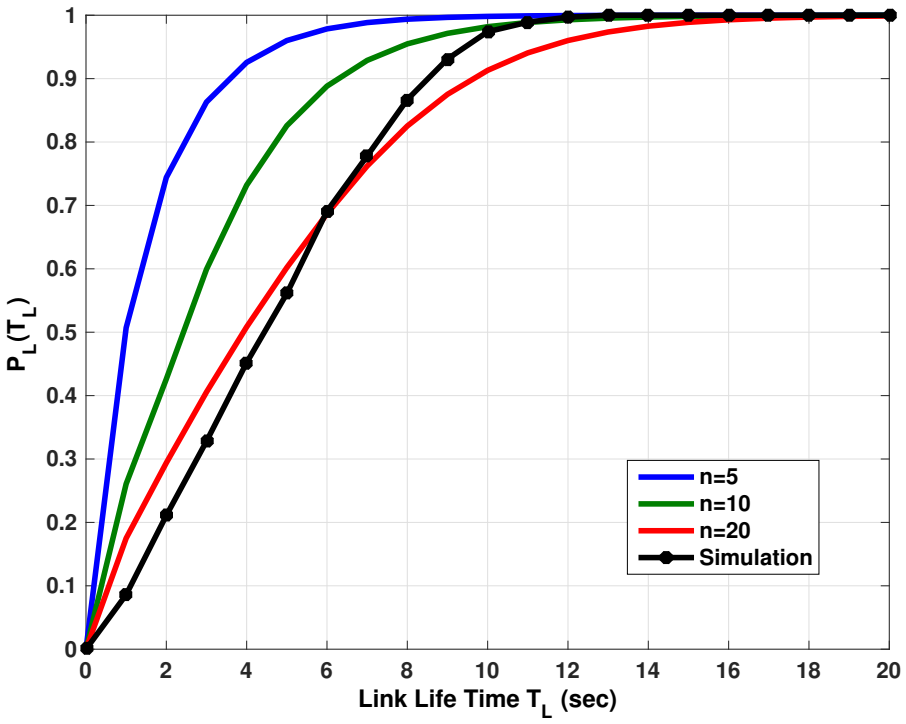

Figure 2.3: CDF of the link lifetime. Accuracy of the analytical model as a function of the number n of states. $R_e = 20\,\mathrm{m}$, $v = 3\,\mathrm{m/sec}$, $\lambda = 0.01\,\mathrm{Blocks}/m^2$, $\Delta t = 1\,\mathrm{sec}$

$$\mathbf{ta} = \Delta t\, \mathbf{N}\, \mathbf{1} \tag{2.17}$$

where $\mathbf{1}$ is a length-n column vector whose entries are all 1.

2.4 Numerical Results

In this section I present our numerical results that illustrate the impact of the blockage on the link lifetime. If not otherwise specified, in the following I consider the RW model and that node B at the initial time t_0 lies in a random state with equal probabilities, i.e, $\pi_i^{(0)} = \frac{1}{n}, i = 1, 2, \ldots, n$.

First I validate my theoretical framework by Monte Carlo simulations where 1,000 randomly generated scenarios are considered. In Figure 2.3,

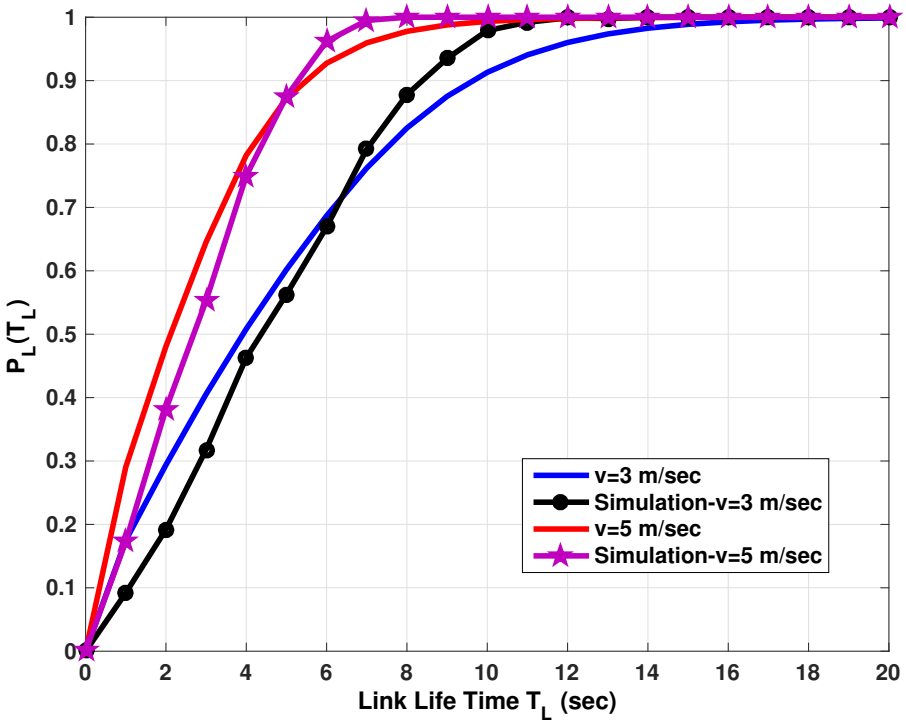

Figure 2.4: CDF of the link lifetime for different values of node's speed. $R_e = 20\,\text{m}$, $\lambda = 0.01\,\text{Blocks}/m^2$, $n = 20$, $\Delta t = 1\,\text{sec}$

the CDF of the link lifetime derived using (3.9) and simulations is shown with different values regarding the number n of states. We observe that the finite-state approximation achieves fairly good accuracy when $n > 10$.

The impact of mobile user's speed is reported in Figure 2.4 where it is evident the strong impact of the speed on link lifetime. A similar behavior can be observed in Figure 2.5 in which the link lifetime CDF for different transmission ranges R_e is shown. Obviously, the smaller the transmission range the higher the probability that at a certain speed the user reaches the circle boundaries.

The joint effect of transmission range, obstacles' density and user's speed can be appreciated in Figures 2.6 and 2.7 where the average link lifetime T_{A} is plotted as a function of λ by varying R_e and v, respectively. In particular, in Figure 2.6 it can be observed that for $\lambda < 0.02\,\text{blocks}/m^2$, the performance

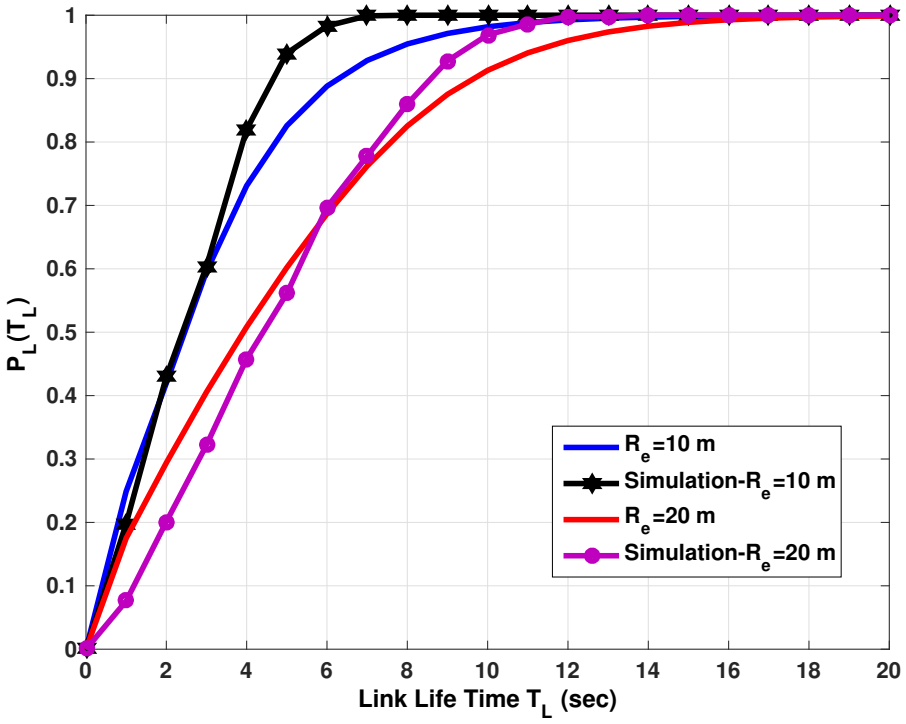

Figure 2.5: CDF of the link lifetime for different values of transmission range R_e. $v = 3\,\mathrm{m/sec}$, $n = 20$ and $\lambda = 0.01\,\mathrm{Blocks}/m^2$, $\Delta t = 1$ sec.

is mainly dominated by the transmission range, whereas for larger values the link lifetime is limited by blockages. From this result one can evaluate the convenience to further increase the transmission range (i.e., the transmitted power) if it leads only to marginal improvements because of blockages. In Figure 2.7 it can be noted that T_{A} is more sensitive to obstacles' density when moving at low speeds. In fact the average link lifetime decreases exponentially with respect to blockage densities regardless the node's speed and it decreases much quickly as the node's speed is high. In general, for an ad hoc network with low mobility T_{A} is dominated by the transmission range R_e. On the contrary, in a network with faster mobile nodes, such as vehicular ad hoc networks, T_{A} is dominated by node's speed.

In Figure 2.8 we study the impact of the initial state $\pi^{(0)}$ on the link lifetime CDF. We note that the probability of link lifetime increases when

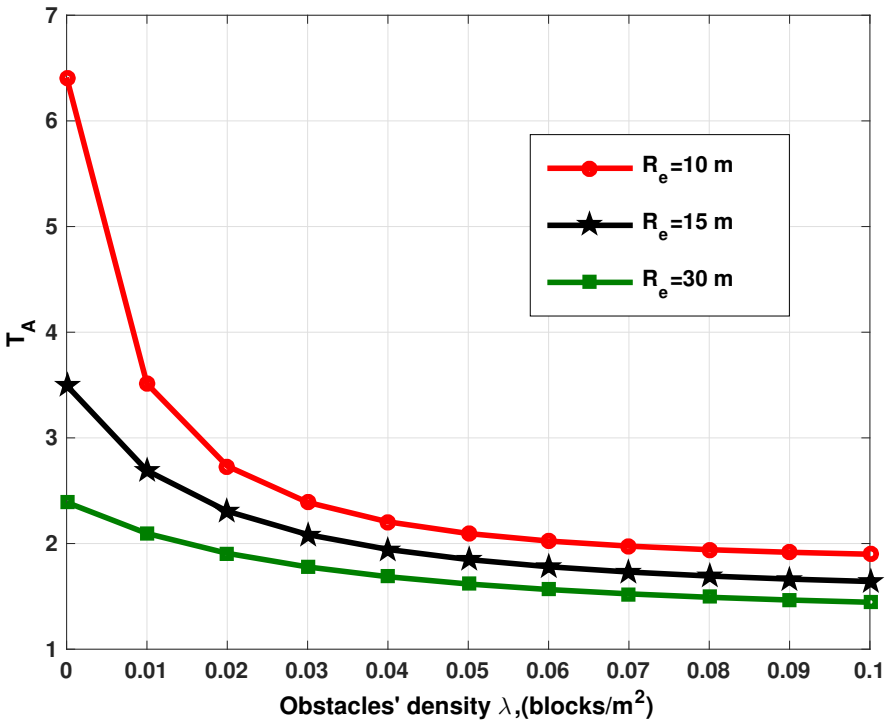

Figure 2.6: Impact of transmission range on the average link lifetime under different blockage densities. $v = 5\,\mathrm{m/sec}$ and $\epsilon = 1\,\mathrm{m}$, $\Delta t = 1\,\mathrm{sec}$

the mobile node is very close to the center where the effects of blockages are less probable.

Finally, in Figure 2.9, the comparison between the two mobility models considered is shown. It is evident that the RW mobility model leads to a significantly worse performance than that obtained with a user moving on a straight line (SL). This can be explained by the fact that the angular velocity in SL is on average higher than that in RW and the link lifetime decreases with the angular velocity.

2.5 Conclusions

In this chapter, I presented a new analytically model to characterize the statistics of the link lifetime in wireless networks in the presence of obstacles.

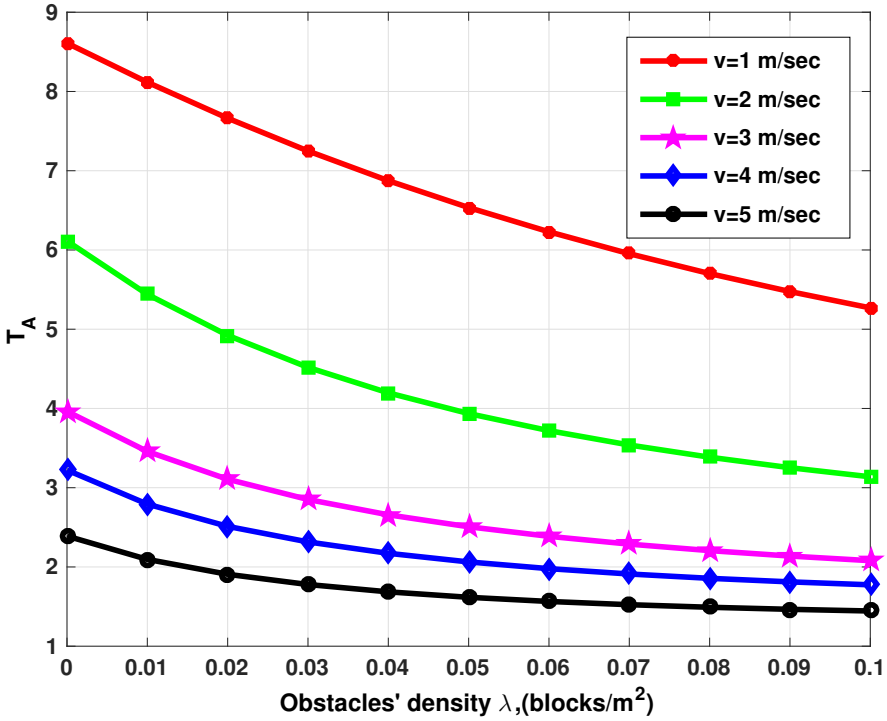

Figure 2.7: Impact of mobile speed on the average link lifetime under different blockage densities. $R_e = 10\,\text{m/sec}$, $n = 10$, $\Delta t = 1\,\text{sec}$.

For this purpose I considered two different mobility scenarios and assumed the distribution of the blockage according to a PPP. I investigated the interplay between obstacles' density, transmission range, and user's mobility by highlighting the main parameters impacting the performance as well as the conditions under which any further increase of the transmission range becomes no more beneficial due to the presence of obstacles and user's mobility.

APPENDIX

Derivation of angle thresholds

As shown in Figure 2.1, I assume node B moves with constant speed v, and that at each time step of Δt seconds it changes randomly its direction. In

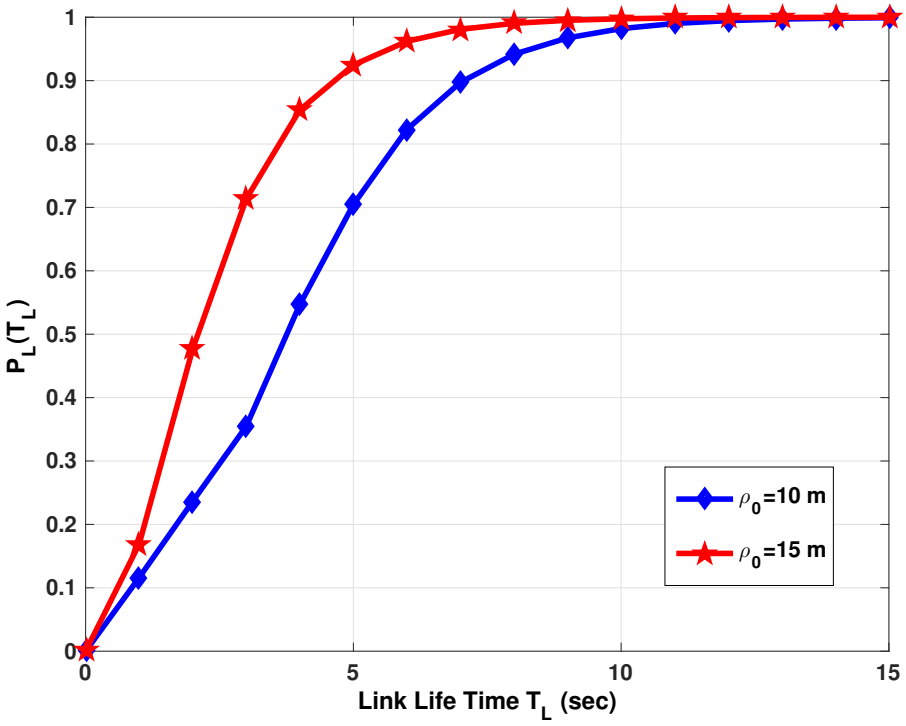

Figure 2.8: Impact of probability of initial state on the link lifetime CDF. $R_e = 20\,\text{m}$, $n = 20$, $v = 3\,\text{m/sec.}$, $\lambda = 0.02\,\text{blocks}/m^2$, $\Delta t = 1\,\text{sec}$

this Appendix I derive the thresholds θ_{ij} on angle θ corresponding to the hop between state S_i and state S_j.

The maximum number of hops compatible with v is given by

$$k = \left\lfloor \frac{v\Delta t}{\epsilon} \right\rfloor \tag{2.18}$$

and the number of potential valid states starting from i is

$$N_i = \min(n, i+k) - \max(1, i-k) + 1 \tag{2.19}$$

so that the potential number of states that can be reached from state S_i becomes

$$N = 2k + 1\,. \tag{2.20}$$

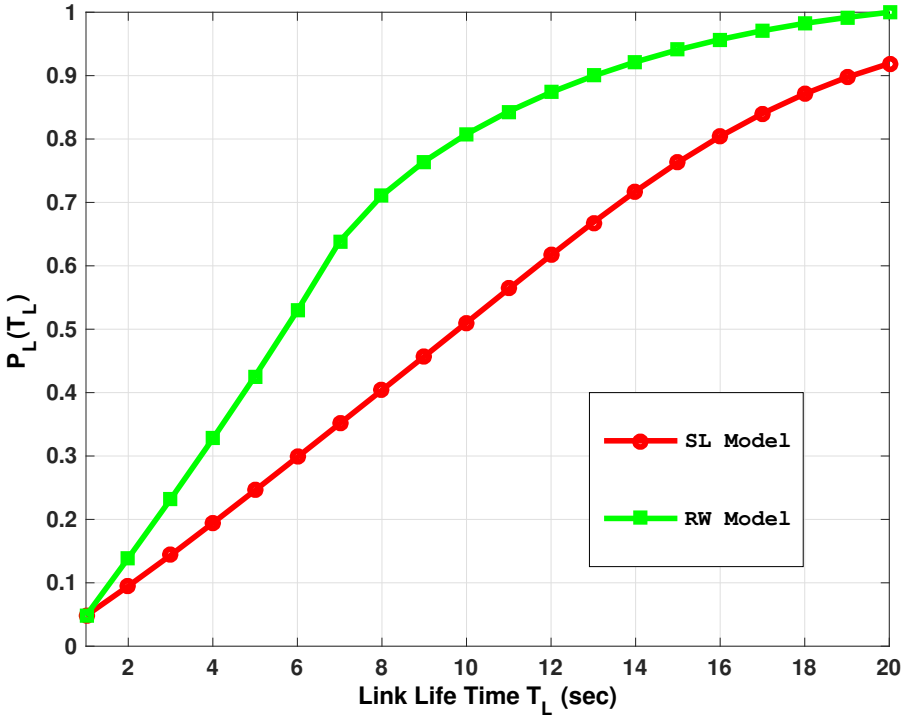

Figure 2.9: Comparison between different mobility models. $R_e = 20$ m/sec, $n = 20$, $v = 2\,\text{m/sec.}$, and $\lambda = 0.02\,\text{blocks}/m^2$.

The main issue is to find a mathematical expression of the probability to get a certain state S_j from state S_i. To this purpose I adopt the following model.

With reference to Figure 2.10(b), when node B remains in state S_i, the angle θ_{ii} formed with respect to node A must satisfy

$$(i\epsilon)^2 = (i\epsilon)^2 + (v\Delta t)^2 - 2iv\epsilon\cos(\theta_{ii}) \tag{2.21}$$

from which it results

$$\theta_{ii} = \cos^{-1}\left(\frac{v\Delta t}{2i\epsilon}\right) . \tag{2.22}$$

When node B moves from its current state S_i to the next state S_j with

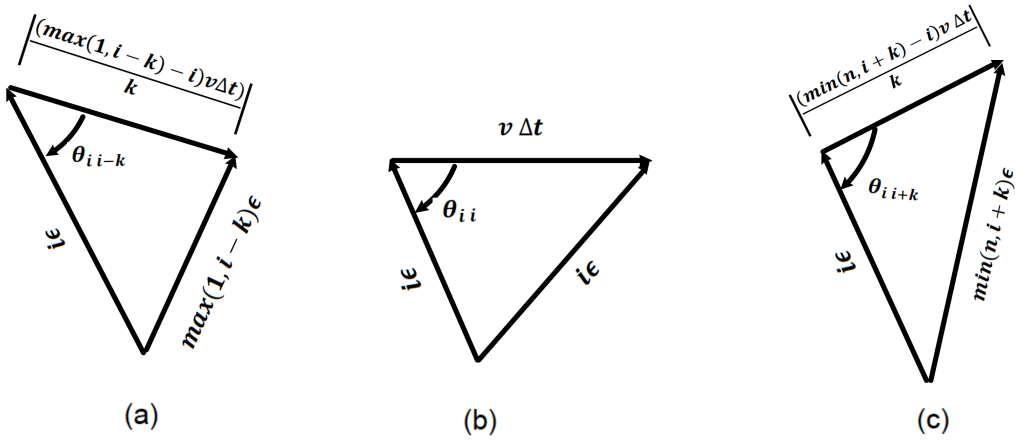

Figure 2.10: (a) Geometric configuration when $S_j < S_i$; (b) Geometric configuration when $S_j = S_i$; (c) Geometric configuration when $S_j > S_i$.

$\max(1, i-k) < j < i$, as shown in Figure 2.10(a), it is

$$(j\epsilon)^2 = (i\epsilon)^2 + (d_1(i))^2 - 2iv(d_1(i))\cos(\theta_{ij} \tag{2.23}$$

where

$$d_1(i) = \frac{|\max(1, i-k) - i|v\Delta t}{k}. \tag{2.24}$$

It results:

$$\theta_{ij} = \cos^{-1}\left(\frac{(i\epsilon)^2 + d_1^2(i) - (j\epsilon)^2}{2i\epsilon d_1(i)}\right). \tag{2.25}$$

In the opposite case where $\min(n, i+k) > j > i$, it is (see Figure 2.10(c))

$$(j\epsilon)^2 = (i\epsilon)^2 + d_2^2(i) - 2iv\, d_2(i)\cos(\theta_{ij}) \tag{2.26}$$

where

$$d_2(i) = \frac{|\min(n, i+k) - i|v\Delta t}{k} \tag{2.27}$$

which leads to

$$\theta_{ij} = \cos^{-1}\left(\frac{(i\epsilon)^2 + d_2^2(i) - (j\epsilon)^2}{2i\epsilon d_2(i)}\right). \tag{2.28}$$

Values θ_{ij} are used in (2.8) as thresholds to determine the probability to jump from state S_i to state S_j given θ is uniform distributed in $[0, \pi)$.

Chapter 3

Characterization of Link Lifetime in the Presence of Random Blocking Objects - Part II

3.1 Introduction

In this chapter I extend part of the analysis developed in chapter 2 by considering obstacles with different sizes. Specifically, I consider one of the most realistic scenario where I assume a mobile device moving along the straight line with constant speed. Further, a random number of obstacles located in random positions with different sizes is present. I derive closed-form expressions for the statistical distribution of link lifetime accounting for the shadowing effect caused by obstacles depending on their dimension and distance from the AP. In the numerical results I investigate the joint effect of the main system parameters such as the density and size of obstacles and the communication distance, from which network design guidelines can be easily obtained. Analytical results are compared with simulations with the purpose to assess their validity.

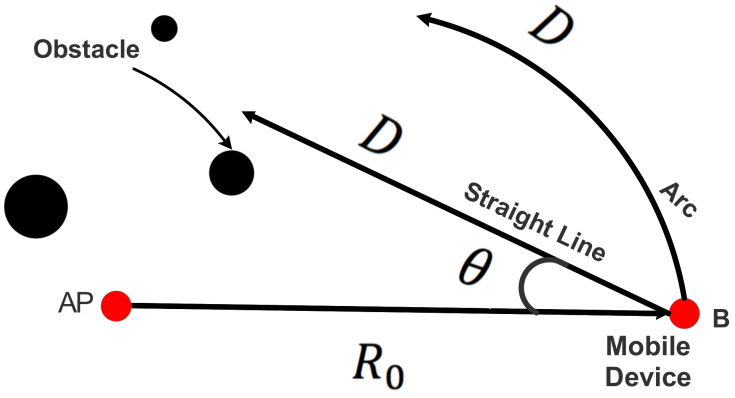

Figure 3.1: Mobility Model

3.2 System Model

As shown in Figure 3.1 I consider a random number of objects (obstacles) distributed according to a PPP in a plane. Objects are completely blocking as usually happens when working at mmW using beamforming techniques. Since I am only interested in the shadowing effect of obstacles when located in between the mobile device and the AP, I approximate them by circles. The assumption might be a good approximation in the mmW wireless networks (D2D and vehicular communications) in which the reflections are weak due to the higher carrier frequency, and signals are highly directive with the deployment of adaptive antenna arrays at both transmitters and receivers [52]. To account for obstacles with different sizes, a number n of classes of objects with radius b_i, $i = 1, 2, ..., n$ distributed according to PPP and density λ_i are considered. The following scenarios for the wireless link between the mobile device and AP are of interest:

- Circle Mobility Model: As shown in Figure 3.1 I consider a wireless link between a mobile device moving for D meters at constant speed along a circle of radius R_0 from the serving AP located in the center. This model approximates situations where the radial movement is small compared to R_0 and/or D. Note that only objects inside the circle of radius R_0 might affect the link between AP and mobile device.

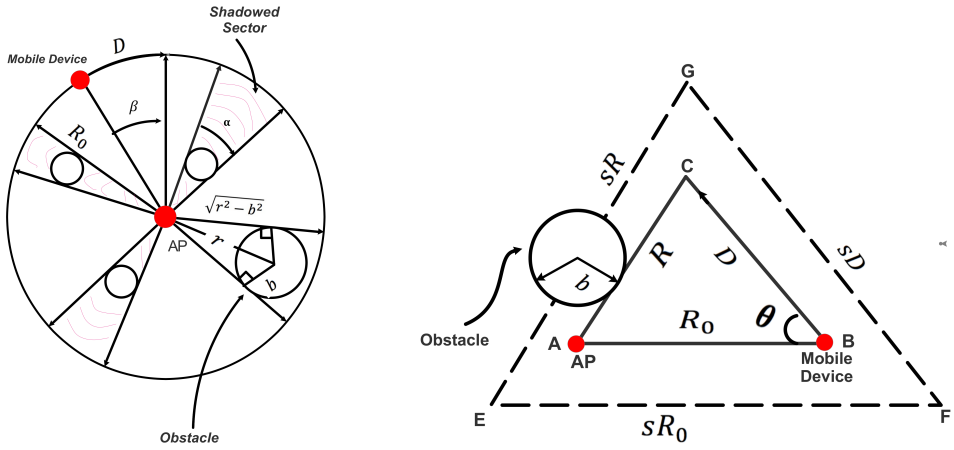

(a) Circle Scenario

(b) Straight Line Scenario; where s is the scale factor

Figure 3.2: Scenarios of a wireless link between a mobile device and AP

- Straight Line Mobility Model: As shown in Figure 3.1 a more realistic scenario considers the mobile device moving for D meters along a straight line with constant speed starting from point B (Mobile Device) with angle θ.

  The link between the mobile device and the AP is established if the mobile device is located in visible region, that is, it is outside all shadow sections determined by the objects. Now define the link drop condition as the event in which the mobile device when moving falls inside at least one shadow region. The link lifetime T_L is the time elapsed from the initial position until the first link drop condition occurs. The purpose is to characterize the statistics of the link lifetime as a function of λ_i, b_i, D, θ and the initial distance R_0 for both mobility models.

3.3 Characterization of the Link Lifetime

3.3.1 Circle Model Scenario

As shown in Figure 3.2(a) I consider the mobile device moving within a sector of angle $\beta = \frac{D}{R_0} \leq \pi$ at distance R_0 from the AP with linear speed v. In

the presence of one object located in a random position within the circle R_0, the probability that the shadow sector of angle α, created by the object, intersects the sector β defined by the mobile device is

$$\mathbb{P}(\text{shadow}|\alpha) = \frac{\beta + \alpha}{2\pi}\,. \tag{3.1}$$

I start the analysis by considering a single object of radius b located at distance r from the AP. As shown in Figure 3.2(a), the angle α of the shadow sector can be calculated by using simple trigonometric rules, where

$$\tan\left(\frac{\alpha}{2}\right) = \frac{b}{\sqrt{(r^2 - b^2)}} \qquad\qquad r > b\,. \tag{3.2}$$

When $r \gg b$ (small obstacles or large distances), (3.2) can be approximated as $\tan\left(\frac{\alpha}{2}\right) \approx \frac{b}{r}$. The accuracy of this approximation will be assessed by simulation in the numerical results. According to the PPP distribution of objects, the number of objects belonging to the ith class that fall inside the circle of radius R_0 is Poisson distributed with mean $\lambda_i \pi R_0^2$ [42]. Their positions are independent and identically distributed (i.i.d.) with uniform distribution so that the p.d.f. of their distance r from the origin is given by

$$f_r\,(r) = \frac{2\,r}{R_0^2}\ , \tag{3.3}$$

where $r \in [0, R_0]$, zero otherwise. Their angle distribution is uniform in $[0, 2\pi)$.

Under the approximation of (3.2), and given (3.3), the CDF of RV α results

$$\begin{aligned} F_\alpha\,(x) = \mathbb{P}\,(\alpha \le x) &= 1 - \mathbb{P}\left(r \le \frac{b}{\tan\left(\frac{x}{2}\right)}\right) \\ &= 1 - \frac{b^2}{R_0^2 \tan^2\left(\frac{x}{2}\right)} \end{aligned} \tag{3.4}$$

for $\alpha \in [2\tan^{-1}(\frac{b}{R_0}), \pi]$, zeros otherwise. The corresponding p.d.f. is

$$f_\alpha(\alpha) = \frac{b^2 \sin(\alpha)}{2R_0^2 \sin^2(\frac{\alpha}{2})} \tag{3.5}$$

defined in the same interval. From (3.5) the expected value of α results

$$\varepsilon(\eta) = \mathbb{E}[\alpha] = \eta(-\eta\pi + 2) + 2(\eta^2 + 1)\tan^{-1}(\eta)\,. \tag{3.6}$$

Note that $\varepsilon(\eta)$ depends only on the ratio $\eta = b/R_0$. The unconditional probability is

$$\begin{aligned} P_1(\beta, \eta) = \mathbb{P}(\text{shadow}) &= \mathbb{E}_\alpha[\mathbb{P}(\text{shadow}|\alpha)] \\ &= \frac{\beta}{2\pi} + \frac{\mathbb{E}[\alpha]}{2\pi} = \frac{\beta}{2\pi} + \frac{\varepsilon(\eta)}{2\pi} \end{aligned} \tag{3.7}$$

which is valid for $0 \leq \beta \leq \pi$. Since there are n classes of objects, each with a random number of objects according to the Poisson distribution, the probability that a mobile device moving in a sector of angle β at distance R_0 is not shadowed by any object is

$$\begin{aligned} P_0^{(arc)}(\beta) &= \prod_{i=1}^{n} \sum_{k=0}^{\infty} [1 - P_1(\beta; \eta_i)]^k \frac{(\pi\lambda_i R_0^2)^k}{k!} e^{-\pi\lambda_i R_0^2} \\ &= \exp\left(-\sum_{i=1}^{n} \frac{\lambda_i R_0^2 \beta}{2}\right) \exp\left(-\sum_{i=1}^{n} \frac{\lambda_i R_0^2 \varepsilon(\eta_i)}{2}\right)\,. \end{aligned} \tag{3.8}$$

Supposing the mobile device moves along the circle at constant linear speed ν, it turns out that the CDF of the link lifetime T_L is

$$P_L^{(arc)}(T_L) = \mathbb{P}(T \leq T_L) = 1 - P_0^{(arc)}\left(\frac{\nu T_L}{R_0}\right)\,, \tag{3.9}$$

being $\nu T_L = D$.

From (3.8) we can note that the first term of $P_0^{(arc)}(\beta)$ gives the probability that no shadows are present in a sector of angle β when considering punctiform objects. In fact $\exp(-\pi\lambda_i R_0^2 \beta/2)$ represents the probability that no

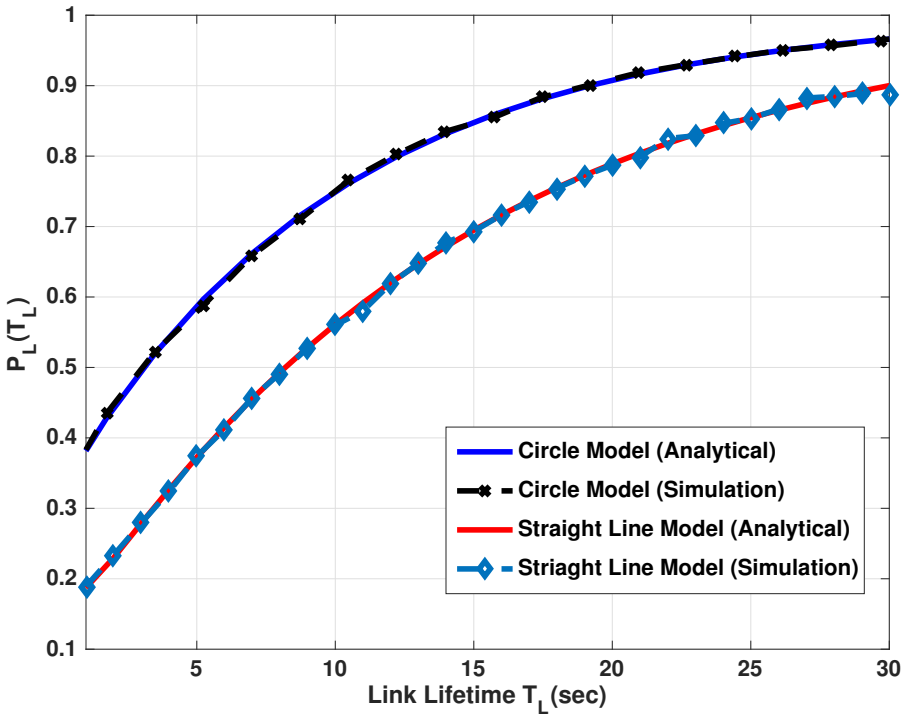

Figure 3.3: Comparison between a user moving on a circle and on the corresponding straight line. One class of obstacles: $b_1 = 1\,\text{m}$, $\lambda_1 = 0.01\,\text{Blocks/m}^2$, $R_0 = 20\text{m}$ and $\theta = \pi/4$.

obstacles of class i have their center in the sector of angle β. The second term accounts for object's dimension and its distance distribution and depends on the ratio $\eta_i = b_i/R_0$ through (3.6) and not on β. This is an interesting result which tells that the effect of object's size is not a function of the distance traveled by the mobile device. From the previous analysis the average link lifetime T_A can be derived by differentiating (3.9) with respect to T_L and taking the expectation resulting in

$$T_A = \sum_{i=1}^{n} \frac{2}{\lambda_i R_0 \nu} \exp\left(-\sum_{i=0}^{n} \frac{\lambda_i R_0^2}{2} \varepsilon(\eta_i) \right). \tag{3.10}$$

The derivation can be found in Appendix A.

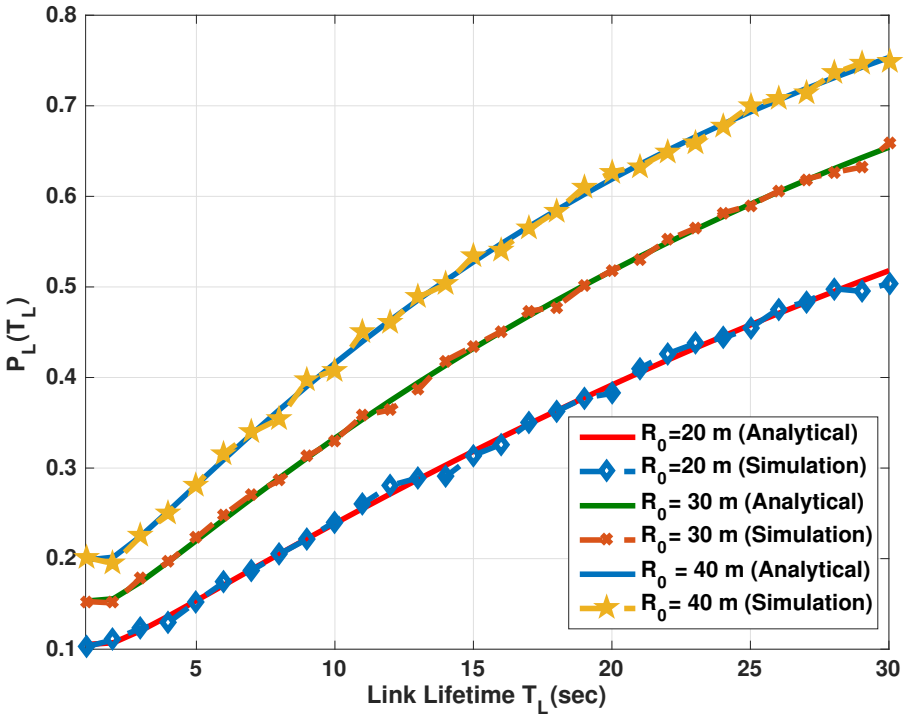

Figure 3.4: Impact of link initial distance R_0 on the link lifetime CDF (Straight Line Model). Two classes of obstacles: $b_1 = 3\,\text{m}$, $b_2 = 1\,\text{m}$, $\lambda_1 = 0.001\,\text{Blocks/m}^2$, $\lambda_2 = 0.002\,\text{Blocks/m}^2$ and $\theta = \pi/4$.

3.3.2 Straight Line Scenario

As shown in Figure 3.2(b) I consider the mobile device moving along the straight line BC with constant speed v and angle θ. The mobile device will keep in contact with the AP for the entire trip from B to C if no object or part of it falls inside the communication region which is defined by the triangle ABC. Given an obstacle of radius b, it falls inside the communication region if its center is located inside the augmented triangle EFG as shown in Figure 3.2(b) .

Since I consider there are n classes of objects distributed according to PPP, then the probability that no object falls inside the communication region can

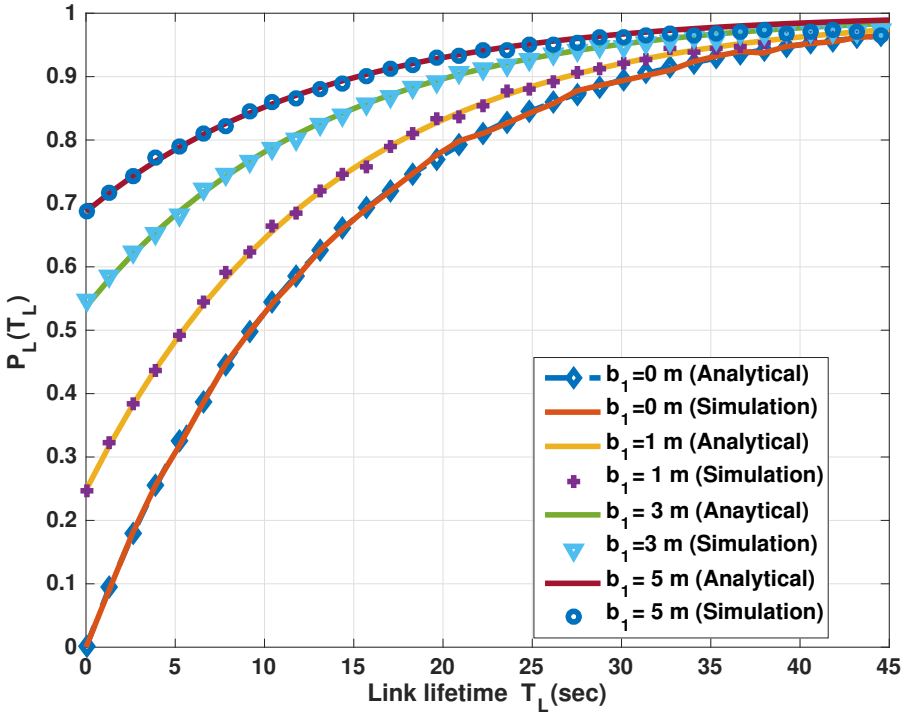

Figure 3.5: Impact of obstacle's size on the link lifetime (Circle Model). One class of obstacles: $R_0 = 15\,\text{m}$, and $\lambda_1 = 0.01$ Blocks/m^2.

be expressed as

$$P_0^{(lin)}(D) = \mathbb{P}(\text{no obstacles in } \triangle \text{EFG}) \approx \exp\left(-\sum_{i=1}^{n} \lambda_i A(D; s_i; R_0, \theta)\right) , \tag{3.11}$$

where (3.11) is approximated since there could be some obstacles with centers located at the edges that do not block the link. Fortunately the probability of this event is very low as confirmed by simulations. $A(D; s_i; R_0, \theta)$ is the area of triangle EFG whose its derivation can be found in appendix B, and s_i is a scale factor which is given by (3.18). Supposing the mobile device moves at constant speed v, it turns out that the CDF of the link lifetime T_L is

$$P_L^{(lin)}(T_L) = \mathbb{P}(T \leq T_L) = 1 - P_0^{(lin)}(\nu T_L)\,, \tag{3.12}$$

being $\nu T_L = D$.
From the previous analysis the average link lifetime T_A can be derived by differentiating (3.12) with respect to T_L and taking the expectation resulting in

$$T_A = \sum_{i=1}^{n} \frac{2b_i R_0}{2b_i + R_0 \sin(\theta)} \times \exp\left(\sum_{i=1}^{n} -b_i \lambda_i (2b_i \csc(\theta) + R_0)\right) K_1\left(\lambda_i b_i \csc(\theta)(2b_i + R_0 \sin(\theta))\right) \quad (3.13)$$

where $K_1(.)$ is the Modified Bessel function of the Second kind.

3.4 Numerical Results

Using the proposed analytical framework, in this section I investigate how the link lifetime in a wireless network is affected by the presence of random blocking obstacles. Moreover, I present some Monte Carlo simulation results to validate our analytical framework. For the sake of illustration and without loss of generality I study the effects of two classes of blocking objects ($n = 2$) if not otherwise specified. I normalize the link lifetime in both proposed models with respect to ν. i.e., $\nu = 1$, so that numerically it corresponds to D.

In Figure 3.3 the accuracy of our model when used to characterize a user moving along a straight line is presented and compared with the circle scenario in term of $P_L(T_L)$. From the results, it can be seen that the circle scenario leads to a significant worse performance compared with a user moving along the straight line (more realistic scenario) and provides an upper bound of the link lifetime.

In Figure 3.4 I study the effect of the initial distance R_0 on $P_{\mathrm{L}}(T_{\mathrm{L}})$ for the straight line scenario. As expected, the initial distance has a significant impact on the link lifetime. In fact, given a fixed obstacles' density, the higher the distance the higher is the probability to encounter obstacles in

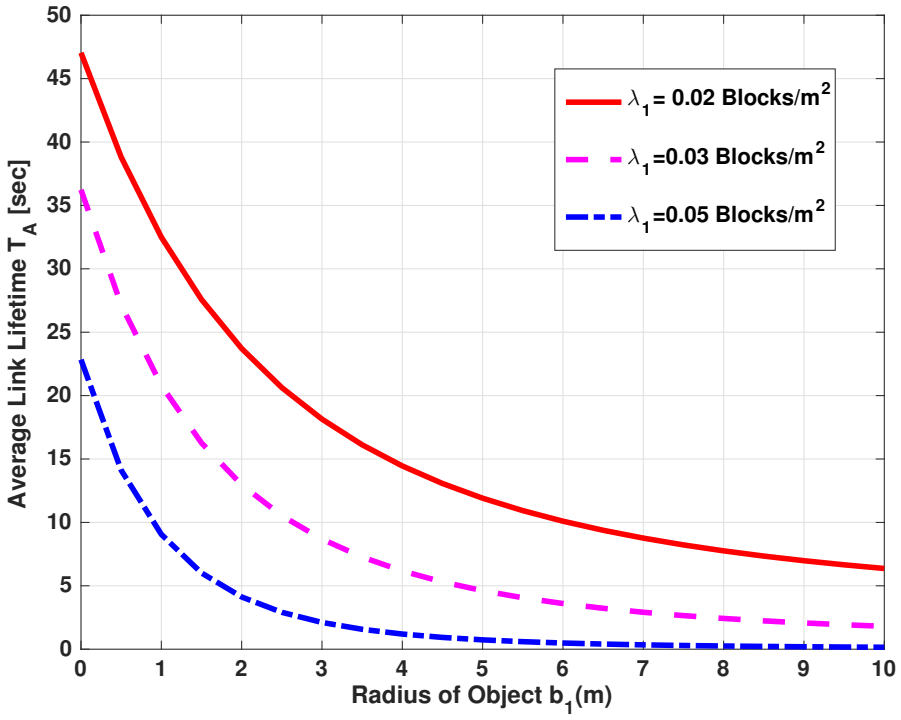

Figure 3.6: Impact of density of obstacles on the average link lifetime (Circle Model). One class of obstacles: $R_0 = 10\,\text{m}$.

between the mobile user and the AP. The effect of obstacle's size is shown in Figure 3.5 in which it is evident that the error one could commit when approximating obstacles with points ($b_1 = 0$) could be significant. The good matching with simulation results validates the accuracy of the analytical framework and the approximation of (3.2) even when b is not much smaller than r.

The behavior of the average link lifetime for the circle model for one class of obstacles as a function of obstacle's size b_1 by varying λ_1 is shown in Figure 3.6. Results indicate that the impact of nodes' density is higher with small objects. In fact the average link lifetime decreases exponentially with respect to the density of obstacles and object's size according to different relationship as evident in (3.6) and (3.10).

3.5 Conclusions

In this chapter I have presented a stochastic analysis of the communication link lifetime between a mobile device and its serving AP in the presence of n classes of randomly located objects characterized by different densities and sizes. I have derived closed-form expressions of the link lifetime CDF and corresponding average, which indicate the exponential behavior of the link lifetime as a function of obstacle's size and allowed to get insights on the interplay between obstacles' density, dimension, and user's distance. Comparisons with simulation results have confirmed the validity of the analytical framework.

Appendix A: Derivation of the average Link life time T_A for the Circle Mobility Model

By differentiating (3.9) with respect to T_L then the p.d.f. of link lifetime $p_L^{(arc)}(T_L)$ can be expressed as

$$p_L^{(arc)}(T_L) = \sum_{i=1}^{n} \frac{\lambda_i R_0 \nu}{2} \exp\left(-\sum_{i=1}^{n} \frac{\lambda_i R_0^2 \beta}{2}\right) \times \exp\left(-\sum_{i=1}^{n} \frac{\lambda_i R_0^2 \varepsilon(\eta_i)}{2}\right) . \tag{3.14}$$

From (3.14), the average link lifetime T_A can be derived

$$T_A = \mathbb{E}[T_L] = \int_0^{\infty} T_L \; p_L^{(arc)}(T_L) dT_L \; , \tag{3.15}$$

where the final result can be found in (3.10) .

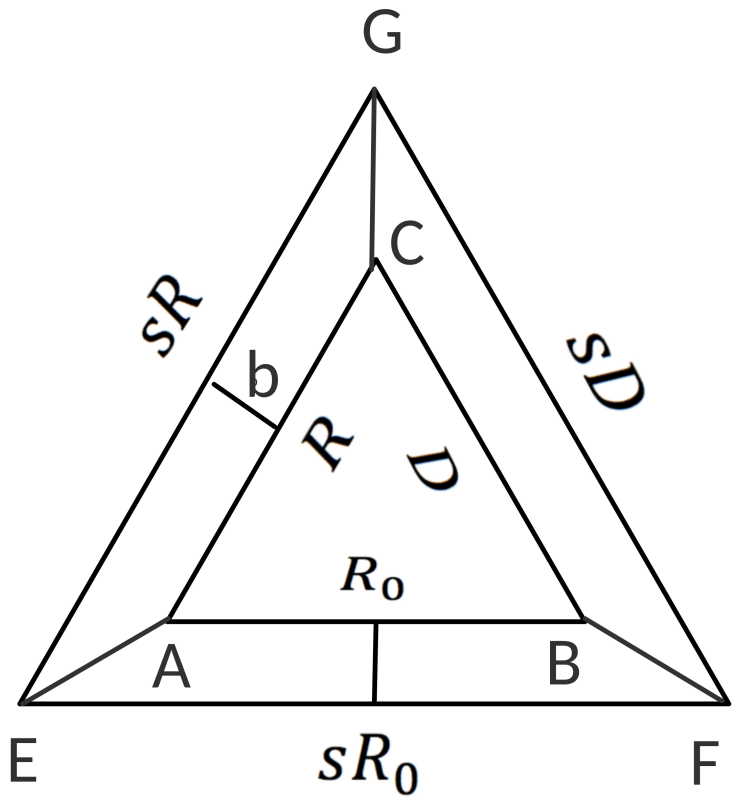

Figure 3.7: The geometric analysis of area of triangle EFG

Appendix B: Derivation of the Area of Triangle EFG Shown in Fig. 3.2

As shown in Figure 3.7 I am interested in scaling the inner triangle ABC with the scale factor s in order to obtain the area of the outer triangle EFG. In fact, based on geometric consideration, the area of triangle EFG is given by

$$A(s, R_0, D, \theta) = s^2 A_{in}(R_0, D, \theta), \tag{3.16}$$

where $A_{in}(R_0, D, \theta) = \frac{1}{2} R_0 D \sin(\theta)$ is the area of triangle ABC. On the other

hand, the left side of (3.16) can also be expressed as

$$\begin{aligned} A(s, R_0, D, \theta) &= \frac{1}{2} R_0 D \sin(\theta) + \frac{1}{2} b(R_0 + sR_0) \\ &+ \frac{1}{2} b(D + sD) + \frac{1}{2} b(R_1 + sR_1) \\ &= A_{in}(R_0, D, \theta) + \frac{1}{2} b P_{in}(R_0, D, \theta) \\ &+ \frac{1}{2} sb P_{in}(R_0, D, \theta), \end{aligned} \tag{3.17}$$

where $P_{in}(R_0, D, \theta)$ is the perimeter of triangle ABC.

By substituting (3.17) in (3.16) the scale factor s results

$$s = \frac{b \csc(\theta)}{D} + \frac{2b \csc(\theta)}{R_0} + 1. \tag{3.18}$$

Finally, by substituting (3.18) in (3.16) the area of triangle EFG can be obtained.

Chapter 4

Device-to-Device Communication and Localization for Road Users

4.1 Related Works

In recent years, vulnerable road users (VRUs), including cyclists, injuries and mortality has rapidly grown due to the increased road traffic: around 2000 people riding bicycle are killed every year in traffic accidents in EU countries [62] and about 30% of cyclist fatalities take place at junction [62,63]. In this scenario, it becomes urgent to develop solutions in order to both encourage people to cycle and make cycling safer at the same time. As regards the last point, increasing road users' awareness of cyclists' presence in the surrounding becomes an essential issue along with the possibility of warning cyclists during cars and heavy goods vehicles (HGVs) dangerous maneuvers.

Today several technologies are available and could be exploited to detect dangerous situations for cyclists. The choice of the proper technology requires a deep analysis of the most dangerous scenarios and situations and must account for several aspects in order to make it effective, reliable, user-friendly, and low-cost.

To this end, in this chapter we first provide a survey of existing technologies, with a particular emphasis on their pros and cons. Second, conscious and inspired by the limits of already available technologies, we propose a new risk detection architecture providing high-accuracy localization and tracking of road users based on the UWB technology [64]. UWB, in its IEEE802.15.4a standard implementation [65], has already proved to be the best candidate in achieving high localization accuracy at low cost thanks to its high temporal resolution, the ability to resolve multipath and to coexist with other wireless technologies [66–68].

The performance of the implemented UWB-based tracking system has been experimentally characterized as discussed in the numerical results. The availability of accurate real-time tracking of road users opens the door to the introduction of advanced RA units, both on vehicles and in the infrastructure (on-site), capable of predicting critical situations and providing a suitable feedback to the road user through ad-hoc HMIs. Moreover, it also enables the possibility of offering additional services to cyclists, such as enhancing the functionality of green waves by accounting for the amount of people approaching the traffic light.[1]

4.2 Analysis of Accident Statistics involving Cyclists

Previous cycling safety research has found that left- and right-turning vehicles had an effect on bicyclist injury occurrence and were frequent in bicycle accidents taking place at intersections [69–72]. These two scenarios are so-called left turn and right turn scenarios. I will proceed to explain them with more detail below.

[1]These applications are currently being investigated in the Europe-funded project XCycle (http://www.xcycle-h2020.eu/).

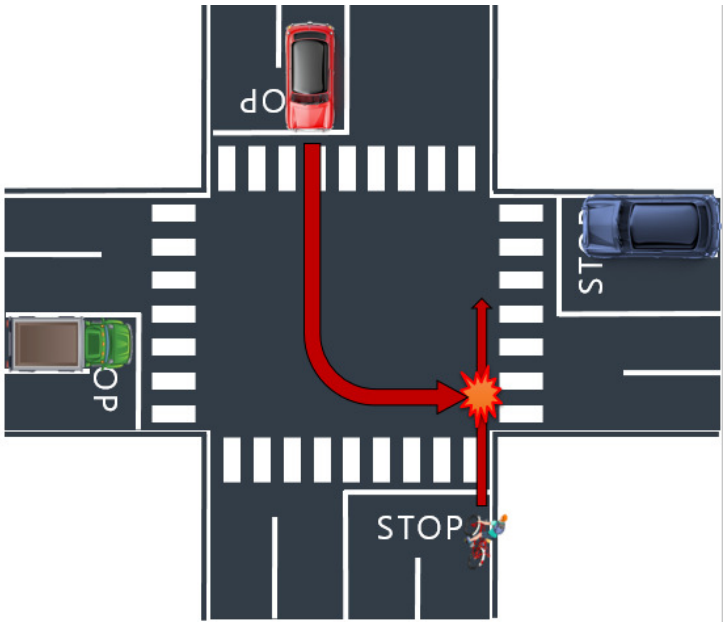

Figure 4.1: Left turn scenario.

4.2.1 Left Turn Scenario

This scenario involves a vehicle turning left at an intersection and the driver failing to yield to a cyclist that approaches the intersection from the opposite direction, or getting in the trajectory of a cyclist approaching on the same direction. In both situations, the cyclist and the driver start their maneuvers on opposite sides of the road. Figure 4.1 displays the maneuver with a cyclist approaching on the opposite direction.

In the case of bicyclists coming in the same direction of the vehicle, blind spots or objects obstructing the view of the motorist could be a contributing factor to the failure to detect them.

4.2.2 Right Turn Scenario

The right turn scenario involves a vehicle failing to yield a bicyclist that rides straightforward in the same direction. It most commonly takes place when a vehicle and a bicycle arrive at the same time at an intersection with at least three branches [72]. Figure 4.2 shows the driver's and cyclist's maneuvers

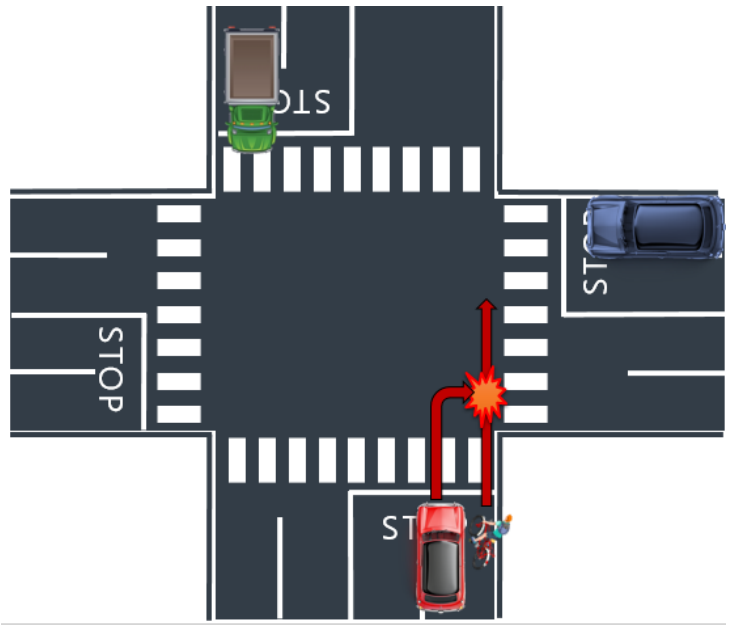

Figure 4.2: Right turn scenario.

involved in the scenario.

Among truck drivers, one of the main contributing factors of this scenario could be that of failing to look/see the bicyclist going straight forward while turning [73]. Blind spots may be the cause, or the contributing factor, of this type of human error.

Cooperative systems, also exploiting infrastructure-based sensors, could be useful to improve detection of cyclists and may assist drivers in minimizing blind spots and "looked-but-failed-to-see" errors. New technological solutions aimed at detecting bicyclists and conveying this information to the driver may play an important role in the prevention of these eventual detection failures and, consequently, of the potential collisions.

4.3 Bicyclists Detection Technologies

The statistical analysis has revealed how accidents occur due to a lack a visibility between the road users, especially at junctions and in the presence of large vehicles. This section aims at describing the main technologies capable

Table 4.1: On-vehicle available technologies.

Technology	Pros.	Cons.
Cameras	Accurate detection and users' discrimination	Difficult operation in bad weather conditions, false alarms
Thermal cameras	Accurate detection and users' discrimination	Cost, false alarms
Ultrasonic sensors	Reliable detection in every weather condition	Poor users' discrimination
Inductive loops	Average users discrimination	Under-surface. Large infrastructure. Very low-range
LIDAR	Accurate detection and users' discrimination	Very high cost, complex deployment and complex data processing
Radar (on-air)	Reliable detection. Good angular resolution	Poor users' discrimination
Radar (under surface)	Average users' discrimination	Under-surface. Battery replacement issues if not powered
RFID	Accurate detection and perfect users' discrimination	Tags needed. Poor angular and ranging resolution
GPS	Localization of different users	GPS receivers needed. Medium localization accuracy, latency

of improving the *visibility* then increasing the safety of road users. Specifically, we will distinguish between *on-site* and *on-vehicle* solutions depending on the sensors' location. For each solution the advantages and disadvantages will be illustrated.

Table 4.1 reports some examples on the panorama of technological solutions for detection of bikes. Sensors, for example cameras of radars, can be placed on the infrastructure (i.e., on-site) or on the vehicles. Most of the detection approaches do not require technology on bike (e.g., radar, cameras or sonar) while other approaches require on-bike modules (e.g., global positioning system (GPS) receivers of radio frequency identification (RFID) tags).

For what concerns the characteristics of the different technologies, narrow-beam radars or sonar-based systems are efficient for detecting the presence of a user in a bicycle-path and providing an alert sign. However, they are not effective in enabling potential collision prediction or multi-target discrimination at junctions. On the other hand, cameras and especially thermo-cameras are effective in large road junctions, and can be used for trajectory (collision) prediction. Some weather conditions make detection with normal cameras difficult (e.g., darkness or rain can decrease the capability of identifying cyclists). Thermo-cameras may solve in part this problem, but they are currently still quite expensive and might fail during the summer because the high temperature of the asphalt might hide the presence of persons. Inductive loops and under-surface radar are effective but have a limited range,

infrastructural problems and poorer target discrimination.[2]

A common shortcoming of all these passive technologies is that there is always a not negligible probability of false alarms that may discourage users to trust the system. On the other side, the main advantage is that they do not require dedicated hardware on bike.

Active technologies, such as GPS and RFID, that require bikes equipped with dedicated technology, respectively, a GPS receiver and a RFID tag, eliminate the presence of false alarms but do not provide a sufficient localization accuracy. Moreover, GPS is expensive, battery hungry, and is characterized by a high response delay that prevents its use in RA.

As regards the on-vehicle technologies, they are often based on proximity sensors, camera or radar and they provide warnings to other road users, such as cyclists, by means of visible alerts. Communication operations between vehicles, infrastructure and cyclists/pedestrians are not provided by such systems as the majority of them relies on LEDs to prevent a possible collision with other road users. Moreover, the few on-vehicle solutions sometimes lack of reliability in terms of misdetections and false alarms.

To conclude, the main disadvantages of the today's solutions also represent incentives for future improvements. Specifically we envisage the following desired capabilities:

- Sub-meter localization and tracking with extreme low-latency ($< 500\,\text{ms}$);
- Possibility to detect and discern different road users (reduce or eliminate false alarms);
- Possibility to predict road users' trajectories;
- Possibility to communicate with other road users (e.g., cyclists or pedestrians) and warn them in a specific way.

Based on the above considerations, it clearly emerges the need of a low-cost, low-latency detection and sub-meter localization and communication

[2]However, they are a good strategy for traffic lights operations. In fact, they are often adopted to detect road users approaching at a specific point, e.g., a junction.

technology to support new generation RA systems capable of predicting the situation of collision and provide a suitable feedback to the vehicle as well as to the cyclist via ad-hoc HMIs.

In the following section we propose on-site and on-vehicle architectures using the UWB technology.

4.4 Proposed System Architectures and Technologies

Inspired by the shortcomings emerged in the current available technologies, in this section we will describe a localization system to improve cyclists visibility and achieve sub-meter accuracy thus guaranteeing an increased safety for the road users.

The proposed architecture is based on active, small, and low-cost tags on the bikes. Contrarily to their passive counterparts, active tags are equipped with a transmitting section and are able to send and/or receive interrogation signals thus also enabling the possibility to communicate with the vehicle and/or the infrastructure and to include HMI.

Tag detection and tracking is performed by analyzing the data exchanged by the tag and a set of reference nodes, called *anchors*, placed in known positions in the space, forming the so called real time locating systems (RTLS). In the following two architectures will be presented. The main difference of the proposed architectures lays on where *anchors* are deployed.

More specifically, we consider an *infrastructure-based* architecture with anchors placed in the correspondence of the crossing's infrastructure (e.g., at traffic-lights) and a *vehicle-based* architecture with reference nodes mounted on vehicles (e.g., cars and trucks). In both solutions several anchors interact with tags by performing different kinds of measurements, as it will be clarified in Sec. 4.4.1; then a central unit gathers the information from all anchors, and fuses it to estimate the position of each tag (i.e., each bike). According to this scheme, in the first architecture the central unit is placed on the infrastructure, while in the second, it is mounted on the vehicle.

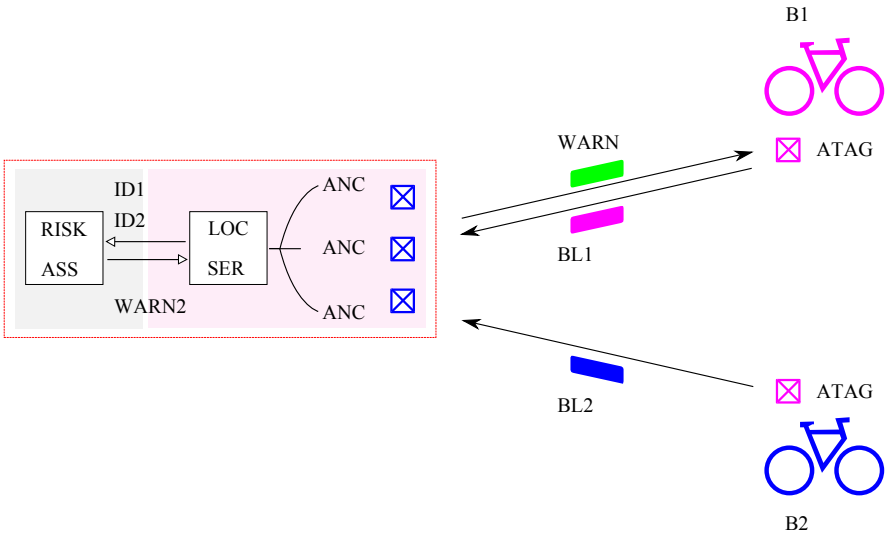

Figure 4.3: Proposed system using active UWB tags.

In the following, we will introduce the underlying UWB technology and communication protocol and then, both architectures will be detailed.

4.4.1 UWB Technology and Communication Protocol

While the IEEE802.11p standard is emerging as the key technology for vehicular communications, a similar counterpart for high-accuracy positioning and tracking for intelligent transportation systems has not been presented yet. Our proposal is to consider UWB signals to achieve the target submeter positioning accuracy. In accordance to the FCC definition, UWB signals are characterized by a bandwidth larger than 500 MHz. The classical and simplest method to obtain UWB signals is by means of impulse radio UWB (IR-UWB). In an IR-UWB system, a sequence of short pulses (typically with duration around 1 ns) is transmitted per information bit in order to collect more energy and allow multi-user access [64]. The short duration of the pulses guarantees a fine resolution in signal time-of-arrival (TOA) measurement and multipath discrimination so that time-based localization algorithms can benefit to obtain accurate localization estimates [67, 74]. The UWB technology is currently utilized as baseline in high-performance short-range RTLS using active tags according to the IEEE 802.15.4a and IEEE

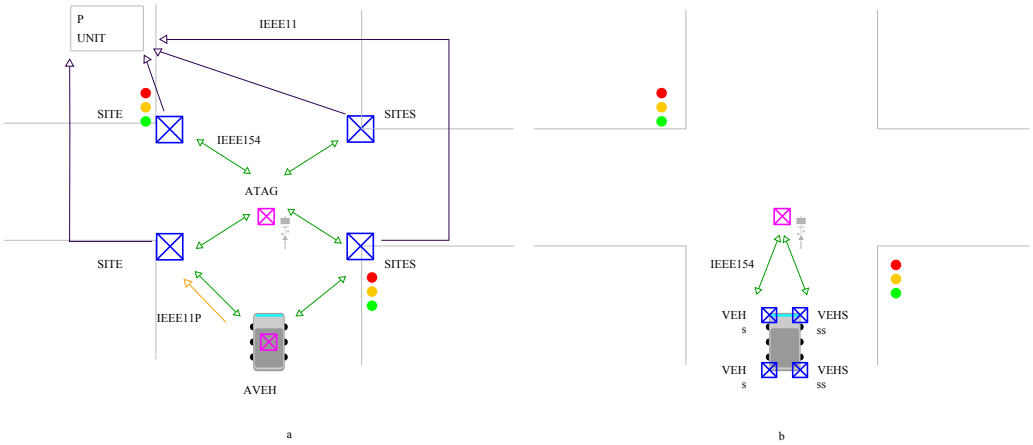

Figure 4.4: Localization architectures with reference nodes placed on the infrastructure (a) or on the vehicle (b).

802.15.4f standards as well as proprietary schemes [65, 75].

In Figure 4.3, the conceptual architecture is shown. As it is possible to see, the different road users periodically transmit a blink packet following the ISO/IEC 24730-62:2013 [76] standard containing their unique 64-bit identification (ID) to the on-site and/or on-vehicle anchors using the UWB link. In our implementation, once a tag enters the monitored area, it is detected by the anchors and the localization server assigns it a temporary 16-bits ID (*tag index*). Such a tag index is used to address the tag until it exits the area and it allows to drastically reduce the size of the exchanged packets during the tracking process thus reducing the risk of packets collision. The anchors receive these blink packets and, thanks to ad-hoc processing schemes determine the road users' positions and other tracking parameters (*localization engine*). Then, if the RA unit predicts a potential dangerous situation, a warning can be sent to a specific bike in order to activate the on-bike HMI.

In the following the two architectures proposed will be analyzed in order to better put in evidence their main peculiarities.

4.4.2 Infrastructure-based Architecture

The infrastructure-based architecture is schematically depicted in Figure 4.4-(a). As previously mentioned, in this solution, anchors are placed on the

infrastructure, for example at the corners of the junction in correspondence of the traffic light towers, while active tags are on bikes. Note that vehicles can be equipped with active tags as well, and thus, they can be tracked by the infrastructure sensors. This allows drawing a virtual map of all the various road users.

Given their active nature, tags periodically send interrogation signals compliant with the IEEE 802.15.4a standard to the anchors. The exchanged messages contain the ID thanks to which each road user can be discriminated. The communication between vehicles and the infrastructure can be ensured by IEEE 802.11p links, whereas infrastructure-to-bike communication is enabled by the UWB IEEE 802.15.4a link.

Each anchor node receives the UWB signals from bikes and vehicles while keeping the synchronization with the other anchors. Starting from the sensed data, the processing unit performs both a localization and RA process, as reported in Figure 4.3. The former consists in estimating the position, relative speed, and acceleration of each active tag. These data are then communicated to the RA unit whose main task is to establish the probability of collisions or more generally the presence of some risky situation. For instance, vehicles can inform the infrastructure whether they intend to start a dangerous maneuver, e.g., the right and left turn, via a IEEE 802.11p link.[3] Based on this information and on the estimated position of all road users present in the junction, the RA unit could detect a dangerous situation and send back a warning message to the involved vehicle and to the cyclist. The on-bike device is able to activate its HMIs (e.g., a visible or audible alert) to proper inform the bicyclist of the potential dangerous situation.

The main advantage of this solution is the good localization coverage that can be achieved thanks to deployment of anchors at the corners of the area to be monitored. On the other hand, this architecture is suitable in situations in which the time needed to prevent a bicycle running into a possible dangerous situation could be relaxed, as for example in the left turn scenario, because of the potentially not negligible latency introduced by the vehicle-infrastructure-bike interaction.

[3] An alternative option could be that of using the UWB technology.

4.4.3 Vehicle-based Architecture

Figure 4.4-(b) reports the vehicle-based architecture. Contrarily to the previous described scenario, here vehicles are equipped with anchors. This means that the processing unit, consisting of the localization and RA engines represented in Figure 4.3, is mounted on vehicles.

The on-vehicle anchors receive the interrogation signals from the on-bike active tags in accordance with the UWB IEEE 802.15.4a standard. Thanks to these interrogations, the location engine running on-vehicle is able to determine the position and other navigation parameters (e.g., speed, acceleration) of the bikes with respect to the vehicle. Then, based on the relative coordinates of both vehicle and bicycle, the RA module, still working on-vehicle, can determine whatever a dangerous situation is present or not and take proper countermeasures. As before, exploiting the same IEEE 802.15.4a links adopted for bicycle localization, the vehicle can send warnings to the on-bike tag regarding the risk and properly activate the on-bike HMI.

The main novelty of this solution is that anchors are closer to each other in comparison with the infrastructure-based approach. Therefore, the tags are always located outside the perimeter described by the anchors. As known in localization theory, this is not the optimal configuration for a localization system, since geometric dilution of person (GDOP) issues can degrade the localization accuracy [77]. For this reason, in 4.5.3, the investigation of the impact of the geometry will be carried out, in order to understand the scale of performance degradation. On the other hand, the main advantage of such a configuration is that bicycle localization can be performed without the need of a specific infrastructure placed at the intersection and no false alarms occur. Moreover, this architecture is more promising when the decision about a possible risky situation and the relative warning message have to be rapidly conveyed to the vehicle driver and to the on-bike module thanks to the direct interaction between the two road users. For example, it is well suited in the right-turn scenario where a stringent latency requirement has to be met.

4.4.4 Enhanced Services

The localization system described in the previous sections could also enable new services as for example those related to green-wave scenarios. Specifically, different green-wave approaches could be implemented: one could be aimed at informing cyclists about how to adjust their speed in order to get the green light at the next junction, while another possibility is that of synchronizing traffic lights based on the number and speeds of cyclists estimated to arrive at next intersections. For this kind of application, the infrastructure-based architecture is the most promising one. Indeed, the anchor nodes placed on the crossing area can monitor the number, direction, relative speed and acceleration of cyclists at the exit of the considered intersection. Based on these parameters, a dedicated processing unit can estimate the number of bikes and the time needed to arrive at the next junction and thus, the traffic lights can be programmed accordingly to allow a safer transit of cyclists. The mechanism through which the cyclists are localized and tracked is the same as described in Sec. 4.4.2.

4.5 The UWB Tracking Sub-system

In this section, the RTLS proposed and implemented for this application is described. As already introduced, the localization process is based on the capability of extrapolating positioning information starting from the UWB signals exchanged between nodes. Specifically, anchors receive the interrogation signals compliant with the IEEE 802.15.4a standard sent by active tags powered by an on-board battery and including a radio transceiver with transmitting/receiving capability.

4.5.1 On-bike Module

The on-bike module implemented, shown in Figure 4.5, is mainly composed of an IEEE 802.15.4a transceiver connected to a UWB antenna. The transceiver communicates via serial peripheral interface (SPI) interface with a microcontroller unit (MCU). The MCU determines the sensor module behavior

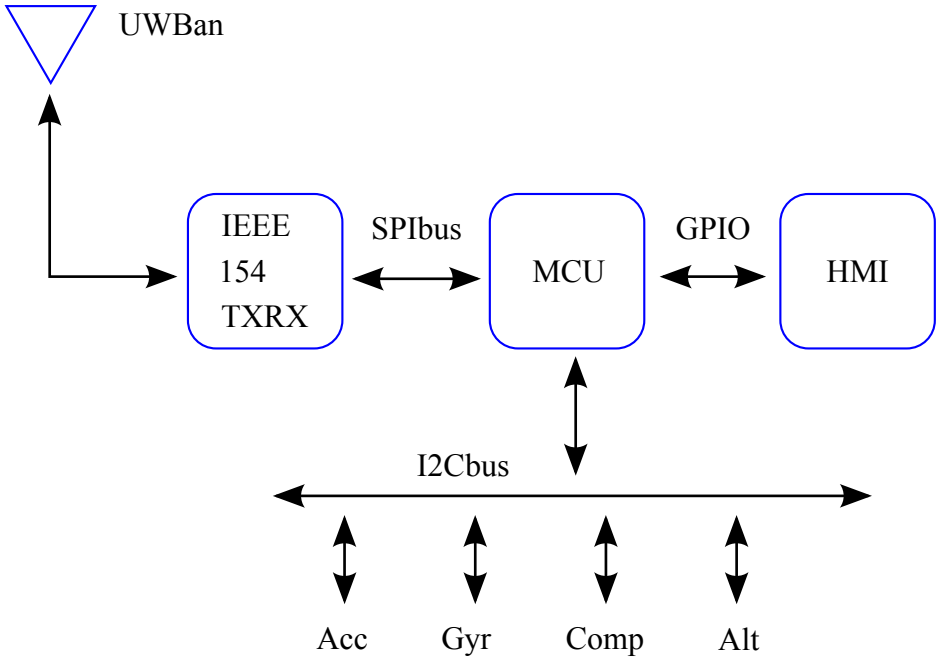

Figure 4.5: On-bike tag module.

and implements all the functionalities needed for enabling localization and communication with vehicle and/or infrastructure. Output ports of the MCU are then adopted for activating the on-bike HMI. As reported in figure, the on-bike module is also equipped with additional 3D sensors (i.e., 3-axis accelerometer, 3-axis gyroscope, 3-axis magnetometer, and pressure sensor) whose output can be processed by the RA unit present on vehicle and/or infrastructure.

All the sensors are periodically interrogated by the MCU. After the interrogation cycle, the sensor outputs are sent via the UWB link as payload of the blink packets to the reference nodes and thus made available for the location process running on vehicle or on infrastructure. The outputs of the localization estimation process consist of the bicycle ID, position coordinates, velocity, acceleration, absolute orientation, and the positioning accuracy.

The on-bike module also contains an HMI to proper inform the bicyclist of a potential danger predicted by the RA unit (either considering bicycle-vehicle interaction or bicycle-infrastructure interaction or simple detection by on-vehicle or infrastructure sensors). The bicycle HMI should be designed

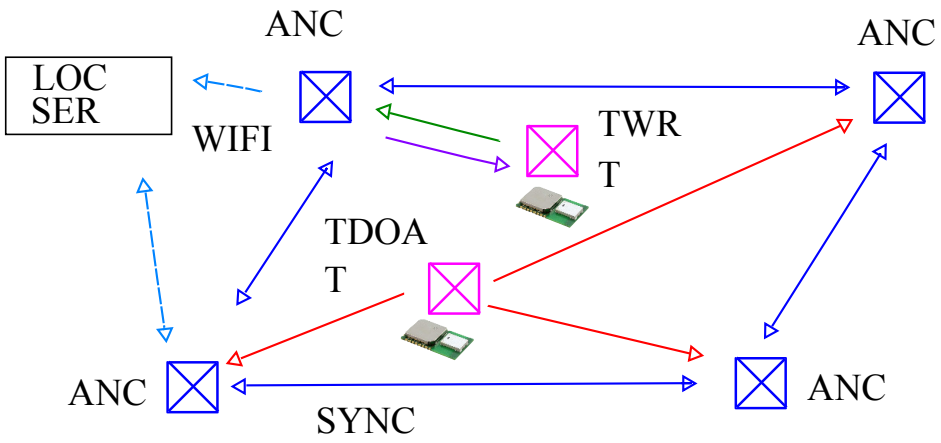

Figure 4.6: Localization scheme using UWB TDOA and TWR tags.

such that it requires minimal attention and does not distract the cyclist. Examples of HMIs are a flashing light display, an auditory alert or a combination of both. The implementation of these should take into account the lighting conditions and background noise when cycling next to a truck. Other possibilities are, for example, HMIs based on helmet or handlebar vibrations. Nevertheless, a detailed analysis of on-bike HMIs is out-of-the-scope of this paper whose main aim is to describe the architectural aspects of the system.

4.5.2 Localization and Tracking Methods

The considered UWB RTLS is capable of providing sub-meter localization accuracy without resorting to costly and less accurate technologies such as GPS. The system deployment mainly consists on the installation of a sufficient number of anchors placed in known positions. The number of anchors depends on the area to be covered: the larger is the space where tags can be placed, the greater the number of anchor nodes should be to guarantee an acceptable level of tracking accuracy.

As shown in Figure 4.6 the main approaches to infer tag's position is by means of two way ranging (TWR) and signals time difference-of-arrival (TDOA) estimation [77]. TWR is based on packet exchanges between a couple of nodes (e.g., the tag and one of the anchors). The round-trip time of this ping-pong is measured and the distance is estimated (*ranging*). This

process must be repeated for any anchor and tag couple. Considering at least three reference nodes performing the TOA measure, it is possible estimate the position of the device resolving a triangulation problem.

The TDOA principle lies on the idea of discovering the position of the transmitting tag by using the difference in time at which the signal arrives at multiple anchors. Therefore, the tag is expected to be placed on a hyperbole where the anchors are in the foci of the curve. Having at least three anchors (i.e., two TDOA measurements) it is possible to estimate the position of the tag. This requires a very accurate synchronization among nodes that has to be guaranteed by distributing a common clock via cable or wirelessly.

If from one side, TWR provides a higher positioning accuracy thanks to the possibility to better counteract oscillators clock drifts, from the other side TDOA permits a drastic reduction in packet exchanges between tags and anchors, thus allowing a significant improvement in terms of refresh rate and multiple tags management. In fact, in TDOA each tag sends a very short blink packet which is received by the network of anchors. Due to the short duration of the blink packet emitted, a large number of tags can be managed at the same time, with both random channel access (e.g., aloha-based solutions) or time-scheduled transmissions (e.g., time division multiple access (TDMA)). In this manner, differently from the TWR scheme, a single uplink tag-anchor is sufficient for positioning (the downlink channel is then used only for infrastructure-to-bike or vehicle-to-bike communication). This solution allows building an extremely simple architecture for the tag, since all the heavy processing for localization is demanded to the central unit placed on infrastructure or vehicle. Moreover, the short blink packets contribute in maintaining the power consumption at tag side low, thus enabling battery-powered, low-cost solutions.

We implemented both the TDOA (with wireless synchronization) and TWR to make some comparisons in terms of performance, as it will be presented in the numerical results. At central unit side, based on the collected measurements, the tag position calculation is performed through state-of-the-art Bayesian filters. Specifically, we implemented a Bayesian filter using the particle filter approach employing measurements fusion mechanisms and

clock drift compensation techniques to enable TDOA. The overall latency is less than 500 ms.

Figure 4.7 shows the classical two steps constituting the Bayesian filtering iterations. As it can be seen, the main objective is to infer an estimate of the state (e.g., tag's position coordinates, absolute orientation, velocity, etc.) and its covariance matrix (i.e., a measure of the estimation uncertainty). More specifically, the first step consists in performing a prediction based on the history of the collected measurements (*time update*). Once new measurements become available (*measurement update*), an estimation correction phase can be undertaken based on the computed Kalman gain which is an indicator of the measurements and prior predictions reliability. In our approach, the observation model is modeled as a uni-modal Gaussian distribution centered in the difference between the estimated TDOA and the true TDOA and with a TOA error standard deviation of 0.2 m characterized from measurements. Regarding the mobility model, we assumed two different solutions depending on the availability of the speed information. In the speed-unawareness case, the density function describing the mobility model corresponds to a Gaussian distribution centered in the previous estimated position whereas in the second case a speed learning approach is adopted where the speed is evaluated from earlier estimated positions with a sliding window. For further details, the reader is invited to refer to [78]. Note that, if tags broadcast their sensor data, inertial measurements fusion techniques can be adopted for improved localization accuracy [78].

4.5.3 Impact of Architecture on the Localization Accuracy: Performance Limits

As anticipated in Sec. 4.4, a discussion about the anchor nodes placement is necessary. In fact, it is well known from the localization literature how the geometrical configuration of anchors impacts the localization accuracy. Such effect, known as GDOP, arises when combining different measurements and can worsen or improve the performance in given position of the space where the tag could be present.

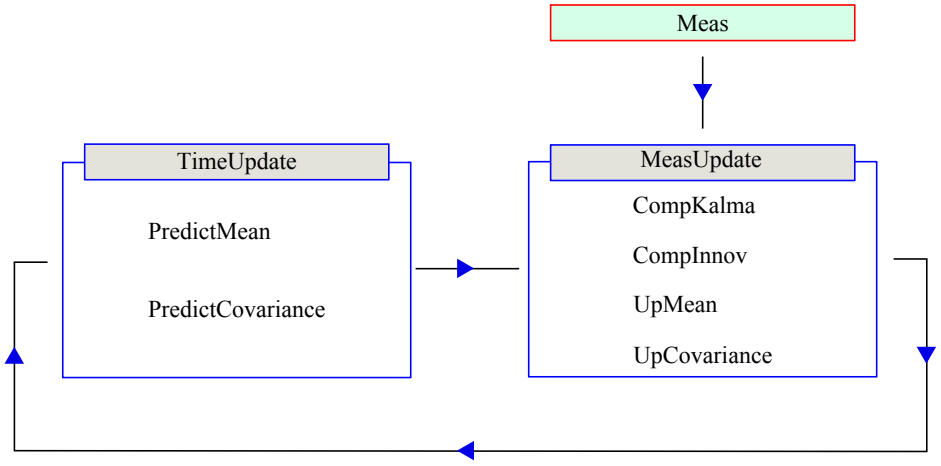

Figure 4.7: Bayesian filtering iterations.

In order to access the potential localization accuracy, in particular in the vehicle-based infrastructure which is known unfavorable from the GDOP point of view, a theoretical analysis based on the position error bound (PEB) is here carried out [79, 80]. PEB is a tool for determining what is the theoretical best positioning accuracy that an algorithm can provide starting from a certain setting in terms of measurements and geometrical configuration of anchors and tag.

In Figure 4.8 the PEB for the infrastructure-based architecture is shown. Specifically, a standard deviation of 20 cm in the ranging is considered, and the presence of 4 anchors placed in the correspondence of the traffic lights in a $30 \times 30\,\mathrm{m}^2$ junction. Anchors are depicted with brown circles and are placed in coordinates (20,10), (20,20), (10,20), (10,10). From the figure, it is possible to see how the localization error is equalized in the entire scenario, always between 10 and 20 cm. On the other hand, Figure 4.9 shows the PEB for the vehicle-based architecture. Again, a ranging standard deviation of 20 cm is considered, and the presence of 4 anchors placed at the corners of (i) a vehicle (small truck) of size $2 \times 5\,\mathrm{m}^2$ and (ii) vehicle (medium-sized truck) of size $2.5 \times 8\,\mathrm{m}^2$. In both cases the truck is assumed in the middle of the scenario. From the figures, it is possible to notice the GDOP effects, which are more pronounced in the direction of the vehicle. In fact, the localization error increases moving away from the vehicle, and such performance degradation is

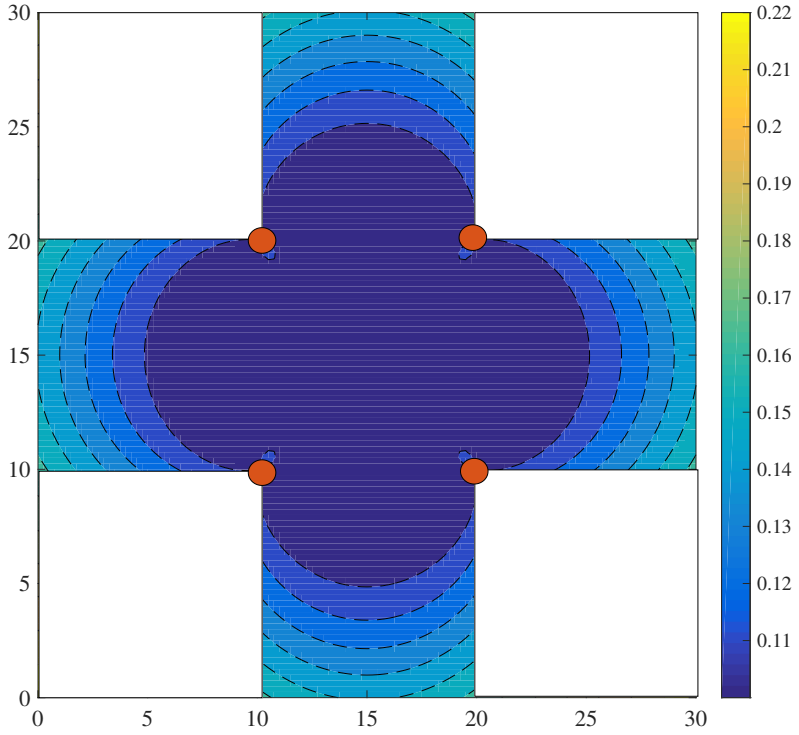

Figure 4.8: PEB [m] for infrastructure-based positioning.

less severe in the orthogonal direction. This is mainly due on the geometrical placement of the anchors along the long vehicle. When adopting vehicle-based architectures, is then fundamental to consider location estimates only in a certain area of some meters around the vehicle, where the location process is effective.

It is important to notice that the final localization accuracy is also impacted by propagation conditions, in particular by the presence of NLOS channels between tags and anchors. Such conditions could occur for several reasons. In an infrastructure-based solution, NLOS condition could be caused by the presence in the crossing area of large trucks blocking the tag-to-anchor signal. Differently, in the vehicle-based solution, the NLOS channel could arise due to the intrinsic shape of the vehicle, which obstructs some of the anchors placed on it. When NLOS channel conditions are present, the

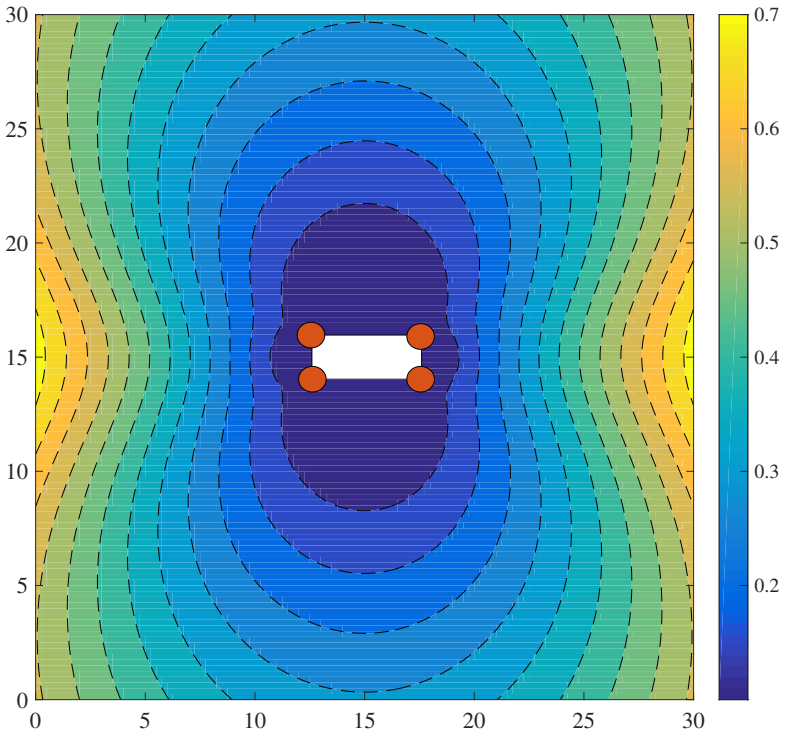

Figure 4.9: PEB [m] for vehicle-based positioning (small truck).

localization accuracy decreases and ambiguities in the position can arise due to an insufficient number of measurements. However, thanks to the considered tracking scheme, where a location engine continuously tracks a given tag starting from new measurements and the prior location estimation, ambiguities can be strongly mitigated. Moreover, NLOS conditions can be reduced by deploying a larger number of anchors nodes and by fusing inertial data. Notice that, thanks to the considered TDOA scheme, this translates only on an increased complexity at the processing unit side, with no modifications required at tag side and no additional complexity.

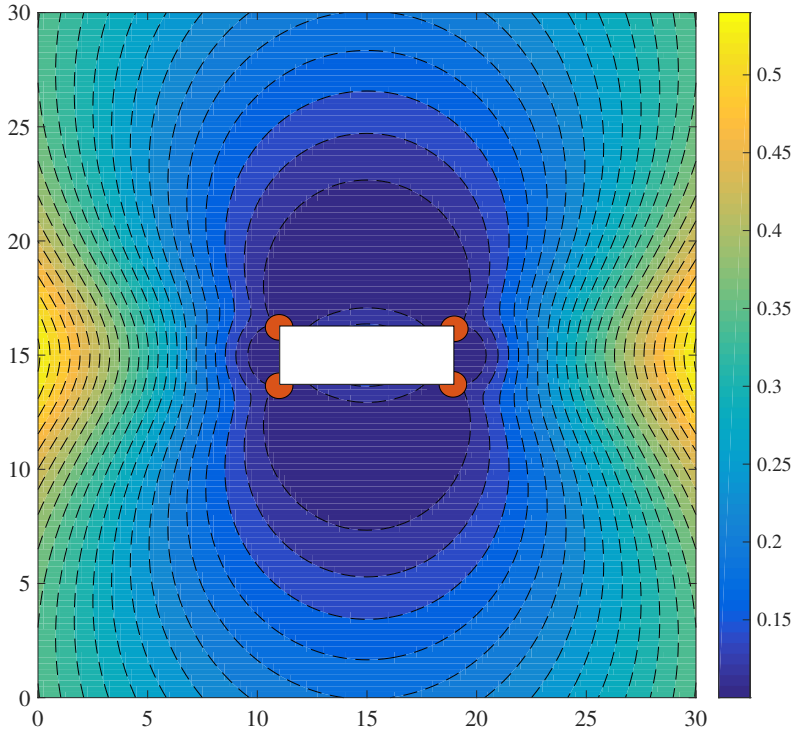

Figure 4.10: PEB [m] for vehicle-based positioning (large truck).

4.6 Experimental Results

In this section preliminary experimental results using the implemented localization system are described in order to assess the localization accuracy in static and dynamic scenarios. The purpose is also to analyze the performance degradation when considering TDOA with wireless synchronization instead of TWR. The measurement campaigns have taken place in the CASY (Center of Complex Automated SYstems) indoor flight arena at the University of Bologna premises.

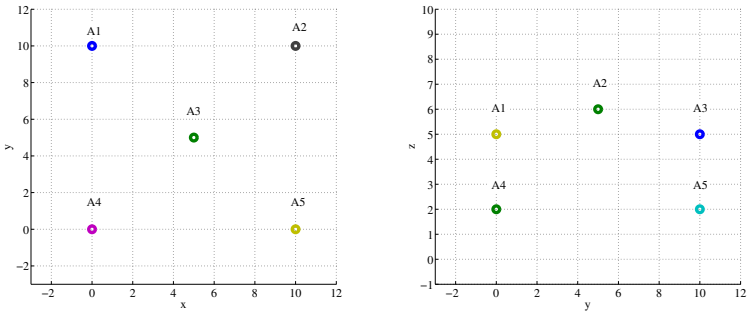

Figure 4.11: Anchors deployment: $x-y$ plane on the left and $y-z$ plane on the right.

4.6.1 Measurement Setup

The measurements have taken place in an area of $11 \times 11 \times 6$ m^3 where tags can move on the $x-y$ plane with a z coordinate that ranges from 1 to 2 m. A set of 22 infrared cameras (VICON Bonita 10) installed in the monitored area have been adopted to infer the exact tags' positions as they can achieve a millimeter localization accuracy. 9 anchor nodes are placed on the infrastructure, according to the deployment represented in Figure 4.11. Specifically, we have considered the following deployments:

- All anchors: when all the reference nodes ($\mathrm{A}_i \quad i = 1, 2, \ldots, 9$) are active;
- Lower Circle: only $\mathrm{A}_i \quad i = 1, 2, \ldots, 4$;
- Upper Circle: only $\mathrm{A}_i \quad i = 5, 6, \ldots, 8$;
- Mixed: mixed combination between lower and upper circle. For example $\mathrm{A}_1, \mathrm{A}_3, \mathrm{A}_6, \mathrm{A}_8$.

As mentioned before, the number of active anchor nodes is one of the parameters that determine the localization accuracy of the system. For this reason a preliminary study concerned the localization performance as a function of the number of reference nodes in static conditions, i.e., with the tag placed in a set of fixed positions. For each test position in space, 500 estimates have

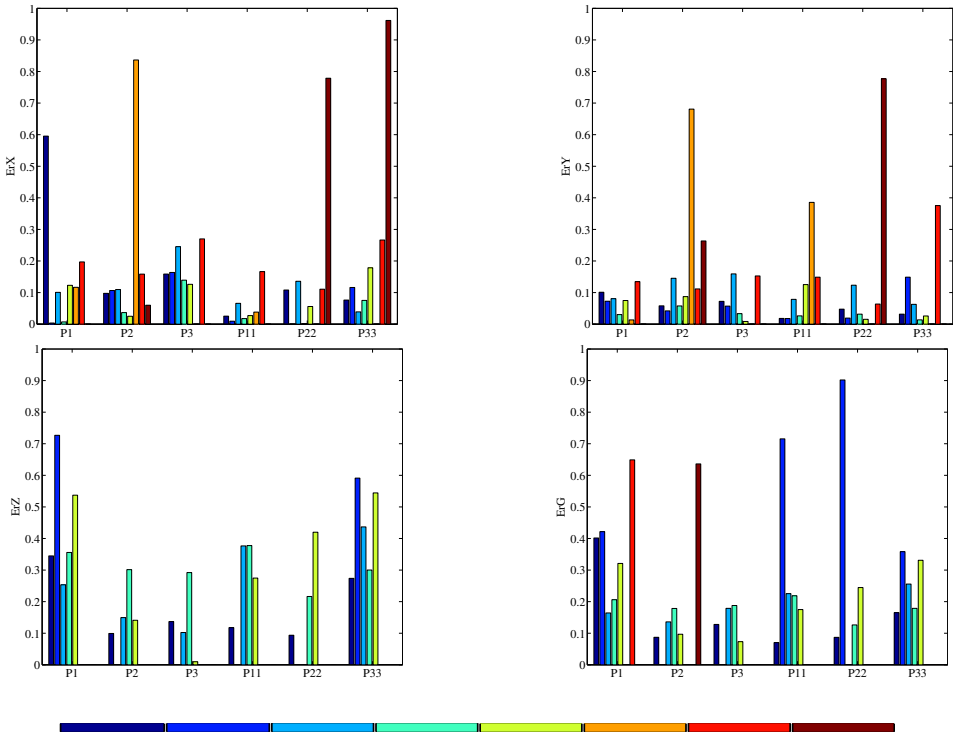

Figure 4.12: Localization error considering static tags.

been collected using a personal computer running the localization algorithm based on Bayesian filtering.

4.6.2 Results

The performance metric adopted for assessing the localization performance is the mean absolute error (MAE) defined as

$$\mathsf{MAE} = \frac{1}{N} \sum_{i=1}^{N} \|\mathbf{p} - \hat{\mathbf{p}}_i\|_2 \tag{4.1}$$

where $\mathbf{p}$ represents the true tag position as derived by the VICON system while $\hat{\mathbf{p}}_i$ is the estimated position. N represents the number of estimates for each set of measurements.

In static configurations, the tag is placed in different fixed unknown po-

Table 4.2: Localization error averaged over different tag positions.

Loc. technique	Anchors config.	x Error [m]	y Error [m]	z Error [m]	Global error [m]
TWR	All anchors	0.26	0.06	0.20	0.15
TWR	Lower-circle	0.44	0.07	1.15	0.83
TWR	Upper-circle	0.13	0.11	2.55	0.74
TWR	Mixed	0.06	0.03	0.31	0.18
TDOA	All anchors	0.10	0.07	0.37	0.20
TDOA	Lower-circle	1.41	1.22	7.49	4.34
TDOA	Upper-circle	0.20	0.19	6.23	3.13
TDOA	Mixed	1.97	2.23	5.44	3.18

sitions inside the area. In the following, we will indicate with $\mathbf{p}^{(j)}$ with $j = 1, 2, 3$ the three testing positions in the $x - y$ plane while as regards to the z coordinate, two different heights, i.e., $z = 1$ m and $z = 2$ m, have been taken into account. For each tag's position, we aim at analyzing the localization performance as a function of the number of anchors and of the chosen localization technique.

Figure 4.12 reports the MAE for each tag's position and coordinate as function of different anchors' deployments and localization approaches. Only anchors geometric configurations resulting in a sub-meter localization error are reported. As one can observe, the TWR technique is more accurate in estimating the x and y coordinates then TDOA, and this is particularly verified for anchors at the same height. Such degradation of the localization performance in TDOA is also due to anchors synchronization mismatches but it can be counteracted using an increased number of reference nodes. When considering a proper anchors deployment TDOA results are satisfactory for the application under consideration.

Table 4.2 reports the mean square error averaged over the tag positions and shows how the UWB localization system is able to infer the tag positions with a centimeter localization accuracy also in indoor environments, especially when operating in TWR fashion and with a high number of anchors. We expect that in outdoor conditions the performance could improve because of the absence of strong multipath caused by signal reflections on the walls as indoor.

In dynamic configurations, the tag was free to move in the flight arena.

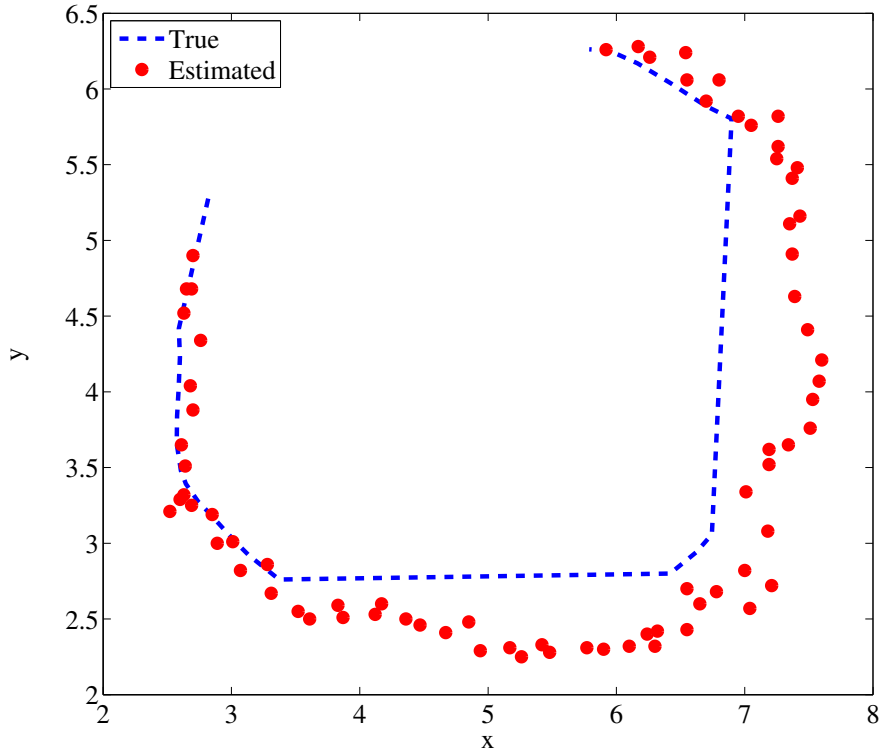

Figure 4.13: Localization error considering dynamic tags.

During this test the tag did not follow only a longitudinal path but also performed rotational movements and modifies its height. The average speed of the tag is 4.5 km/h and the distance covered is approximately 100 m.

Figure 4.13 reports the true and estimated tag trajectories. It is possible to observe that the estimated trajectory, marked with red circles, diverges from the true one, indicated with a dashed blue curve, especially in correspondence of rapid changes of direction. Nevertheless, this inconvenience could be solved by refining the mobility model in the Bayesian tracking algorithm which is one of future tasks.

4.7 Conclusions

Starting from a deep analysis of road users' behavior and of typical dangerous situations, in this paper two architectures performing RA and providing

a feedback to road users and, in particular, to cyclists on potentially dangerous situations have been presented. Reference nodes can be placed both at the junctions (*infrastructure-based architecture*) or on vehicle (*vehicle-based architecture*). To enable such architectures, we proposed a localization system based on the UWB technology capable of guaranteeing high-accuracy localization and tracking, in which bikes are equipped with low-cost and low-complexity active tags and with HMI. Preliminary experimental activities have been conducted to assess the feasibility of the proposed solutions in static and dynamic conditions. Results show the possibility of achieving centimeter-level localization accuracy and good tracking capabilities, even in harsh propagation environments.

Conclusions

The main topic investigated in this thesis is related to characterization of the performance of D2D wireless networks. Given this broad objective, analytical framework models based on stochastic geometry have been proposed. One of them deals with the study of the coverage probability of both cellular networks and D2D networks whereas the others are related to dynamic mobility models in which the effects of blockages on the link lifetime have been studied. On the other hand, the experimental activity based on UWB using passive tags has been presented in which a localization system based on the ultra-wideband (UWB) technology and high-level architectures to improve the cyclists safety has been proposed.

Specifically, in chapter 1 a new analytical framework based on stochastic geometry for analyzing the coverage probability in coexisting cellular networks and D2D networks has been proposed. The closed-form expressions for coverage probability based on the spatial HPPP model, for the distribution of BSs, and for any non-uniform distribution of D2D links to capture the tendency of D2D users to work in groups have been derived. Both power control, compensating path loss and shadowing, and fixed power strategies for the D2D link have been investigated. The reciprocal impact of D2D and cellular communications on the downlink coverage has been investigated as a function of the D2D links maximum range and density. The analytical framework model has been used to get engineering insights regarding to the amount of the traffic that could be offloaded through D2D communications. Finally, the accuracy of our theoretical analysis has been corroborated by simulation results.

In chapter 3 a stochastic analysis of the communication link lifetime be-

tween a mobile device and its serving AP in the presence of n classes of randomly located objects characterized by different densities and sizes has been presented. Closed-form expressions of the link lifetime CDF and corresponding average have been derived in which these expressions indicate the exponential behavior of the link lifetime as a function of obstacle's size and allowed to get insights on the interplay between obstacles' density, radius of objects, and user's distance. The validity of the analytical framework have been confirmed through comparisons with simulation results .

In chapter 4 a different category of D2D network related to road users has been considered two architectures performing risk assessment (RA) and providing a feedback to road users and, in particular, to cyclists on potentially dangerous situations have been presented. Reference nodes can be placed both at the junctions (*infrastructure-based architecture*) or on vehicle (*vehicle-based architecture*). To enable such architectures, I proposed a localization system based on the UWB technology capable of guaranteeing high-accuracy localization and tracking, in which bikes are equipped with low-cost and low-complexity active tags and with HMI. Preliminary experimental activities have been conducted to assess the feasibility of the proposed solutions in static and dynamic conditions. Results show the possibility of achieving centimeter-level localization accuracy and good tracking capabilities, even in harsh propagation environments.

In the future work, I will explore the D2D underlay multi-tier multi channel downlink cellular networks and possibly using multiple antennas, which is more complicated due to the mutual interference between D2D links and multi-tier cellular links. In addition, the investigation of the blockage lifetime is of interest. The extension towards this direction can be done by using similar argument.

Regarding to experimental activity, the next activity foresees the assessment of the two architectures in a real outdoor scenario by following a multidisciplinary approach with the two-fold objective of analyzing road users behaviors and testing user-friendly technologies to enhance cyclists safety. The behavioral investigation takes a central role in evaluating different HMI solutions, to alert cyclists of dangerous situations in order to enhance their

comfort and safety, without being source of distractions or annoying the final users, thus establishing the technology acceptance. The behavioral analysis plays a crucial role because it puts the final user at the center of all the investigation and the ultimate aim of the technologies that will be developed.

Publications

Journal papers

- [J1] A. Al-Rimawi, and D. Dardari, "Analytical Characterization of Device-to-Device and Cellular Networks Coexistence ", submitted to *IEEE Transactions on Wireless Communications with Minor Revision*, October, 2016.

- [J2] A. Al-Rimawi, and D. Dardari: "Characterization of Link lifetime and Blockage lifetime", *in preparation for submission*, 2016.

- [J3] A. Al-Rimawi, and D. Dardari: "Characterization of Link lifetime under Human Blockage Effects", *in preparation for submission*, 2016.

- [J4] D. Dardari, N. Decarli, A. Guerra, A. Al-Rimawi, V. Puchades, G. Prati, M. Angelis, F. Fraboni, L. Pietrantoni, "High-accuracy Tracking using Ultra-wideband Signals for Enhanced Safety of Cyclists",*accepted in mobile information systems, special issue on connected vehicles, applications and communication challenges*, November, 2016.

Conference papers

- [C1] A. Al-Rimawi, D. Dardari, "Analytical Modeling of D2D Communications over Cellular Networks ", accepted for presentation to *IEEE ICC 2015, Wireless Communications Symposium* , London, United Kingdom, June,2015.

- [C2] A. Al-Rimawi, D. Dardari, "Modeling non-uniform D2D distributions in downlink cellular networks ", accepted for presentation to

IEEE 2015 Europoean Conference on Networks and Communications: Track 2 : Wireless Networks (WIN) , Paris, France, June,2015.

- [C3] A. Al-Rimawi, D. Dardari, "characterization of link lifetime in presence of Random Blockages ", accepted for presentation to *IEEE ICC 2017, Wireless Communications Symposium* , Paris, France, May, 2017.

Technical Documents

- [D1] H2020 XCYCLE Deliverable 3.1: "Specification of in-vehicle and on-bicycle systems", March 2016.

Acknowledgements

At the end of my PhD I would like to express my deepest gratitude and appreciation to all people who in different ways have guided and supported me in these years.

First of all, sincere thanks to my advisor, Prof. Davide Dardari; without his inspirational ideas, patience and guide this dissertation would not have been possible. His daily presence and humanity have allowed me to grow along the way, not only professionally, but also as a person. His encouragement to work hard with perseverance and dedication, even in research "difficulties", as well as to attend various conferences and training courses have instilled passion for this work. I always felt privileged to be your student.

A special thank to Prof. Lorenzo Favalli and Dr.Mohammed Jubran for having reviewed the thesis and for all the insightful comments and suggestions that have helped in improving the quality of the manuscript.

Special thanks to all the telecommunications group of Cesena. Thanks to all the teachers, Prof. Marco Chiani, Prof. Enrico Paolini, Prof. Andrea Giorgetti who accompanied me during their university studies and all the lab partners, Anna, Ahmed, Mario, Matthew, Daniel, francesco with whom I shared funny work days and happy.

A special thanks to my family. Words cannot express how grateful I am to my mother-in law, father-in-law, my mother, and father for all of the sacrifices that youve made on my behalf. Your prayer for me was what sustained me thus far. I would also like to thank all of my friends who supported me in writing, and incented me to strive towards my goal. At the end I would like express appreciation to my beloved wife Baraa who spent sleepless nights

with and was always my support in the moments when there was no one to answer my queries.

List of Figures

Bibliography

[1] J. G.Andrews, H. Claussen, M. Dohler, S. Rangan, and M. C. Reed, "A tractable approach to coverage and rate in cellular networks," vol. 59, pp. 56–62, May 2011.

[2] V.Chandrasekhar, J. Andrews, and A.Gatherer, "Femtocell networks: A survey," vol. 46, no. 9, pp. 59–67, September 2008.

[3] G.Fodor, E. Dahlman, G. Mildh, S. Parkvall, N. Reider, G. Mikls, and Z. Turnyi, "Design aspects of network assisted device-to-device communications," vol. 50, no. 3, pp. 170–177, March 2012.

[4] K. Doppler, M. Rinne, C. Wijting, C. Ribeiro, and K. Hugl, "Device-to-device communication as an underlay to LTE-advanced networks," vol. 47, no. 12, pp. 42–49, December 2009.

[5] J. G.Andrews, F. Baccelli, and R. K. Ganti, "A tractable approach to coverage and rate in cellular networks," vol. 59, no. 11, pp. 3122–3134, November 2011.

[6] M. Haenggi, J. Andrews, F. Baccelli, O. Dousse, and M. Franceschetti, "Stochastic geometry and random graphs for the analysis and design of wireless networks," *IEEE Journal on Selected Areas in Communications*, vol. 27, no. 7, pp. 1029–1046, September 2009.

[7] M. D. Renzo, A. Guidotti, and G. E. Corazza, "Average rate of downlink heterogeneous cellular networks over generalized fading channels - A stochastic geometry approach," *CoRR*, vol. abs/1303.0529, 2013. [Online]. Available: http://arxiv.org/abs/1303.0529

[8] A. M. Ibrahim, T. ElBatt, and A. El-Keyi, "Coverage probability analysis for wireless networks using repulsive point processes," in *2013 IEEE 24th International Symposium on Personal Indoor and Mobile Radio Communications (PIMRC)*, Sept 2013, pp. 1002–1007.

[9] H. S. Dhillon, R. K. Ganti, F. Baccelli, and J. G. Andrews, "Modeling and analysis of k-tier downlink heterogeneous cellular networks," vol. 30, no. 3, Appril 2012.

[10] F. Wang and W. Wang, "Analytical modeling of downlink power control in two-tier femtocell networks," in *2013 IEEE 9th International Conference on Wireless and Mobile Computing, Networking and Communications (WiMob)*, Oct 2013, pp. 559–564.

[11] M. Di Renzo, A. Guidotti, and G. Corazza, "Average rate of downlink heterogeneous cellular networks over generalized fading channels: A stochastic geometry approach," *IEEE Transactions on Communications*, vol. 61, no. 7, pp. 3050–3071, July 2013.

[12] T. Samarasinghe, H. Inaltekin, and J. Evans, "On optimal downlink coverage in Poisson cellular networks with power density constraints," *IEEE Transactions on Communications*, vol. 62, no. 4, pp. 1382–1392, April 2014.

[13] M. Di Renzo and P. Guan, "Stochastic geometry modeling of coverage and rate of cellular networks using the Gil-Pelaez inversion theorem," *IEEE Communications Letters*, vol. 18, no. 9, pp. 1575–1578, Sept 2014.

[14] ——, "A mathematical framework to the computation of the error probability of downlink MIMO cellular networks by using stochastic geometry," *IEEE Transactions on Communications*, vol. 62, no. 8, pp. 2860–2879, Aug 2014.

[15] Q. Ying, Z. Zhao, Y. Zhou, R. Li, X. Zhou, and H. Zhang, "Modeling spatial distributions of base stations in cellular networks," *CoRR*, vol. abs/1404.1143, 2014. [Online]. Available: http://arxiv.org/abs/1404.1143

[16] N. Deng, W. Zhou, and M. Haenggi, "Outage and capacity of heterogeneous cellular networks with intra-tier dependence," in *2014 Sixth International Conference on Wireless Communications and Signal Processing (WCSP)*, Oct 2014, pp. 1–5.

[17] Y. Zhou, Z. Zhao, Q. Ying, R. Li, X. Zhou, and H. Zhang, "Two-tier spatial modeling of base stations in cellular networks," *CoRR*, vol. abs/1404.1142, 2014. [Online]. Available: http://arxiv.org/abs/1404.1142

[18] A. Al-Rimawi and D. Dardari, "Analytical modeling of D2D communications over cellular networks," in *IEEE ICC 2015 - Wireless Communications Symposium (ICC'15 (02) WC)*, London, United Kingdom, Jun. 2015.

[19] ——, "Modeling non-uniform D2D distributions in downlink cellular networks," in *2015 European Conference on Networks and Communications: Track 2: Wireless Networks (WIN) (EuCNC 2015 - Track 2-Wireless Networks (WIN))*, Jun. 2015.

[20] C. H. Yu, O. Tirkkonen, K. Doppler, and C. Ribeiro, "On the performance of device-to-device underlay communication with simple power control," in *Vehicular Technology Conference, 2009. VTC Spring 2009. IEEE 69th*, April 2009, pp. 1–5.

[21] N. Lee, X. Lin, J. G. Andrews, and R. W. H. Jr., "Power control for d2d underlaid cellular networks: Modeling, algorithms and analysis," *CoRR*, vol. abs/1305.6161, 2013. [Online]. Available: http://dblp.uni-trier.de/db/journals/corr/corr1305.html/abs-1305-6161

[22] C. H. Yu, K. Doppler, C. B. Ribeiro, and O. Tirkkonen, "Resource sharing optimization for device-to-device communication underlaying cellular networks," *IEEE Transactions on Wireless Communications*, vol. 10, no. 8, pp. 2752–2763, August 2011.

[23] J. Gu, S. J. Bae, B.-G. Choi, and M. Y. Chung, "Dynamic power control mechanism for interference coordination of device-to-device communication in cellular networks," in *2011 Third International Conference on Ubiquitous and Future Networks (ICUFN)*, June 2011, pp. 71–75.

[24] D. Feng, L. Lu, Y. Yuan-Wu, G. Li, G. Feng, and S. Li, "Device-to-device communications underlaying cellular networks," *IEEE Transactions on Communications*, vol. 61, no. 8, pp. 3541–3551, August 2013.

[25] Z. Wang, H. Tian, and N. Chen, "Reliability improvement using power control in device-to-device networks," *Journal of Networks*, vol. 9, no. 2, 2014. [Online]. Available: http://ojs.academypublisher.com/index.php/jnw/article/view/jnw090249

[26] S. Shalmashi, G. Miao, and S. Ben Slimane, "Interference management for multiple device-to-device communications underlaying cellular networks," in *2013 IEEE 24th International Symposium on Personal Indoor and Mobile Radio Communications (PIMRC)*, Sept 2013, pp. 223–227.

[27] B. Cho, K. Koufos, and R. Jantti, "Spectrum allocation and mode selection for overlay D2D using carrier sensing threshold," in *2014 9th International Conference on Cognitive Radio Oriented Wireless Networks and Communications (CROWNCOM)*, June 2014, pp. 26–31.

[28] B. Kaufman, J. Lilleberg, and B. Aazhang, "Spectrum sharing scheme between cellular users and ad-hoc device-to-device users," *IEEE Transactions on Wireless Communications*, vol. 12, no. 3, pp. 1038–1049, March 2013.

[29] C. Xu, L. Song, and Z. Han, "Resource management for device-to-device underlay communication," *CoRR*, vol. abs/1311.1018, 2013. [Online]. Available: http://arxiv.org/abs/1311.1018

[30] F. Tong, Y. Wan, L. Zheng, J. Pan, and L. Cai, "A probabilistic distance-based modeling and analysis for cellular networks with underlaying device-to-device communications," *IEEE Transactions on Wireless Communications*, vol. PP, no. 99, pp. 1–1, 2016.

[31] J. Lianghai, A. Klein, N. Kuruvatti, and H. D. Schotten, "System capacity optimization algorithm for d2d underlay operation," in *2014 IEEE International Conference on Communications Workshops (ICC)*, June 2014, pp. 85–90.

[32] M. Ji, G. Caire, and A. F. Molisch, "Wireless device-to-device caching networks: Basic principles and system performance," *IEEE Journal on Selected Areas in Communications*, vol. 34, no. 1, pp. 176–189, Jan 2016.

[33] Z. Gong and M. Haenggi, "Interference and outage in mobile random networks: Expectation, distribution, and correlation," *IEEE Transactions on Mobile Computing*, vol. 13, no. 2, pp. 337–349, Feb 2014.

[34] X. Liang, X. Zheng, W. Lv, T. Zhu, and K. Xu, "The scaling of human mobility by taxis is exponential," *CoRR*, vol. abs/1109.5460, 2011. [Online]. Available: http://arxiv.org/abs/1109.5460

[35] B. Zhang, Y. Li, D. Jin, and Z. Han, "Network science approach for device discovery in mobile device-to-device communications," *IEEE Transactions on Vehicular Technology*, vol. 65, no. 7, pp. 5665–5679, July 2016.

[36] J. Tengviel and K. Diawuo, "Comparing the impact of mobile nodes arrival patterns in mobile ad hoc networks using poisson and pareto models," *CoRR*, vol. abs/1309.5725, 2013. [Online]. Available: http://arxiv.org/abs/1309.5725

[37] D. M. Blough, G. Resta, and P. Santi, "A statistical analysis of the long-run node spatial distribution in mobile ad hoc networks," in *Proceedings of the 5th ACM International Workshop on Modeling Analysis and Simulation of Wireless and Mobile Systems*, ser. MSWiM '02. New York, NY, USA: ACM, 2002, pp. 30–37. [Online]. Available: http://doi.acm.org/10.1145/570758.570765

[38] G. Fodor, D. D. Penda, M. Belleschi, M. Johansson, and A. Abrardo, "A comparative study of power control approaches for device-to-device

communications," in *2013 IEEE International Conference on Communications (ICC)*, June 2013, pp. 6008–6013.

[39] N. Jindal, S. Weber, and J. G. Andrews, "Fractional power control for decentralized wireless networks," *CoRR*, vol. abs/0707.0476, 2007. [Online]. Available: http://arxiv.org/abs/0707.0476

[40] C. Vitale, V. Mancuso, and G. Rizzo, "Modelling d2d communications in cellular access networks via coupled processors," in *2015 7th International Conference on Communication Systems and Networks (COMSNETS)*, Jan 2015, pp. 1–8.

[41] P. Robertson, E. Villebrun, and P. Hoeher, "A comparison of optimal and sub-optimal map decoding algorithms operating in the log domain," in *1995 IEEE International Conference on Communications. ICC '95 Seattle, 'Gateway to Globalization',*, vol. 2, Jun 1995, pp. 1009–1013 vol.2.

[42] A. Zanella, M. Stramazzotti, F. Fabbri, E. Salbaroli, D. Dardari, and R. Verdone, "Comments on "probability distributions for the number of radio transceivers which can communicate with one another"," *IEEE Transactions on Communications*, vol. 46, no. 5, pp. 1287–1289, May 2009.

[43] J. M. Kelif, S. Sénécal, M. Coupechoux, and C. Bridon, "Analytical performance model for poisson wireless networks with pathloss and shadowing propagation," *CoRR*, vol. abs/1411.5173, 2014. [Online]. Available: http://arxiv.org/abs/1411.5173

[44] Y. Li, B. Ai, X. Cheng, P. Liu, Y. Li, and Z. Zhong, "Interference model with channel shadowing and fading for device-to-device communications," in *General Assembly and Scientific Symposium (URSI GASS), 2014 XXXIth URSI*, Aug 2014, pp. 1–4.

[45] S. Mukherjee, in *Analytical Modeling of Heterogeneous Cellular Networks*. Cambridge University Press, 2011.

[46] T. Bai, A. Alkhateeb, and R. Heath, "Coverage and capacity of millimeter-wave cellular networks," *IEEE Communications Magazine*, vol. 52, no. 9, pp. 70–77, September 2014.

[47] T. Bai and R. Heath, "Coverage and rate analysis for millimeter-wave cellular networks," *IEEE Transactions on Wireless Communications*, vol. 14, no. 2, pp. 1100–1114, Feb 2015.

[48] G. Franceschetti, S. Marano, and F. Palmieri, "Propagation without wave equation toward an urban area model," *IEEE Transactions on Antennas and Propagation*, vol. 47, no. 9, pp. 1393–1404, Sep 1999.

[49] S. Marano and M. Franceschetti, "Ray propagation in a random lattice: a maximum entropy, anomalous diffusion process," *IEEE Transactions on Antennas and Propagation*, vol. 53, no. 6, pp. 1888–1896, June 2005.

[50] M. Franceschetti, J. Bruck, and L. Schulman, "A random walk model of wave propagation," *IEEE Transactions on Antennas and Propagation*, vol. 52, no. 5, pp. 1304–1317, May 2004.

[51] T. Bai, R. Vaze, and R. Heath, "Using random shape theory to model blockage in random cellular networks," in *2012 International Conference on Signal Processing and Communications (SPCOM)*, July 2012, pp. 1–5.

[52] T. Bai, R. Vaze, and R. W. Heath, "Analysis of blockage effects on urban cellular networks," *IEEE Transactions on Wireless Communications*, vol. 13, no. 9, pp. 5070–5083, Sept 2014.

[53] B. Van Quang, R. Prasad, I. Niemieeger, and N. Huong, "A study on handoff issues in radio over fiber network at 60 ghz," in *2010 Third International Conference on Communications and Electronics (ICCE)*, Aug 2010, pp. 50–54.

[54] W. Wang and M. Zhao, "Joint effects of radio channels and node mobility on link dynamics in wireless networks," in *IEEE INFOCOM 2008. The 27th Conference on Computer Communications*, April 2008, pp. –.

[55] L. E. Miller, "Distribution of link distance in a wireless network," *Journal of Research of National Institute of Standards and Technology*, vol. 106, April 2001.

[56] A. Gudipati, D. Perry, L. E. Li, and S. Katti, "Softran: software defined radio access network," in *Proceedings of the Second ACM SIGCOMM Workshop on Hot Topics in Software Defined Networking, HotSDN 2013, The Chinese University of Hong Kong, Hong Kong, China, Friday, August 16, 2013*, 2013, pp. 25–30. [Online]. Available: http://doi.acm.org/10.1145/2491185.2491207

[57] S. Shelly and A. Babu, "Probability distribution of link life time in vehicular ad hoc networks," in *2013 International Conference on Advances in Computing, Communications and Informatics (ICACCI)*, Aug 2013, pp. 1418–1423.

[58] J. Boleng, W. Navidi, and TracyCamp, "Metrics to enable adaptive protocols for mobile ad hoc networks," in *Proceedings of the International Conference on Wireless Networks (ICWN '02)*, June 2002, pp. 293–298.

[59] M. Zhao and W. Wang, "The impacts of radio channels and node mobility on link statistics in mobile ad hoc networks," in *Global Telecommunications Conference, 2007. GLOBECOM '07. IEEE*, Nov 2007, pp. 1206–1210.

[60] S. Gambs, M.-O. Killijian, and M. N. n. del Prado Cortez, "Next place prediction using mobility markov chains," in *Proceedings of the First Workshop on Measurement, Privacy, and Mobility*, ser. MPM '12. New York, NY, USA: ACM, 2012, pp. 3:1–3:6. [Online]. Available: http://doi.acm.org/10.1145/2181196.2181199

[61] S. Vural and E. Ekici, "On multihop distances in wireless sensor networks with random node locations," *IEEE Transactions on Mobile Computing*, vol. 9, no. 4, pp. 540–552, April 2010.

[62] ERSO, "Traffic safety basic facts 2015: Cyclists," European Road Safety Observatory, Tech. Rep., 2015.

[63] "CARE database," http://ec.europa.eu/transport/road_safety/specialist/index_en.htm, European Commission.

[64] M. Z. Win, D. Dardari, A. F. Molisch, W. Wiesbeck, and J. Zhang, "History and applications of UWB," *Proc. IEEE*, vol. 97, no. 2, pp. 198–204, 2009.

[65] "IEEE standard for information technology - telecommunications and information exchange between systems - local and metropolitan area networks - specific requirement part 15.4: Wireless medium access control (MAC) and physical layer (PHY) specifications for low-rate wireless personal area networks (WPANs)," *IEEE Std 802.15.4a-2007 (Amendment to IEEE Std 802.15.4-2006)*, pp. 1–203, 2007.

[66] H. Soganci, S. Gezici, and H. Poor, "Accurate positioning in ultra-wideband systems," *IEEE Wireless Communications*, vol. 18, no. 2, pp. 19 –27, Apr. 2011.

[67] D. Dardari, A. Conti, U. Ferner, A. Giorgetti, and M. Win, "Ranging with ultrawide bandwidth signals in multipath environments," *Proc. IEEE*, vol. 97, no. 2, pp. 404–426, Feb. 2009.

[68] Y. Shen and M. Z. Win, "Fundamental limits of wideband localization – Part I: A general framework," vol. 56, no. 10, pp. 4956–4980, Oct. 2010.

[69] M. Räsänen and H. Summala, "Attention and expectation problems in bicycle–car collisions: An in-depth study," *Accident Analysis & Prevention*, vol. 30, no. 5, pp. 657–666, 1998.

[70] R. Aldred and S. Crosweller, "Investigating the rates and impacts of near misses and related incidents among UK cyclists," *Journal of Transport & Health*, vol. 2, no. 3, pp. 379–393, 2015.

[71] L. Miranda-Moreno, J. Strauss, and P. Morency, "Disaggregate exposure measures and injury frequency models of cyclist safety at signalized intersections," *Transportation Research Record: Journal of the Transportation Research Board*, no. 2236, pp. 74–82, 2011.

[72] W. Niewoehner and F. A. Berg, "Endangerment of pedestrians and bicyclists at intersections by right turning trucks," *Statistics*, pp. 1–15, 2005.

[73] HVU, "Ulykker mellem hjresvingende lastbiler og ligeudkrende cyklister (accidents between trucks turning right and bicycles going straight ahead)," Havarikommissionen for Vejtrafikulykker (Danish Road Traffic Accident Investigation Board), Tech. Rep., 2006.

[74] M. Z. Win and R. A. Scholtz, "Impulse radio: How it works," *IEEE Commun. Lett.*, vol. 2, no. 2, pp. 36–38, 1998.

[75] Z. A. Lu, S. Gezici, and G. Ismail, *Ultra-wideband Positioning Systems: Theoretical Limits, Ranging Algorithms, and Protocols.* Cambridge University Press, 2008.

[76] "ISO/IEC 24730-62:2013 standard," 2013.

[77] D. Dardari, E. Falletti, and M. Luise, *Satellite and terrestrial radio positioning techniques: a signal processing perspective.* Academic Press, 2011.

[78] D. Dardari, P. Closas, and P. M. Djurić, "Indoor tracking: Theory, methods, and technologies," *IEEE Trans. Vehicular Techn.*, vol. 64, no. 4, pp. 1263–1278, 2015.

[79] D. B. Jourdan, D. Dardari, and M. Z. Win, "Position error bound for UWB localization in dense cluttered environments," *IEEE Trans. Aerospace Electronic Syst.*, vol. 44, no. 2, pp. 613–628, 2008.

[80] N. Decarli, F. Guidi, and D. Dardari, "A novel joint RFID and radar sensor network for passive localization: Design and performance bounds," *IEEE J. Sel. Topics Signal Process.*, vol. 8, no. 1, pp. 80–95, 2014.